Feasibility of in-orbit CubeSat Laser Ablative Propulsion

Master Thesis

Renato Meier

Delft University of Technology

TU Delft

Feasibility of in-orbit CubeSat Laser Ablative Propulsion

by

Renato Meier

to obtain the degree of Master of Science

at the Delft University of Technology,

to be defended publicly on September 11, 2025

Student number:	5818710
Project duration:	November 2024 – September 2025
Thesis supervisor:	João de Teixeira da Encarnação

Cover: Laser Station emitting a laser for LAP
AI created using ImageFX, improved with DALL-E

An electronic version of this thesis is available at `http://repository.tudelft.nl`
The code repository of the simulation is found at
`https://doi.org/10.4121/437b2e25-1ac1-4f6b-8f20-5b67123766e3`

TU Delft

Abstract

This thesis investigates the feasibility of the usage of space-based Laser Ablation Propulsion (LAP) to perform orbit maintenance on CubeSat in Low Earth Orbit (LEO). The thesis is motivated by the growing need for efficient, compact propulsion systems for small satellites and explores LAP as a method that eliminates the need for onboard fuel by generating momentum via directed laser beams from orbital laser stations.

A detailed simulation framework is developed to model the physical environment in LEO, including atmospheric drag, solar radiation pressure, and third-body gravitational effects. The propagation of high-powered lasers through space is modeled considering diffraction, absorption, and current limits of aiming precision. The propulsion interaction between laser and CubeSat is simulated through a dynamic model based on material properties and laser beam parameters.

Power generation and energy storage are analyzed in the context of space-based constraints, comparing solar arrays, battery technologies, and their degradation over time. A financial model evaluates system-level trade-offs, including station cost, maintenance intervals, and replacement economics. Optimizations are performed to understand how propulsion efficiency, energy storage capacity, and environmental variability affect system performance and scalability.

Simulation results show that LAP is viable under current technological constraints, provided stations are deployed in sufficient numbers and at the right altitudes. The system can service a meaningful number of CubeSats while remaining competitive with the cost of satellite replacement. Technological limitations such as aiming accuracy and beam control are identified as key challenges, with recommendations for future work including the expansion of in-orbit LAP to networks, and further applications.

Contents

Nomenclature

Roman symbols

A	Area [m^2]
a	Acceleration [m/s^2]
a_{tr}	Semi-major axis of transfer orbit [m]
c	Speed of Light [m/s]
C_D	Drag coefficient [-]
C_m	Momentum coupling coefficient [N/W]
C_r	Solar radiation coefficient [-]
d	Distance [m]
f	Frequency [Hz]
F_D	Air drag [N]
F_T	Thrust [N]
G	Gravitational constant [m^3/kgs^2]
h	Altitude [m]
h_p	Planck constant [Js]
I_{sp}	Specific impulse [s]
L	Ablation plate side length [m]
L_d	Spacecraft lifetime in orbit [days]
M	Mass [kg]
m	Mass flow [kg/s]
P	Power [W]
p_{srp}	Solar radiation pressure [Pa]
R_{sun}	Distance to the Sun [AU]
r	Radius [m]
$\vec{r}$	Position vector [m]
$S_\odot$	Solar constant [W/m^2]
v	Velocity [m/s]
w	Laser beam radius [m]

Greek symbols

α	Absorption coefficient [1/m]
ϵ	Specific orbital energy [m^2/s^2]]
η_{AB}	Ablation efficiency [-]
η_{abs}	Absorption efficiency [-]
η_{Array}	Solar array efficiency [-]
η_{diff}	Diffusion efficiency [-]
θ	Field of View semi-vertex angle [°]

λ	Wavelength [m]	ϱ_E	Specific energy [J/kg]
μ	Earth gravitational parameter [m^3/s^2]	ϱ_P	Specific power [W/kg]
ρ	Density [kg/m^3]	φ	Aiming accuracy angle [rad]
ρ_s	Specular reflectivity [-]	χ	Sun exposure parameter [-]

Acronyms

AU Astronomical Unit. iv, 19, 39

CCD Charge Coupled Device. 9

CubeSat Cube Satellite. i–iii, viii–x, 1, 3, 4, 8, 10, 12, 13, 15–19, 21–27, 31–36, 38–40, 42–46, 48–51, 55–59, 61–64, 67–72, 74–78

DC Direct Current. 9

ESA European Space Agency. 9

EU European Union. 4

FoV Field of View. iv, viii, 23–25, 45, 48, 74, 76–78

GAP Glycidyl Azide Polymer. 5, 6, 8

ISS International Space Station. ix, 10, 64–66

JIMO Jupiter Icy Moons Orbiter. 11

L'ADROIT Laser Ablative Debris Removal by Orbital Impulse Transfer. 7–9, 13

LAP Laser Ablation Propulsion. i–iii, viii, x, 2–13, 15–17, 28–30, 32–35, 40, 45, 46, 49, 51, 54–57, 69, 71, 72, 76, 78

LBLRTM Line-By-Line Radiative Transfer Model. 21

LEO Low Earth Orbit. i, 3, 10, 13, 15, 29, 33, 34, 43, 71

LMT Laser Micro-Thrusters. viii, 8, 9, 13

LODR Laser Orbit Debris Removal. 3, 8, 13

LOWESS LOcally WEighted Scatterplot Smoothing. 37, 40

NASA National Aeronautics and Space Administration. 10, 11, 36, 64, 65

Nd:YAG Neodymium-doped Yttrium Aluminum Garnet. 22

PET Polyethylene Terephthalate. 8

PTD Pathfinder Technology Demonstrator. 36

RTG Radioisotope Thermoelectric Generator. 10, 11, 27

SRP Solar Radiation Pressure. x, 19, 39, 40, 42, 67

TEG Thermoelectric Generator. 10, 11, 27

TOF Time of Flight. 6

TRL Technology Readiness Level. 17, 27

Tudat TU Delft Astrodynamics Toolbox. 18–20, 27, 30, 38, 88

UV Ultraviolet. 8, 19

List of Figures

List of Tables

1 Introduction

From early gunpowder-powered projectiles to modern spacecraft, the history of propulsion has witnessed a century-long development. In the thirteenth century, the Chinese had already been using projectiles for military purposes, which were propelled by a solid propellant primarily consisting of gunpowder. Konstantin Tsiolkovsky, who formulated the ”Rocket Equation”, also proposed the usage of fluid propellant in the early twentieth century [1]. Since then, multiple means of propulsion systems have been developed. In the case of rocket launchers, propulsion is achieved through chemical reactions, such as the burning of liquid oxygen and hydrogen, which provide high thrust. Shortly thereafter, the Space Shuttles were launched using a combination of fluid and solid rocket propellant. Around the same time, multiple propulsion systems have been developed for satellites. On one hand, this includes propulsion methods, such as mono- and bi-propellant systems. They provide high, constant thrust to a satellite; however, they may require preheating to initiate the chemical reaction, which can cause thermal issues in the remaining satellite, especially for small satellites, as insulation on that scale is challenging. On the other hand, electric propulsion systems such as Hall effect and ion thrusters provide many more options for propulsion. Although electric systems provide only low thrust, they offer significantly higher I_{sp}s than chemical thrusters, and thus are more efficient. All presented thrusters have in common that they require tanks filled with a propellant, which takes up considerable fractions of space in a spacecraft and adds mass to it. For example, CU Aerospace produces a compact propulsion unit for 3U Cube Satellites (CubeSats) (see section 1.2) taking up 0.35U of space [2]. The consequence is that either less payload can be carried per spacecraft, or it must be built bigger, ultimately increasing the launch cost.

In 1953, photon propulsion —- a form of propulsion utilizing light —- was proposed as a novel approach, several years before the invention of lasers. Further research showed that, in the ideal case, only a force of 6.7 nN per watt of the incoming light is exerted; this ratio is henceforth referred to as the coupling coefficient. To put this value in perspective, an industrial laser of 100 W would have to be active for 17 days and 6 hours to accelerate a resting body of 1 kg to a speed of 1 m/s, assuming

no external forces act upon it. In 1971, it was first suggested that ablating, in other words, removing, and thereby accelerating a solid onboard propellant using a laser would be more effective. This process is called Laser Ablation Propulsion (LAP) [3].

1.1. Laser Ablation Propulsion (LAP)

Laser ablation is a manufacturing process used in industry for high-precision engraving, cutting, or drilling. A high-power laser is directed toward a material to accelerate and remove its atoms or ions, allowing it to shape workpieces. With short pulses of the order of femto- to nanoseconds, this process affects only thin layers of a material, thus ensuring high precision. Since this process can be applied to metals, ceramics, and polymers, laser ablation is used in various industries, such as the automotive industry or household appliances [4].

The same principles are applicable for LAP. The ablatant can be composed of various materials, which in turn influence the magnitude and efficiency of the thrust. Using polymers allows a laser to penetrate far into the propellant, removing a significant amount of propellant mass, whereas for a metallic ablative, less is ablated since the laser can only penetrate the surface. Consequently, the former leads to an increased coupling coefficient and thrust, whereas exhaust velocity and I_{sp} are low. The inverse effects take place for the latter [5]. By varying the laser intensity, those parameters can also be adjusted to accommodate a satellite's mission profile [6]. As is presented in sections 2.1 and 4.4, the coupling coefficient and thrust are directly tied to it.

1.1.1. Applications of LAP

Currently, LAP is a mainly conceptual topic, as will be further addressed in chapter 2. Regardless, multiple future applications for LAP have been identified:

- Asteroid deflection: In 2013, a meteorite 20 meters in diameter exploded in an airburst, yielding 400 to 500 kilotons of TNT of energy near Chelyabinsk, Russia. The resulting shockwave broke windows in an area of several thousand square kilometers [7]. This is an example of an asteroid that crossed Earth's orbit and posed a threat to people and the environment. One concept of LAP is the alteration of an asteroid's trajectory so that it just misses Earth, so that events as those in Chelyabinsk are prevented. A possible realization could entail a number of satellites in formation flying alongside an asteroid, each equipped with a laser aimed at it, thereby contributing to the total thrust. This would allow for scaling dependent on the asteroid's size and time left for redirection [8]. The practicability is highly reliant on the asteroid's velocity and mass, as the faster and more massive it is, the larger the thrust and/or the further away

the thrust must be applied for a successful deflection. Accordingly, such an asteroid must be detected early enough so that a mission can be initiated, and the satellites can reach the asteroid. In the case of Chelyabinsk, the asteroid was not detected as it approached Earth from a sunward direction; otherwise, it would only have been detected months before impact [9], which is still a very short time span to react.

- Laser Orbit Debris Removal (LODR): Low Earth Orbit (LEO) is filled with millions of objects ranging from paint pieces to rocket parts and satellites that reached their end of life. These objects are estimated to total approximately 6000 tons of mass, making it ”the world’s largest garbage dump” [10]. The debris can cause significant damage to spacecraft due to large velocity differences. LAP offers a solution to reducing space debris by slowing down single objects by inducing a thrust in the opposite direction as they are moving. At lower altitudes, they are then further slowed down by the denser atmosphere, and ultimately burn up in Earth’s atmosphere [3].

- Launch to orbit: Chemical rocket launches require a lot of infrastructure that is difficult to move. Therefore, these systems are not capable of high-frequency launches. Laser launchers have the potential to reduce overall costs, as they can launch multiple vehicles per day [3]. It has been estimated that with a daily launch frequency of 100, the cost to reach LEO can be reduced to approximately $100/kg, whereas today’s LEO launch costs lie at roughly $3000/kg [11].

- Interstellar flight: Some concepts propose a spacecraft to be propelled with high-power lasers, accelerating it to a fraction of the speed of light to reach neighboring star systems within short time spans. Undertaking such a mission would require powerful lasers to generate high thrust and counteract losses (see section 4.2.1) as well as enough energy to provide that power over an extended period. Therefore, laser-powered interstellar flight is a topic that might become interesting in the far future [12].

- Orbit maintenance: Satellites in LEO are still affected by drag from Earth’s atmosphere. Therefore, satellites must be propelled regularly to maintain their altitude. LAP provides an option where no large tank of fuel, no pumps, and other propellant control components that might fail have to be integrated into a spacecraft, therefore reducing its size, as they are replaced only by a surface of ablative propellant. For example, the 2.5U-sized BIT-3 ion thruster package, designed for 6U CubeSat, is equipped with a 300 cm^3 tank made of thermoplastic material. The tank holds 1.5 kg of iodine and provides 3000 m/s of ΔV [13]. In contrast, a 10 cm x 10 cm plate of iron used for LAP that has a mass of 1.5 kg, can only provide up to 1475 m/s with LAP; the space used, however, is reduced to roughly 0.19U [14].

This thesis focuses on the application of LAP for satellite orbit maintenance, as elaborated in the last point, since research in this area is scarce; so there is the potential for a specific type of mission where LAP orbit maintenance can be more advantageous compared to the known methods.

1.2. CubeSats

The CubeSat is an approximately 25-year-old standard of satellites. Its primary difference from conventional satellites lies in its size. A CubeSat is made of cubes of 10 cm x 10 cm x 10 cm, also called 1 unit (1U), that are combined to larger satellites up to 16U. Due to the limited space, the mass of such a CubeSat is limited and tends to go only up to 32 kg [15]. Traditional satellites, on the other hand, take up significantly more space and have a higher mass. For example, the European Union (EU)'s global navigation satellite system Galileo is equipped with satellites of 2.5 m x 14.67 m x 1.1 m with deployed solar wings and a mass of 700 – 732 kg [16]. The CubeSats' small size creates opportunities such as significantly lower prices for production and launch [15]. On the other hand, however, it also limits the satellite's capabilities. First, the small size restricts the area of solar arrays, thereby limiting power generation, which in turn requires onboard systems and instruments to function at low power levels or to be operated in turns. Second, there are limits to the miniaturization of instruments due to physical constraints [17]. Imagery instruments, for example, require a certain mirror size to produce high-resolution pictures; the higher the resolution, the larger the mirror must be [18].

Initially intended for educational purposes, CubeSats have also been used commercially for optical high-resolution imagery of Earth as well as weather forecasting. Furthermore, they are being used for technology demonstrations [19]. An example is the SLP-1K thruster test, further elaborated in section 2.2.3. Due to their modularity, CubeSats can be adapted to a project's purpose and built with off-the-shelf components. Most importantly, they can be developed and deployed into orbit within one to two years [15].

2
State of the Art

This chapter explains what the most recent research found on LAP and other topics that are crucial to this thesis, as well as the current state of technology and its properties. The information discussed here provides a basis for the methods and parameters that the thesis can build upon. Section 2.1 elaborates on the current state in LAP, secondly section 2.2 discusses different concepts of LAP orbit maintenance and in what way LAP has been used. Thirdly, section 2.3 discusses the currently achievable aiming accuracy. Finally, section 2.4 discusses methods of how to generate and store energy in space.

2.1. Current LAP properties

As hinted in section 1.1, the efficiency and thrust are dependent on the choice of the material that is ablated. The formulation of those are presented in section 4.4, as this section focuses mostly on the coupling coefficient, compares it with other thrusters, and discusses other effects that occur with LAP. The material choice is essential for LAP, as the energy required to achieve a desired maneuver is directly tied to it.

Table 2.1 compares the measured coupling coefficients of different electric propulsion systems and LAP materials. All presented means of propulsion outperform photon propulsion by at least three orders of magnitude, indicating that pure photon propulsion is not a viable option due to its limited thrust performance. Furthermore, the table displays that LAP systems using Glycidyl Azide Polymer (GAP), gold, and iron can compete with, and in some cases, surpass existing thrusters regarding propulsion efficiency. Due to the significant differences in the coupling coefficient C_{m} among the LAP materials, research and innovation on other materials might lead to better-performing ablation materials.

Table 2.1: Comparison of coupling coefficients of different propulsion systems

	C_m [µN/W]	Source
Photon propulsion	$6.7 \cdot 10^{-3}$	[3]
Ion Thrusters	17.0 – 45.7	[11]
Hall Effect Thrusters	31.3 – 68.8	[11]
LAP (Aluminum)	30	[11]
LAP (Copper)	$\leq$ 220	[14]
LAP (GAP:C)	$\leq$ 1170	[20]
LAP (Gold)	$\leq$ 100	[11]
LAP (Iron)	$\leq$ 181	[14]

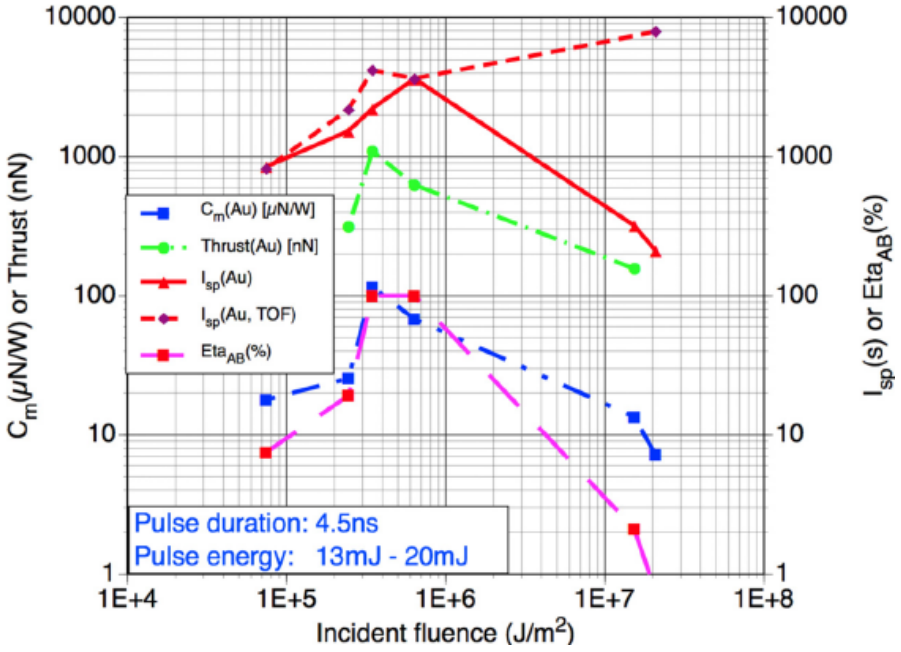

Figure 2.1: Experimental data for LAP on gold [11]. The divergence of the two I_{sp} curves indicates a reduced mass loss (solid red), while the Time of Flight (TOF), thus the ion speed, increases with increased fluence (dashed red).

Experimental measurements show that the coupling coefficient is highly dependent on the incident energy fluence, the amount of energy per area, to the ablative surface. In the case of gold LAP in table 2.1, the value refers to the blue curve in figure 2.1. For a fluence of 100 kJ/m^2, 20 µN/W was measured, whereas for a fluence of 330 kJ/m^2, a coupling coefficient of 100 µN/W was reached. With higher fluences, it decreased again to 70 µN/W with a fluence of approximately 620 kJ/m^2 and decreased further with higher laser fluence. Similar behavior is observed for the ablation efficiency depicted in pink. A reason for this behavior is that with increased power and therefore increased

mass flow, the laser is obstructed by the propelled material so that eventually not the full power reaches the ablative plate [11]. Therefore, to use LAP efficiently, not only the choice of ablative material but also the properties of the laser are paramount variables that must be considered.

2.2. Space applications for LAP

After discussing the material properties of different ablatants, this section aims to discuss in what ways LAP has been conceptualized and implemented, as a means to obtain a benchmark on what can be achieved by it.

2.2.1. Ground-based laser stations

The approaches of how LAP can be used to propel a satellite in orbit are manifold. Extensive research has been done on ground-based lasers [3, 5, 21]. Their main advantage over space-based lasers is that they do not require space infrastructure for installation or maintenance and, therefore, are comparably cheap. Furthermore, electricity supply can be ensured by building a large-scale power station or connecting it to the grid [5]. Their disadvantage lies in the reduced efficiency of the laser caused by the densest part of Earth's atmosphere present at low altitudes and meteorological phenomena such as clouds that absorb the laser's energy drastically [22]. Consequently, a ground laser would have to compensate for those effects by using excess power. Additionally, the continuously changing outgoing laser angle at the spacecraft alters the incoming laser energy intensity and thus the thrust generated over time due to the varying laser's distance traveled in said lower altitudes [11]. As a countermeasure, the implementation of a satellite equipped with a relay mirror system, which is already in orbit, has been conceptualized, so that the distance traveled in the denser part of the atmosphere is kept minimal. Although the modeled relay stations have been intended to facilitate the final phase of a launch, when a spacecraft has to gain horizontal speed, the detriment of the dense atmosphere is also valid for orbit maintenance, since they both aim to accelerate a spacecraft to bring it to its final orbit [23].

2.2.2. L'ADROIT

L'ADROIT, short for Laser Ablative Debris Removal by Orbital Impulse Transfer, is a concept intending to remove the risk of space debris colliding with satellite infrastructure using LAP. It proposes a laser station in an elliptical polar orbit at altitudes between 560 and 960 km. The main concept is to slow down small objects, up to 10 cm in size, so that they burn up in Earth's atmosphere. In contrast, larger objects are either decelerated or accelerated to change their altitude to establish a secure distance between satellites and debris. Simulations showed that the proposed laser station

could provide a ΔV of 236 m/s to 100000 objects within four months at a cost of $8 per kg of removed debris. Furthermore, for large objects with a mass of 1000 kg, it would take four years to raise or lower the orbit by 40 km with a cost of $280 per kg. For the simulation, a neodymium Ultraviolet (UV) laser with a wavelength of 355 nm, with a fluence of 8.5 kJ/m^2 at 32 Hz was taken [24]. To that extent, L'ADROIT is one of the most advanced analyses conducted on space-based LAP and its applicability. While it focuses on LODR and not orbit maintenance per se, increasing debris orbit altitudes is practically identical to orbit maintenance. Therefore, L'ADROIT is of high comparable value for this thesis.

2.2.3. Laser Micro-Thrusters (LMT)

Another approach to LAP has been followed with Laser Micro-Thrusters (LMT). Instead of directing a high-power laser across several kilometers to a satellite or debris, a LMT works with a small laser diode installed on board. Figure 2.2 depicts how LMTs work. An ablative layer is attached to a transparent tape or layer. To create thrust, a laser, depicted in blue, originating from the diode, beams through the transparent tape onto the ablative layer. This causes a high-velocity jet of plasma and residual particles of the propellant, giving the satellite an impulse. The tape with the ablative layer is continuously moved sideways so that another part of the ablative material is ablated and the thrust is maintained over a longer period [25].

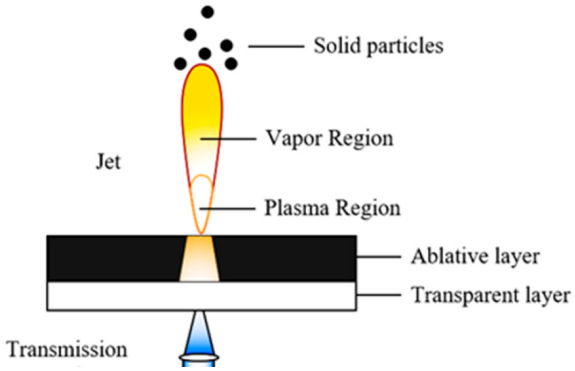

Figure 2.2: Schematic of the LMT thrust generation [25]

In 2022, a LMT was successfully tested in orbit for the first time with a thruster called SLP-1K. The thruster was designed for attitude control and was mounted on a 6U CubeSat. It used Polyethylene Terephthalate (PET) as the transparent tape with Glycidyl Azide Polymer (GAP) as the ablative material [25, 26]. Mechanical tests before launch and in orbit showed that the thruster could perform tests of up to approximately 300 µN, requiring 6.55 W of power, thus resulting in a coupling coefficient of

45.80 µN/W. LMTs have been the first proof that LAP is possible in space. However, the study has so far only shown that it is practical for attitude control; whether it is suitable for maneuvers is yet to be found out [25]. Furthermore, in contrast to concepts such as L'ADROIT that proposes a laser station, orbit maintenance by LMT would have to be performed by every satellite individually; thus, each satellite would require an individual thruster.

2.3. Aiming accuracy

High aiming accuracy is paramount for LAP in space, if lasers are emitted over many kilometers. Over long distances, even if atmospheric effects were ignored, minimal inaccuracies can lead to a laser missing its target. From trigonometry, it can be derived that at a deviation of 0.01°, the laser misses its target by approximately 17.5 m for every 100 km of distance the laser covers. This does not yet account for natural phenomena such as diffraction, elaborated in section 4.2. Missing a target can imply that the laser ablates the target's surroundings or another object. Both can be fatal for the spacecraft, as unforeseeable thrust will be generated, altering its orbit and, depending on the material and components hit, possibly reducing the satellite's functionality.

Research on aiming accuracy in optical communications for space applications goes back to the 1970s [27]. It has promising properties, such as a high transmission rate and being hardly jammable [28]. The primary focus lies in the research on pointing and tracking for this thesis. Since laser communication and LAP both rely on light beams sent over long distances in space, they follow the same physical principles. Consequently, insights from one can be applied to the other, and the same aiming technology can be used.

In 1994, the Japanese Ministry of Posts and Telecommunications developed a laser tracking device that, with coarse tracking, achieved an accuracy of 32 µrad, using a Charge Coupled Device (CCD). Precision tracking was performed using a four-quadrant detector, achieving an accuracy of 2 µrad. ESA achieved the same accuracy for an inter-satellite optical communication link only using a Direct Current (DC) stepper motor and a fast mirror in 2002 [27]. More research has been conducted in the meantime, and other aiming devices have been constructed; none of them, however, has been able to improve accuracy beyond 2 µrad; the accuracies have remained in the range of <10 to 200 µrad [27, 29]. Regarding slew speed, a 50° retargeting in 2 seconds, thus 25°/s, could be achieved for mirrors the size in the order of 1-2 meters in diameter [30].

Returning to trigonometry with the currently most sophisticated accuracy of 2 µrad, the deviation of this angle corresponds to 20 cm per 100 km of distance passed by the laser. Here lies the problem with ground-based lasers: even without considering atmospheric influences and being pointed directly at the zenith, the laser would have to cover approximately 400 to 600 km to reach a satellite in LEO, resulting in a deviation of up to 80 to 120 cm. Since the deviation exceeds the size of entire CubeSats, such a method of propulsion is not reasonable unless significant improvements in aiming accuracy are achieved. Space-based lasers, on the other hand, can aim the laser at shorter distances, which means that the ablative surface can be targeted with minor deviations.

2.4. Energy Management for LAP

The laser used for LAP requires a power supply to work. Therefore, there must be a method to generate power, whose options are discussed in section 2.4.1. Furthermore, since it must be expected that the power supply is interrupted, energy storage is paramount to ensure continuing operation.

2.4.1. Power generation in Space

For spacecraft instruments to function, they require power from electricity. Therefore, they must generate and store electricity to continue their functionality throughout their mission. So far, two means of energy production have been used in spacecraft: solar panels and Radioisotope Thermoelectric Generators (RTG). Additionally, the use of Thermoelectric Generators (TEG) has been proposed.

Solar cells are the preferred choice for spacecraft operating relatively close to the Sun, as they provide a substantial amount of free energy. The Sun delivers approximately 1.4 kW/m^2 in an Earth orbit. Therefore, spacecraft with a high power consumption, such as the International Space Station (ISS), have large arrays to deliver useful power levels. In 2021, the ISS was equipped with roll-out solar arrays the size of 18.2 x 6 m, each array producing 20 kW to upgrade its power system [31, 32]. Since spacecraft in Earth's orbit go through an eclipse, power cannot be provided continuously. Thus, they also require power storage, bridging the supply for a particular time, which then is recharged as soon as the solar arrays are exposed to the Sun again. Other disadvantages are found in the low efficiencies of solar panels, which necessitate the installation of larger solar arrays to compensate; the latest designs achieve only 30% efficiency. Furthermore, they are prone to degradation due to solar heating and radiation [33].

RTGs produce power by converting the heat caused by plutonium-238 decay into electricity. NASA first implemented a RTG in 1968 for its Nimbus B-1 meteorological satellite and continued implementing them for the Apollo missions as well as the Pioneer and Voyager spacecraft, with the latter

ones still being in use, despite having been launched in the 1970s. Therefore, RTGs have proven highly reliable. So far, RTGs provided power in the range of 20 to 300 W. NASA's future generation RTG that is planned to be flight-ready by 2030 has the objective to provide roughly 250 W; thus, there is no indication of any higher performing radioactive decay power sources. The advantage of this method for powering a spacecraft lies in its reliable, continuous power generation, regardless of the spacecraft's location and attitude [34]. The radioactivity of the plutonium-238, however, raises multiple challenges and disadvantages. The design and assembly of RTG-powered satellites are more expensive due to the cost of plutonium and the protection measures required against radioactivity during production, launch, and operation. From a legal standpoint, although the Safety Framework for Nuclear Power Source Applications in Outer Space exists, it is not legally binding; legal constraints may arise solely due to national regulations [35].

Research on TEGs has been conducted for over 50 years. TEGs aim to exploit the heat flow from a hot to a cold location. In space applications, this can be the heat flow from the spacecraft hull heated by the Sun to the surrounding space. It has been shown that for this method of energy generation, Brayton, Rankine, and Stirling cycles are suitable and, therefore, follow the same thermodynamic processes as gas turbines and combustion engines. The Brayton cycles for space have been researched since the 1960s; at that time, one Brayton generator could already produce 10 kW [36]. The other cycles have also been considered for space applications in the meantime, such as during NASA's Jupiter Icy Moons Orbiter (JIMO) project in the early 2000s, Stirling generators were considered in design studies. For instance, a free-piston Stirling engine was developed in 2001, producing 108 W/kg with an efficiency of 28.5% [36].

2.4.2. Energy storage in Space

As elaborated in section 2.4.1, there are presently no means to produce enough electrical power to operate a space-based laser without scaling those sources into larger generators, resulting in a significant addition of mass and volume to a laser station. An option would be to implement energy storage, which allows the power generators to remain small-scale. The energy required for a laser emission can be accumulated over time. Energy can be stored chemically using batteries, electrostatically in capacitors, mechanically using flywheels, or nuclearly using RTGs. All those methods have been used for space applications except for flywheels, whose specific energy is limited due to their material's tensile strength [37]. Nuclear options use the radioactive energy stored in a RTG's plutonium and have been discussed in section 2.4.1.

Batteries can be categorized into primary and secondary, or in other words, single-use and rechargeable batteries. Both types have countless different examples that have been developed for specific applications. Sputnik was equipped with a silver-zinc battery due to its high specific power supply of up to 2.5 kW/kg. Nickel-cadmium batteries, such as those used in the Landsat D mission, were chosen for their ability to power satellites for multiple years. The Hubble telescope has been equipped with nickel-hydrogen batteries, as they are designed to operate for 15 years or 60000 discharge cycles [37].

Primary batteries have been used in planetary probes, such as during the Cassini mission. The lithium-sulfur dioxide (Li-SO_2) battery used there had an energy capacity of approximately 800 kJ/kg and offers one of the highest specific power levels among primary lithium cells. The lithium-thionyl (Li-$SOCl_2$) battery has been designed for long-term missions and, therefore, has a high specific energy capacity of roughly 1.4 MJ/kg but provides only low power levels in the order of 100 W/kg. It has been used on the Mars rover Sojourner [37]. While secondary batteries such as the silver-zinc cell used in the 1960s have been decommissioned due to rapid degradation and short life cycles, alternatives have been developed. Nickel-cadmium batteries have proven reliable for over fifty years, with low maintenance requirements and the ability to operate for over ten years with 80000 cycles of charging and decharging. However, with a specific energy capacity of 180 kJ/kg, they count towards the less energy-dense cells. Nickel-hydrogen batteries have been widely employed in spacecraft due to their decade-long lifespan, as previously elaborated. Nevertheless, this battery type has a specific energy capacity comparable to that of the nickel-cadmium cell, providing only an advantage in operational duration [37]. Finally, there is a considerable variation in lithium-ion batteries. Among these, lithium-sulfur cells offer the highest energy density, at 1.44 MJ/kg, and high discharge rates of 800 to 1500 W/kg. However, they only operate in the order of some hundred to a thousand charging cycles [38].

Supercapacitors offer a solution similar to secondary batteries. Experiments have shown that supercapacitors are a reasonable option for space applications such as CubeSats. For instance, this was demonstrated with a capacitor with a diameter of 35 mm in diameter holding 20 kJ/kg of energy and providing 7.9 kW/kg [39]. Recent research has shown that higher energy densities are achievable with asymmetric supercapacitors compared to their ”simple” counterparts. For example, a capacitor made of transition-metal-oxide nanowires and single-walled carbon nanotubes can provide 92 kJ/kg and 50.3 kW/kg [40]. In sum, capacitors tend to provide high power levels while they store a significantly lower amount of energy than batteries, whereas the opposite is the case for batteries [37].

3
Research Proposal

So far, in the field of LAP, only LMT have been launched into orbit. Ground-based and in-orbit lasers remain in the conceptual or experimental stage. The latter, however, has hardly been considered except for L'ADROIT, a concept for space-based LODR. While L'ADROIT offers a cheap solution to remove space debris, it only hints at the potential for orbit maintenance due to the opposite goal of LODR to remove objects out of orbit. Thus, space-based laser orbit maintenance is a field that has not been touched so far. This thesis aims to determine whether operating an in-orbit laser station for orbit maintenance is viable and financially feasible, and to identify the characteristics that such a laser station must possess to achieve this.

3.1. Research Questions

Sub-questions have been defined to help answer the main research questions, each one trying to do so from a different perspective.

The first question focuses on the laser station's orbit characteristics to enable it to reach a CubeSat with its laser. It primarily arises due to energy losses that a laser experiences during its path from the station to a satellite and efficiency losses. Furthermore, a station must reach many satellites; the requirements that arise from this must also be defined. Since there is the possibility that these requirements do not allow for a solution, one must assess the technological advancements necessary to operate a laser station. Consequently, the following questions were developed.

RQ-1 What are the possible orbits in LEO for the laser station so that the losses of laser energy are minimal, the number of reachable satellites is maximal, and the orbit maintenance of the laser station is minimal?

RQ-1.1 What are possible altitudes for the laser station to propel CubeSats in LEO?

RQ-1.2 What are the possible altitudes of the laser station so that its own orbit has to be maintained as rarely as possible while still being able to reach other satellites with its laser?

RQ-1.3 What is the farthest distance the laser station can be away from a satellite to still provide orbit maintenance due to the aiming accuracy limits of today's technology?

RQ-1.4 What types of lasers suit a laser station?

RQ-1.5 To what extent can the laser station's orbit be improved with more accurate aiming technology in the future?

When a laser station propels a satellite, assuming it was in a circular orbit beforehand, its orbit will become elliptical. It may have to be accelerated a second time to put it back into a circular orbit at a higher altitude. Depending on the constellation of this satellite and laser station, their difference in velocity, and the distance between them, another laser station may have to induce that thrust, as the satellite is out of reach for the original station, which raises the second question.

RQ-2 How many laser stations are required to ensure a circular orbit for the satellites?

Research question 3 aims at inspecting the energy limits of a laser station. The number of satellites the laser station can propel is directly tied to the amount of energy produced on the station, the capacity at which it can be stored onboard, and how much energy is drawn to create a laser. Since solar cells and batteries degrade over time due to solar radiation and repeated charging and discharging, the number of satellites a laser station can maintain in orbit is bound to decrease. The consequence is that to ensure the orbit maintenance of a given number of satellites, that number must include a certain tolerance so that components of the space station can be replaced.

RQ-3 What is the maximum number of satellites that can be propelled due to energy limitations?

RQ-3.1 What power supply options provide the most energy to the laser station to enable high-power lasers to be emitted?

RQ-3.2 *removed*

RQ-3.3 What are the power supply and storage degradation implications over time?

RQ-3.4 What dimensions must the laser station have to house energy storage and power generators?

Despite the physical and technological challenges that the operation of an in-orbit laser station entails, to be reasonable to pursue it, it also must be financed. Since an orbit maintenance laser station would compete with actors that would launch a replacement of a decommissioned satellite, the former has to undercut the latter or offer an additional value that a satellite replacement cannot provide. Therefore, the fourth question is as follows:

RQ-4 Is pursuing laser-based orbit maintenance of satellites financially viable as opposed to replacing satellites?

3.2. Reference case

The scenario used for answering the research questions listed in section 3.1 is made from the perspective of a company offering LAP orbit maintenance to CubeSat operators.

The laser stations maintain only CubeSats in circular or nearly circular LEOs. LEO is assumed since this is the common orbital region where CubeSat are used [15]. Accounting for more eccentric or higher altitude orbits adds a large variation of cases and would be beyond the scope of the thesis. Nearly circular orbits are considered to account for the loss of altitude that a satellite experiences due to atmospheric and other external influences, which will be discussed in chapter 4. Similarly, the scenario assumes circular orbits for the laser stations, which are also affected by atmospheric drag. For the altitude changes, the CubeSats only undergo accelerations parallel to the velocity vector, as they require the least amount of ΔV.

Next, it is assumed that each laser station is fully self-sufficient energy-wise and, accordingly, obtains all energy from solar arrays or onboard generators. Equally, the laser stations do not serve as a relay station for ground-based lasers, comparable to [23]'s proposal presented in section 2.2.1. The only exception made is for its own orbit maintenance, where a station is either propelled by LAP or conventional means, which would require refueling. A station's laser system is equipped with one laser and can, therefore, propel only one satellite at a time. Technology-wise, the laser stations are fitted with components that already exist today.

The CubeSats are assumed to be of the size of 6U in a 2-by-3 formation, as depicted conventionally in figure 3.1, and the mass of 12 kg. The format results in more atmospheric drag than a 1-by-N formatted one, slowing down the CubeSats additionally. This format is popular; for instance, Kepler Communications has been planning a fleet of 140 6U CubeSats for inter-satellite communications [41]; and therefore allows the results to be representative for a possible implementation for LAP for CubeSats. This mass is chosen to increase the satellites' inertia with the consequence that

a laser needs to propel for a more extended period than for smaller CubeSats. Furthermore, the ablative surface is set to 10 cm x 10 cm; since this is a universal size for all CubeSats. The plate is positioned centered on the side oriented in the opposite direction as the velocity vector, indicated by the blue square in figure 3.1. Finally, for simplicity's sake, it is assumed that the satellites are nominally Earth-pointing. This implies that the thrust generated through LAP is deemed tangential to the velocity vector.

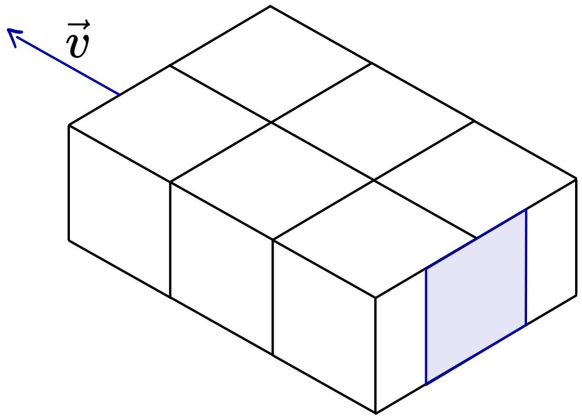

Figure 3.1: Conceptional depiction of the CubeSat used in this thesis

3.3. Requirements

The requirements for the laser station are derived from the research questions and the reference case. They are divided into three categories: operational, state of technology, and financial.

The operational requirements set the boundaries within which the laser station must perform. Energy management and laser propulsion are in constant interplay throughout the lifetime of such a laser station. The limits of both dictate the number of satellites whose orbits can be maintained. To ensure long-term operation, the space station must generate sufficient energy for its own needs. Furthermore, the time spent on one satellite must be limited to provide service to the maximum number of satellites; thus, the thrust event must be efficient so that losses are minimized. From this, it follows that the laser must always hit the ablative surface, as otherwise the laser must be activated again to conduct a CubeSat's maintenance event. For this reason, it is also reasonable that a maneuver is completed with one thrust event. Finally, the plane that the laser station and CubeSats orbit Earth determines the energy generation and therefore the energy storage on the laser station. In a polar orbit, the time the spacecraft are in eclipse varies, with the extreme case of

not going into eclipse at all. An equatorial orbit is guaranteed to have the spacecraft go into eclipse. Therefore, if the energy calculation is made for the equatorial plane, it is also valid for orbits in all inclinations, as it is a worst-case scenario regarding energy budgeting.

OPS-1 The laser station shall operate energy-efficient.

- **OPS-1.1** The CubeSats shall perform Hohmann transfers for their orbit maintenance.
- **OPS-1.2** The laser stations shall generate all electrical power on board and, therefore, be self-sufficient.

OPS-2 The laser station shall spend minimal amount of time per CubeSat for orbit maintenance.

- **OPS-2.1** The laser station shall be able to aim at the CubeSat's ablative surface so that the laser never misses it.
- **OPS-2.2** CubeSats shall only be propelled once to initiate and terminate the transfer orbit.
- **OPS-2.3** The laser station shall be capable to propel CubeSats of the mass of 12 kg with an ablative surface of 10 cm x 10 cm.

OPS-3 The CubeSats and laser stations shall orbit Earth in the equatorial plane.

The state of technology limits the capabilities of the laser station. Simulating with technological limits that have not yet been reached has the consequence that the results are not meaningful beyond identifying the areas that require further research and innovation, as well as the characteristics that need to be achieved. Therefore, it is only reasonable to make a feasibility study based on current capabilities and resort to future possibilities for improvement. Hence, the following requirements have been defined.

SOT-1 The laser stations shall be equipped with current technology that has a Technology Readiness Level (TRL) of 8 or higher.

Feasibility of LAP entails also its financial viability. If ”conventional” orbit maintenance methods are cheaper, and LAP cannot compete against them, then its pursuit is not reasonable.

FIN-1 The operation of a system of laser stations shall be profitable and competitive.

- **FIN-1.1** The company selling laser-based orbit maintenance shall achieve at least 5% of profit.

4
Methodology

A simulation framework has been developed to assess the feasibility of space-based laser stations, addressing the research questions and requirements outlined in chapter 3. In the following sections, its elements are discussed. First, section 4.1 describes the environment within which the CubeSats and laser stations are simulated. It discusses the external forces that act on them and alter their trajectories, which are then implemented into the simulation. Next, section 4.2 discusses the choice of the laser for the simulation and elaborates on the implementation of the laser model. Section 4.3 describes the energy model of the laser stations. The effect of the laser, the propulsion model, is presented in section 4.4. Finally, the grounds of the financial calculations are presented in section 4.5.

4.1. Environment Model

The environment model is based on the TU Delft Astrodynamics Toolbox (Tudat) that supports the simulation of astrodynamics and orbit propagation. This thesis's simulation mainly utilizes the environmental functionalities and the positioning of celestial bodies. Finally, it is also used to propagate the CubeSats' and laser stations' orbits around Earth.

4.1.1. Atmosphere model

As already elaborated in section 1.1, there are remains of Earth's atmosphere, with the consequence that spacecraft are decelerated over time and lose altitude due to air drag. Air drag F_{D} is defined as follows.

$$F_{\mathrm{D}} = \frac{C_{\mathrm{D}}}{2} \rho v^2 A \tag{4.1}$$

C_{D} represents the drag coefficient; its magnitude depends on the geometry of the satellite and is determined in section 5.4.2. ρ stands for the atmosphere's density, v for the spacecraft's velocity, and A is the area of the satellite projected to a plane perpendicular to the direction of motion. Since

all spacecraft are assumed to rotate with their direction of motion, A reduces to their frontal area. The calculation of the air drag is taken over by Tudat since it calculates the velocities and contains a model of Earth's atmosphere. It also considers the 11-year solar cycle, which influences Earth's atmosphere. Increased solar activity, of which mainly UV and x-ray emissions, causes the thermosphere to heat up so that the atmosphere expands, consequently increasing air drag to which a spacecraft is affected by.

4.1.2. Solar radiation pressure

Solar Radiation Pressure (SRP) is created from the interaction of solar photons with a spacecraft's hull. Incident photons exchange momentum with the spacecraft and are either absorbed or reflected; the reflectivity coefficient $C_\mathsf{r} \in [1, 2]$ gives the respective ratio. A value of 1 means that all photons are absorbed, while a value of 2 indicates that all photons are reflected. SRP p_srp is defined by the solar constant $S_\odot$ giving the Sun's radiation flux at a distance of 1 AU, which is 1361 W/m^2. The resulting acceleration a_srp at a distance R_Sun from the Sun is given below [42]. The reflectivity coefficient can be approximated with the specular reflectivity ρ_s [43].

$$a_\mathsf{srp} = p_\mathsf{srp} \left(\frac{1\ \mathsf{AU}}{R_\mathsf{Sun}} \right)^2 C_r \cdot \frac{A_\mathsf{sat}}{M_\mathsf{sat}} \quad \text{with} \quad p_\mathsf{srp} = \frac{S_\odot}{c} = 4.53\ \mu Pa \quad \text{and} \quad C_\mathsf{r} = 1 + \rho_\mathsf{s} \tag{4.2}$$

SRP only is effective on a spacecraft as long as it is directly exposed to the Sun. In eclipse, there is no acceleration in combination with SRP. Tudat considers the constellations of the Sun, Earth, and spacecraft for the simulation of SRP; thus, Tudat has been used for this part of the simulation as well.

As the sensitivity study in section 5.1.2 shows, SRP has a significant influence on the orbit, and it becomes relevant to consider how the spacecraft surfaces are composed. For simplicity, it is assumed that the sides of all CubeSats are either covered by solar arrays or are made of aluminum. Solar arrays have a specular reflectivity of 0.0727, and aluminum has a ρ_s of 0.8, thus resulting in reflectivity coefficients of 1.0727 and 1.8, respectively [44]. It is assumed that the CubeSats' solar arrays are positioned on their 2x3 sides, as those areas are the largest and therefore the most energy can be generated. Covering the entire area results in approximately 24.5 W of power with a solar array efficiency of 30%. The remaining sides are simulated to be aluminum. Overall, this gives a weighted average C_r of 1.403.

4.1.3. Third-body gravity

The first step in deciding which celestial bodies, besides Earth, to include in the model involves determining the highest possible gravitational acceleration for each. This was done by assuming the closest possible distances between the spacecraft and each body separately. As the difference in distance between the spacecraft and the other planets deviates only minimally from the distances between them and Earth, and therefore their gravitational acceleration, the latter were used. Due to its proximity, the altitude was used to determine the Moon's influence. Since the spacecraft's altitude is not yet defined, an altitude of 400 km was chosen. Additionally, the accelerations were set relative to Earth's gravity at this altitude. The results are shown in table 4.1. The gravitational acceleration a is defined as presented in equation 4.3, G being the gravitational constant, M_{Body} representing the mass of the celestial body attracting the spacecraft, and d standing for the distance between the centers of mass of the two.

$$a = G \cdot \frac{M_{\text{Body}}}{d^2} \tag{4.3}$$

Table 4.1: Third-body gravitational influence on a spacecraft at 400 km altitude. Derived from [45]

	Max. Gravitational acceleration [m/s^2]	Relative to Earth gravity
Earth	8.70	1.00
Sun	$5.94 \cdot 10^{-3}$	$6.82 \cdot 10^{-4}$
Mercury	$2.66 \cdot 10^{-9}$	$3.06 \cdot 10^{-10}$
Venus	$1.88 \cdot 10^{-7}$	$2.16 \cdot 10^{-8}$
Moon	$3.36 \cdot 10^{-5}$	$3.86 \cdot 10^{-6}$
Mars	$7.01 \cdot 10^{-9}$	$8.06 \cdot 10^{-10}$
Jupiter	$3.21 \cdot 10^{-7}$	$3.69 \cdot 10^{-8}$
Saturn	$2.32 \cdot 10^{-8}$	$2.67 \cdot 10^{-9}$
Uranus	$7.81 \cdot 10^{-10}$	$8.98 \cdot 10^{-11}$
Neptune	$3.63 \cdot 10^{-10}$	$4.17 \cdot 10^{-11}$

A comparison of the values in table 4.1 with the estimation of air drag deceleration in section 4.1.1 was made to determine what celestial bodies are of relevance. The air drag estimation at 400 km altitude was $1.24 \cdot 10^{-7}$ m/s^2. Accordingly, the gravitational influences of the Sun, Venus, the Moon, and Jupiter are more extensive than Earth's atmospheric drag at that altitude; thus, they must be considered in the simulation. Furthermore, the influence of the remaining planets' gravity is to be evaluated in the sensitivity study in section 5.1.3. To simulate the accelerations of all celestial bodies, Tudat was used, as it allows for simply adding and removing them in the simulation.

4.2. Laser Model

This section, on the one hand, describes the physical implications of emitting a laser over long distances and what measures must be taken to still hit the ablative surface at the CubeSat. On the other hand, it elaborates on the laser activation conditions and the constraints on emission distance.

4.2.1. Losses

Lasers experience losses when passing through a medium. In the model, the lasers are expected to travel distances in the order of multiple 10 km to a few 100 km, with the consequence that losses can significantly influence the laser beam. The simulation includes two sources of losses. First, there is absorption, the transmission of energy to the atmosphere. Second, there is diffraction, the deviation of single light waves from the intended beam direction, so that they miss the target surface. Both can be expressed as efficiencies as presented in equations 4.4 and 4.5, respectively [11, 46, 47].

$$\eta_{\text{abs}} = e^{-\alpha d} \tag{4.4}$$

$$\eta_{\text{diff}} = 1 - \exp\left[-2\left(\frac{w_{\text{d}}}{w_0}\right)^2\right] \tag{4.5}$$

$$\text{with } w_0 = w_{\text{d}} \cdot \sqrt{1 + \left(\frac{d}{d_0}\right)^2} \tag{4.6}$$

$$d_0 = \frac{\pi w_{\text{d}}^2}{\lambda} \tag{4.7}$$

In equation 4.4, α represents the absorption coefficient, and d denotes the distance the laser covers. In equation 4.5, w_{d} stands for the laser beam radius at the aperture where the laser leaves the laser station and w_0 for the laser beam radius at the ablative surface of a CubeSat. d and d_0 in equation 4.6 respectively represent the distance between a laser station and a CubeSat, and the Rayleigh range, which is the distance the laser beam remains approximately parallel before spreading due to diffraction [47]. Finally, λ symbolizes the laser wavelength.

The absorption coefficient α is dependent on the atmospheric density and therefore also on altitude. Since the absorption only plays a role in this model, and is not of central interest in this thesis, the inclusion of a Line-By-Line Radiative Transfer Model (LBLRTM), using HITRAN, would have been out of scope. Therefore, an overestimating constant value of $1.25 \cdot 10^{-5}$ m^{-1}, which is more appropriate for approximating the absorption from ground to orbit where more absorption occurs, is assumed [46].

The consequence of this choice is that the simulation calculates a lower laser efficiency than would be the case. Therefore, thrust events are estimated to last longer, which reduces the maximum number of CubeSats that can be maintained per laser station.

4.2.2. Laser variants

From the coupling coefficients given in table 2.1 and the discussions in section 4.2.1, it is apparent that high-power lasers must be used to propel the CubeSats. CO_2 and solid-state lasers are the most typical types in that category. The former type of laser emits beams at wavelengths of 10.6 µm and provides power levels up to 100 kW. However, a Neodymium-doped Yttrium Aluminum Garnet (Nd:YAG) laser, offering the highest power levels of the latter category, only provides 10 to 20 kW at a wavelength of 1.06 µm [48].

4.2.3. Aiming & Emission distance

As elaborated in section 2.3, the most precise aiming has a deviation of 2 µrad. This value is used as a fixed value in the model to ensure that requirement SOT-1 is fulfilled. The aiming accuracy is the limiting factor regarding the distance over which the laser can be sent.

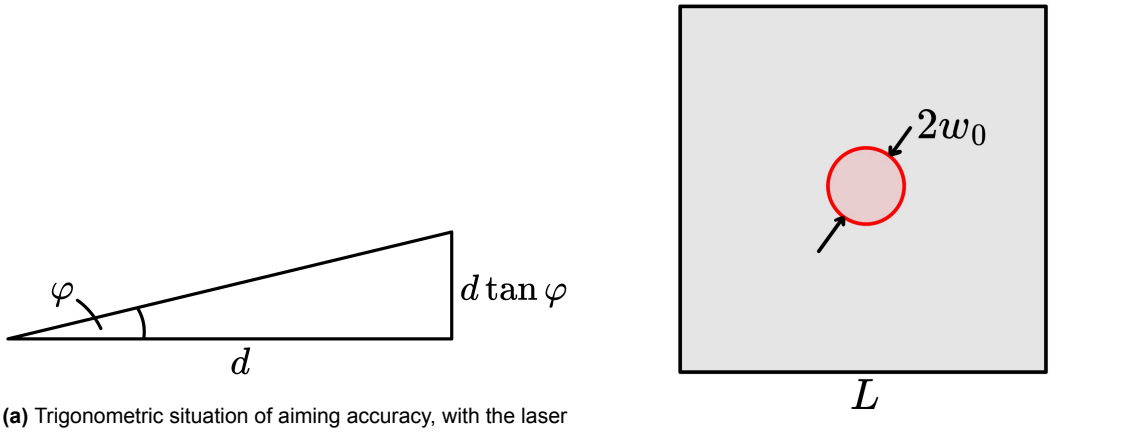

(a) Trigonometric situation of aiming accuracy, with the laser station located on the left and the CubeSat ablative plate on the right of the triangle.

(b) Frontal perspective of a laser beam (red) with diameter $2w_0$ on the ablative plate

Figure 4.1: Geometries present for aiming the laser at an ablative plate of a CubeSat

The laser beam is not allowed to be larger when it arrives at the ablative plate than the plate itself, as otherwise, energy would be wasted into space, or damage to the satellite parts would occur due to their ablation. Therefore, it can be deducted from figure 4.1a, illustrating the trigonometry at hand with a deviation of φ, and figure 4.1b, depicting a schematic of a laser beam in red reaching the

square ablation surface, that $2w_0 = 2d \cdot \tan\varphi$ cannot be larger than the side length L of the ablation surface. For the laser to entirely hit the ablation surface, the deviation must remain smaller than $\frac{L}{2} - w_0$. With the help of figure 4.1b, depicting the laser with radius w_0, the maximum distance over which a laser beam may travel is described as presented with equation 4.8. Since the laser beam can arrive at the ablative plate at an angle, and not only perpendicularly, as is assumed in figure 4.1b, the projected plate side length can shrink. This is accounted for by adding the $\cos\theta$ term to the equation.

$$d_{\text{max}} = \frac{L\cos\theta - 2w_0}{2\tan\varphi} \geq d \tag{4.8}$$

4.2.4. Laser activation conditions

It is only reasonable to activate the laser when the constellation of a laser station and a CubeSat allows the latter to be accelerated. In other words, the laser station must be able to aim at the rear end of the CubeSat. Since the laser stations orbit Earth at higher altitudes and, therefore, at a lower velocity, this constellation is achieved after a CubeSat has passed a laser station. The constellation is depicted in figure 4.2 with the laser station being the upper larger box, and the CubeSat represented by the small box at the bottom, the two spacecraft being in parallel flight. The blue vectors depict the respective velocities, and $\vec{r}_{\text{rel}}$ is the relative position of the CubeSat with respect to the laser station. With the laser station and CubeSats moving in the equatorial plane, as defined by requirement OPS-3, only at different altitudes, figure 4.2 is representative, with the exception that the rotation of the spacecraft is not considered. Nevertheless, it is sufficient to derive a formulation for the laser activation conditions.

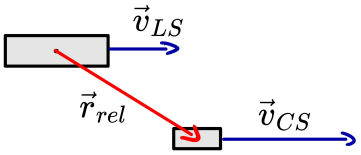

Figure 4.2: Schematic constellation for orbit maintenance

Since the laser can pan and assuming that the laser can hit the ablative plate at a limited angle, the CubeSat and the laser station having a cone-shaped Field of View (FoV); for the former, it is positioned on the ablative surface, looking away from the direction of motion, and for the latter, it is placed at the laser emitter oriented into the direction of movement. If the two ”see” each other, the laser is activated. The FoVs are formulated in equations 4.9 and 4.10, with θ being the respective

semi-vertex angles; the subscripts CS and LS stand for CubeSat and laser station, respectively.

$$\frac{\vec{r}_{\text{rel}} \cdot \vec{v}_{\text{LS}}}{\|\vec{r}_{\text{rel}}\| \cdot \|\vec{v}_{\text{LS}}\|} \leq \cos\theta_{\text{LS}} \tag{4.9}$$

$$\frac{\vec{r}_{\text{rel}} \cdot \vec{v}_{\text{CS}}}{\|\vec{r}_{\text{rel}}\| \cdot \|\vec{v}_{\text{CS}}\|} \leq \cos\theta_{\text{CS}} \tag{4.10}$$

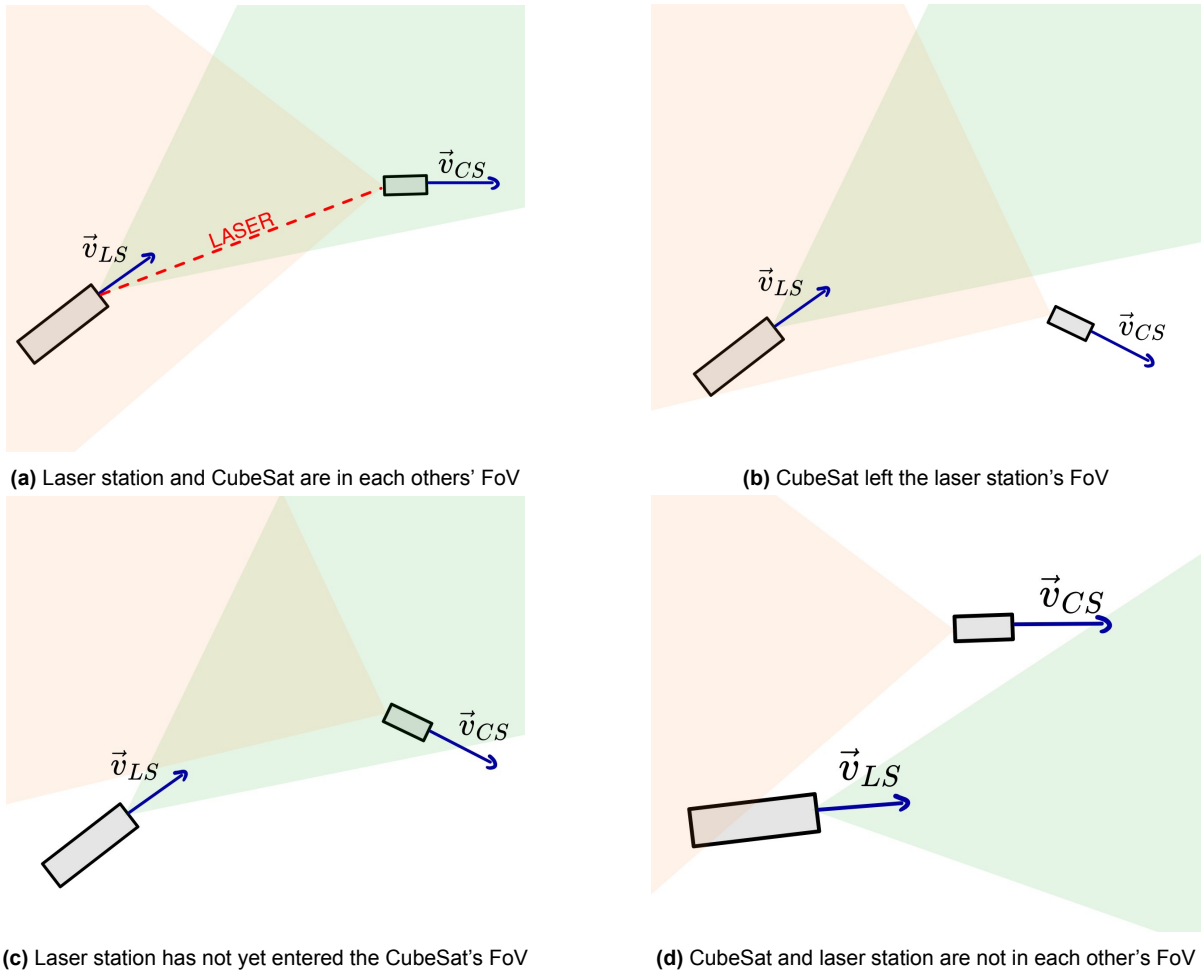

(a) Laser station and CubeSat are in each others' FoV

(b) CubeSat left the laser station's FoV

(c) Laser station has not yet entered the CubeSat's FoV

(d) CubeSat and laser station are not in each other's FoV

Figure 4.3: FoV for a CubeSat and laser station in proximity. (a) shows a constellation where all laser activation criteria are met. In (b), (c), and (d) at least one criterium is not fulfilled.

Figure 4.3 illustrates the FoVs; the laser station is shown on the left, and the CubeSat on the right of both figures. The respective FoVs are colored green and orange; the θs from the equations above determine both fields' opening angle. The required situation to propel a laser is shown in figure 4.3a,

where the spacecraft are in each other's FoV. Situations where the laser cannot be activated are pictured in figures 4.3b to 4.3d, with the laser station not being able to "see" the CubeSat, while the opposite is indeed the case. Further constellations where no laser beam can be emitted are, on the one hand, that the laser station can see the CubeSat but is not seen by it, as shown in figure 4.3c, and on the other hand, that both cannot see each other which can occur in a constellation as illustrated in figure 4.3d. This setup is flexible and allows for laser activation in situations where a laser station and CubeSat are at different altitudes.

So far, the maximum distance over which a laser can be emitted is defined by the aiming accuracy. This, however, does not consider, first, whether Earth obstructs the direct path, and second, how close the laser beam comes to Earth if the laser can be aimed at its target. The latter is paramount, as the laser beam should not be directed through significantly denser parts of the atmosphere than it already is, to prevent losses due to absorption. Those two points are addressed with one addition to the laser model, which has been made with the help of figure 4.4.

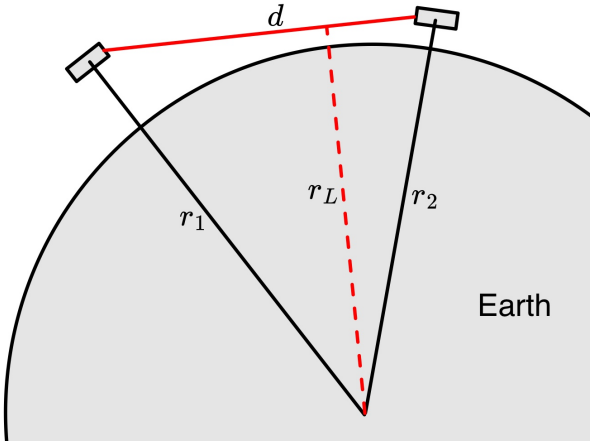

Figure 4.4: Sideways view on a laser station propelling a CubeSat

Figure 4.4 illustrates a laser beam in red going from one spacecraft to the other, represented by the two boxes, over a distance d. The radii of the spacecraft are labeled r_1 and r_2, and the smallest distance to Earth is given in r_L. The spacecraft radii are given by their momentary position during the simulation; therefore, the maximum distance over which the laser can be beamed directly depends on the choice of r_L. The maximum distance is described as follows.

$$d_{max} = \sqrt{r_1^2 - r_\mathrm{L}^2} + \sqrt{r_2^2 - r_\mathrm{L}^2} \tag{4.11}$$

4.2.5. Doppler Effect

Since the laser stations and CubeSats revolve around Earth on nearly circular orbits at different altitudes, they have different velocities. For completeness, it has been analyzed whether the Doppler effect should be considered in the simulation, as light changes its energy density with varying wavelengths. The consequence is that the incident laser power would change as well, ultimately changing the thrust of a CubeSat in a maneuver. For electromagnetic waves such as light, the change in frequency, applied to the thesis, is defined as shown in equation 4.12, with δv being the velocity difference between a laser station and CubeSat.

$$\frac{f_{\text{CubeSat}}}{f_{\text{Laser station}}} = \sqrt{\frac{c+\delta v}{c-\delta v}} \qquad \delta v < 0 \text{ for increasing distances} \tag{4.12}$$

$$E_{\text{photon}} = h_p \cdot f = \frac{h_{\text{p}} \cdot c}{\lambda} \tag{4.13}$$

For simplicity, the worst-case scenario with the highest possible velocity difference has been considered for the analysis. δv is at maximum when a laser station and CubeSat move precisely in the opposite direction, thus being the sum of the respective velocities. Table 4.2 shows the relative change of the laser frequency incident on the ablative surface on a CubeSat compared to the one sent from the laser station in the combination of multiple altitudes. As expected, the Doppler effect is more substantial the lower the altitudes of both laser station and CubeSat due to their higher velocities. Regardless, it is apparent that with a relative change in the order of 10^{-5}, the Doppler effect is only of minimal significance for this application. For example, if both the laser station and CubeSat orbit Earth at 200 km altitude, a laser emitted with a 1064 nm wavelength would hit the ablative surface with a wavelength of 1064.055 nm. Using those numbers in equation 4.13, it shows that one photon's energy in the laser beam, and by extension, therefore the entire laser beam energy, reduces with the same relative deviation. While this change in wavelength impacts the energy reaching the CubeSat due to the change in wavelength and diffusion efficiency, it is minimal. Hence, the Doppler effect has been neglected in the simulation.

Table 4.2: Relative incident laser frequency and energy change on the ablative surface due to the Doppler effect

$f_{CS}/f_{LS} - 1$		Altitude Laser Station					
		200 km	300 km	400 km	500 km	600 km	700 km
Altitude CubeSat	200 km	$-5.20 \cdot 10^{-5}$	$-5.18 \cdot 10^{-5}$	$-5.16 \cdot 10^{-5}$	$-5.14 \cdot 10^{-5}$	$-5.12 \cdot 10^{-5}$	$-5.10 \cdot 10^{-5}$
	300 km	-	$-5.16 \cdot 10^{-5}$	$-5.14 \cdot 10^{-5}$	$-5.12 \cdot 10^{-5}$	$-5.10 \cdot 10^{-5}$	$-5.08 \cdot 10^{-5}$
	400 km	-	-	$-5.12 \cdot 10^{-5}$	$-5.10 \cdot 10^{-5}$	$-5.08 \cdot 10^{-5}$	$-5.06 \cdot 10^{-5}$
	500 km	-	-	-	$-5.08 \cdot 10^{-5}$	$-5.06 \cdot 10^{-5}$	$-5.04 \cdot 10^{-5}$
	600 km	-	-	-	-	$-5.04 \cdot 10^{-5}$	$-5.03 \cdot 10^{-5}$
	700 km	-	-	-	-	-	$-5.01 \cdot 10^{-5}$

4.3. Laser Station Energy Model

Energy availability is the limiting factor for the number of CubeSats a laser station can propel and, therefore, is essential to the entire simulation. The model consists of three parts: energy generation, capacity, and the energy used to power the laser. The following sections discuss those three parts.

4.3.1. Energy generation

Energy generation has been determined to be realized using solar arrays. TEGs are to be excluded due to the requirement SOT-1 which mandates a TRL of 8 or higher. As elaborated in section 2.4.1, they never surpassed the prototyping phase and, accordingly, are below TRL 8. The usage of RTGs would increase the development and assembly cost of the laser stations while also providing relatively low power levels, which will very likely not be enough for the chosen laser's power level, as elaborated in section 4.2.2. Furthermore, high costs are to be expected at the end-of-life of RTG-powered stations to be de-nuclearized before burning up in the atmosphere. Operating solely on batteries without a power source is impractical, considering the significant energy consumption of the laser, which must be sustained for multiple years. Thus, the only remaining option is the use of solar arrays.

Solar arrays gather the power equivalent of the solar constant $S_\odot$ = 1361 W/m^2. Therefore, the power intake is customizable by varying the area of solar arrays A_{Array} on the laser stations. The total power generation P_{gen} is calculated as presented in equation 4.14, with η_{Array} being the solar arrays' efficiency. The calculation of χ is performed with Tudat's shadow function.

$$P_{\text{gen}} = \chi \cdot \eta_{\text{Array}} A_{\text{Array}} S_\odot \qquad \chi = \begin{cases} 1 & \text{, if laser station exposed to the Sun} \\ 0 & \text{, if laser station is in eclipse} \end{cases} \tag{4.14}$$

4.3.2. Energy storage

Since high levels of power are used to power the laser, it is not reasonable to rely on primary batteries that cannot be recharged, as an immense number of batteries would be required to uphold the LAP system for multiple years, as stated in the requirements. Nuclear options are also not considered for the reasons given in section 4.3.1. Therefore, a secondary battery or supercapacitors are the only suitable options.

A laser station requires energy storage that can store enough energy for at least one thrust event and provide the necessary operational power. Connecting multiple cells enables the required energy capacity and power levels to be achieved. On the one hand, the battery must be capable of providing enough power to the laser. On the other hand, it must also have the capacity to store enough energy during eclipse. Unless the energy and power requirements align with the battery's specific energy and power, only one of the two is responsible for the battery mass, and by extension, battery size, while the other remains in excess. This is formulated in equation 4.15. P_{Laser} and E_{Capacity} stand for the power used for emitting the laser and the energy capacity, respectively, and ϱ stands for the specific power and energy of the energy storage.

$$M_{\text{bat. min}} = \max\left(\frac{P_{\text{Laser}}}{\varrho_{\text{P}}}, \frac{E_{\text{Capacity}}}{\varrho_{\text{E}}}\right) \tag{4.15}$$

Therefore, regarding launch costs, the preferable option would be a cell with high specific power as well as high specific energy, which, however, as established in section 2.4.2, does not exist. Furthermore, the number of cycles in which the energy storage is charged and depleted must be sufficiently high to allow for the long-term operation of the laser stations, which will be determined during the simulations.

The energy storage options discussed in section 2.4.2 were considered regarding the established properties and listed, in table 4.3. Excluded from the table were batteries, such as the silver-zinc battery, that are no longer used. Furthermore, experimental solutions, such as the metal-oxide/carbon nanotube supercapacitor, were not considered to meet the SOT-1 requirement.

Based on the cycle life values in table 4.3, supercapacitors and nickel-cadmium batteries are the most reasonable choices, as they allow for a high number of recharges, thus allowing for a long lifetime. Ni-H_2 batteries provide no advantage compared to their nickel-cadmium counterparts and were therefore not further considered. Li-S batteries cannot compete with the others on table 4.3 and are impractical for long-term missions. While the numbers indicate that supercapacitors have a significantly higher cycle life, a laser station equipped with them would entail roughly nine times

Table 4.3: Energy storage options overview

Type	ϱ_E [MJ/kg]	ϱ_P [kW/kg]	Cycles	
Nickel-cadmium	0.18	0.45 [49]	80 000	
Ni-H_2	0.18	0.28 [50]	60 000	
Li-S	1.44	0.8	<1000	
Supercapacitors	0.02	7.9	>100 000	[51]

the mass of one with nickel-cadmium batteries. Furthermore, superconductors cost approximately $5500/kg, resulting in a total cost of $275 million, while the batteries, with a cost of $1000/kW, only amount to $100000 to equip an entire station [51]. Therefore, the most reasonable choice is nickel-cadmium batteries.

4.3.3. Energy usage

With the chosen laser that operates with 100 kW, the vast majority of the energy stored on the laser station is used for LAP. Other energy is consumed for systems such as attitude control, communication, and thermal control. The actual energy usage for these functions cannot be entirely determined due to the laser station's design variables and is outside the scope of this thesis. Mainly, attitude control falls in that category since, with variable energy capacity, the volume and mass of the on-board batteries are unknown. The energy consumed to adjust the laser station's rotation increases with a higher mass, due to its increased inertia. While the mass and the dimensions of the laser station are to be defined in section 5.4.2, a rough estimate is made here, based on the Hubble Space Telescope, as it is a larger spacecraft in LEO. On average, it consumes 2.1 kW of power [52]. Since the distribution of that energy is not publicly available for the Hubble telescope, an in-depth estimate for the laser station is not possible. Therefore, the power level of 2.1 kW is also assumed, in the full knowledge that it is most likely too high an estimate. The overestimation, thus, is considered to be a buffer.

4.3.4. Energy system sizing

The next step, after defining the method for generating, storing, and using energy on the laser station, was to determine how much capacity the battery must hold to provide power to the laser while the station is in eclipse and how large the solar arrays have to be so that the battery does not fully deplete. To do so, the scenario of highest energy consumption during an eclipse has been chosen, as in less consuming cases, the battery and solar arrays can provide power and energy with reserves at the end of the eclipse.

First, the battery capacity was defined based on the amount of energy consumed during an eclipse and the number of thrust events that can occur within a specific time interval. Equation 4.16 describes the calculation of the battery capacity required for one eclipse. η_{bat} represents the battery efficiency. $t_{\text{thrust event}}$ is the maximum thrust event time and thus also defines the time over which the laser is activated. Finally, t_{sunlit} and $t_{eclipse}$ represent the time the laser station is exposed to the Sun and the time in eclipse, respectively; P_{systems} is the power the systems besides the laser consume, and N stands for the number of thrust events.

$$E_{\text{bat}} = \frac{1}{\eta_{\text{bat}}} \cdot P_{\text{Laser}} \cdot t_{\text{thrust event}} \cdot N_{\text{in eclipse/orbit}} + \frac{P_{\text{systems}} \cdot t_{eclipse}}{\eta_{\text{bat}}} \tag{4.16}$$

$$E_{\text{bat, degr}} = \frac{E_{\text{bat}}}{K_{\text{t}}} \quad \text{with} \quad K_{\text{t}} = 1 - t \cdot r_{\text{cycle}} \tag{4.17}$$

$$E_{\text{sunlit}} = \cdot P_{\text{Laser}} \cdot t_{\text{thrust event}} \cdot N_{\text{in Sun/orbit}} + P_{\text{systems}} \cdot t_{sunlit} \tag{4.18}$$

E_{bat} does not account for the battery's degradation over time. To ensure the required battery capacity E_{bat} at the end of life of the battery and/or laser station, capacity must be added, which is described in equation 4.17, where K_{t} is the relative capacity after a time t. It is defined by the cyclic degradation r_{cycle} induced by draining the battery. Experiments have shown that for nickel-cadmium batteries, after 1200 cycles the battery degrades to a capacity of 97%, which equates to 0.0025% degradation per cycle [53]. Finally, equation 4.18 describes E_{sunlit} as the energy that is used while the laser station is exposed to the Sun.

With the defined amount of energy that the battery has to be charged with, and the maximum laser power given from section 4.2.2, the area of solar arrays required to power the laser station can be described with equation 4.19. The energy needed to charge the battery and provide sufficient power to the laser is added and then divided by the energy that the solar arrays can produce while they are illuminated.

$$A_{\text{SolarArray}} = \frac{S_{\odot} \eta_{\text{Array}} t_{\text{sunlit}}}{N_{\text{per orbit}} \cdot t_{\text{thrust event}}} \tag{4.19}$$

4.4. Propulsion Model

The propulsion model is partly built on Tudat and partly developed from scratch. The former option allows for the simulation of thrust acting on a spacecraft. However, LAP is not included and consequently had to be created separately. In detail, Tudat requires values for thrust F_{T}, its direc-

tion, and the specific impulse I_{sp}. Those were obtained from the model presented in this section, which includes the ΔV estimation in section 4.4.1, the transformation of the laser's energy to thrust (section 4.4.2), and the laser model (section 4.2).

4.4.1. ΔV estimation

To determine the thrust magnitude a CubeSat must experience to return to its intended orbit, the necessary ΔVs are calculated to enter the transfer and circular orbit again. This is done using the vis-viva equation (see equation 4.20). The derived expressions for the ΔVs for entering the transfer orbit and re-entering a circular orbit are given in equations 4.21 and 4.22, respectively. ε stands for the specific orbital energy, μ is Earth's gravitational parameter, r represents the distance between Earth and the satellite, and $a_{\text{tr}} = \frac{1}{2}(r_1 + r_2)$ stands for the semi-major axis of the satellite transfer orbit. The indices 1 and 2 denote the current and the targeted orbit [54].

$$\varepsilon = \frac{v^2}{2} - \frac{\mu}{r} \tag{4.20}$$

$$\Delta V_1 = \sqrt{\frac{\mu}{r_1}} \left(\sqrt{\frac{r_2}{a_{\text{tr}}}} - 1 \right) \tag{4.21}$$

$$\Delta V_2 = \sqrt{\frac{\mu}{r_2}} \left(1 - \sqrt{\frac{r_1}{a_{\text{tr}}}} \right) \tag{4.22}$$

The simulation's maneuvers ensue in a transfer orbit mode and a correction-to-circular-orbit mode. The maneuver of the first mode is triggered as soon as a CubeSat's altitude crosses a lower altitude threshold and a laser station is available. As soon as the ΔV_1 from equation 4.21 has been fully used, the CubeSat transitions into the second maneuver mode, where ΔV_2 from equation 4.22 is used. In this mode, the laser is activated when the CubeSat is close to apogee and a laser station is available. As soon as this maneuver is completed, the maneuver mode falls back to the transfer orbit mode, to be activated at a later stage when the CubeSat has lost enough altitude.

Since equations 4.21 and 4.22 describe the optimal case for a transfer orbit, ignoring perturbations such as atmospheric drag, they do not lead to the actual ΔVs that are needed, and measures for over- and underestimation have been added to the simulation. An overshoot beyond the goal altitude would be expected for the former situation. Therefore, the remaining ΔV for the maneuver is set to 0, and the maneuver mode is changed. In the case of an underestimation, the CubeSat undergoes

an altitude increase but does not reach the goal altitude, and the standard process, as described in the previous paragraph, takes place; however, the next thrust event must take place sooner. The ΔVs are converted to the required propellant mass using the rocket equation.

4.4.2. Thrust generation

The coupling coefficient C_m is paramount for the thrust generation; as the ratio of thrust generated per unit of laser power links the incident laser power to the thrust a CubeSat experiences. The thrust is described in equation 4.23, η_AB representing the ablation efficiency, and P_in being the incident laser power. Regarding absorption efficiency, the literature supports the assumption of a constant value of 40% for the ablative surface [21, 55].

$$F_\mathsf{T} = \eta_\mathsf{AB} \cdot C_\mathsf{m} P_\mathsf{in} \tag{4.23}$$

$$m = \frac{C_\mathsf{m} P_\mathsf{in}}{2 \cdot \eta_\mathsf{AB}} \tag{4.24}$$

$$I_\mathsf{sp} = \frac{2\eta_\mathsf{AB}}{\psi \cdot C_\mathsf{m}} \tag{4.25}$$

The mass flow of the ablatant is described in equation 4.24 and is used in the simulation to calculate whether sufficient ΔV has been delivered. At each time step, m is calculated based on the current efficiencies of the laser, resulting in a change in the ablated material mass. The stepwise removal of blatant mass is added over time. Propulsion continues until the summed-up mass is smaller than the initially set propulsion mass that must be ablated.

During simulations, it was discovered that with the set laser power of 100 kW, thrust events lasted for less than 10 µs. Since this time was smaller than the minimum step size given to the integrator, excessive thrust was simulated, resulting in inaccurate results. Consequently, a check was implemented to ensure that, whenever the thrust event was shorter than the minimum time step size, the laser power would be reduced, thereby prolonging the thrust event to 1 ms so that it could be computed accurately.

Finally, the effect of an angled incidence angle has been debated. Since a laser beam is a stream of photons, said effects are purely caused by photon propulsion, which are negligible compared to LAP, as can be deduced from the findings in section 2.1. Furthermore, the thrust created by LAP is generated from the energized particles on the ablative surface from which they spread away. The

laser does not direct the plasma and particles in any direction, so that the thrust is directed perpendicularly away from the ablative surface on average. Therefore, any effects are not considered in the simulation.

4.5. Financial Model

Development, assembly, launch, and operation costs have been considered to model the total cost of in-orbit LAP. Furthermore, to assess profitability and competitiveness, as demanded by requirements FIN-1 and FIN-2, the cost is contrasted with the expenses that arise for a conventionally operated satellite mission. The proposal's competitiveness is ensured by undercutting the competitors. Profitability is achieved by pricing services above the actual cost of operating in-orbit laser stations. If the proposed operation is less expensive than current space missions, a price range for laser propulsion as a service can be determined.

The model categorizes costs into one-time and recurring expenses. The former entails the development of the spacecraft, while the latter encompasses assembly, launch, and operating costs. Assembly and launch occur each time a spacecraft must be replaced; the simulation treats operating costs as daily costs. The following sections list the prices used in the simulation, section 4.5.1 for the LAP setting, section 4.5.2 for non-propelled and propelled conventional missions, assuming they all aim for a long-term mission in LEO. Regarding the end-of-life of both spacecraft, it is assumed that they fully burn up in the atmosphere, so debris removal is ignored, thus adding no cost.

4.5.1. Cost estimations for LAP constellations

This section discusses the price estimations for the proposed orbit maintenance system using LAP. The prices found in table 4.4 are based on prices found on the market for CubeSat parts and components. While the cost for a satellite's payload is highly dependent on what it consists of, a range of $50000 to $200000 has been found, which includes attitude control, communications, and optics [56]. The cost of the ablative plate depends on the material it is made of and the amount of ablative material mounted onto the satellite. For the CubeSat platform, a product versatile in its usage, sold by EnduroSat, has been chosen, as it features a 2-by-3 format and weighs approximately 12 kg with its payload [57]. For launching the satellites into orbit, SpaceX's rideshare program has been selected. It lets smaller spacecraft ”hitchhike” in smaller spaces on a rocket, which has been chosen, as with a price of $300000 for masses up to 50 kg, this is a comparatively low price to reach orbit [58].

Mission design, spacecraft design, the communication system, and operational risk shape the operational cost of a space mission [54]. Historical data indicates that these costs fall within a range of approximately 8 to 23% of the total mission cost [59].

Table 4.4: Cost estimates for a LAP CubeSat

Main category	Sub-part / Provider	Cost [k$]	Reference
Subsystems	CubeSat payload	125	[56]
Assembly cost	Platform	140 – 260	[57]
	Ablative plate	to be derived	
Launch cost	SpaceX rideshare	300	[58]
Operating cost		8 – 23%	[59]

The general cost breakdown of laser stations is comparable to that of CubeSats . The operating and launch costs were taken from literature, the references shown in the tables, and listed prices. The power system cost, which includes the cost of the batteries, is derived from the calculation presented in section 4.3.2.

Lasers that might be used for LAP are currently still in development [60]; therefore, only development contracts are available for consultation. From a contract between Dynetics, Lockheed Martin, and the US Army, it can be taken that the cost of a high-power laser is $130 million [61]. This is also the case for the structure and the payload of a laser station. LEO satellites with a life-span of up to 5 years cost up to $20 million for assembly and operation [62]. The cost will be scaled based on the actual lifetime of the laser station. The cost of the laser and battery was added, since high-power lasers are not standard equipment for a satellite, and the battery must provide more power and energy than common satellites require. The development cost and power system cost are dependent on the size of the laser station and the battery, as well as the solar array size, respectively, and will, therefore, be defined in section 5.4.2. Their price, mass, and dimensions are scaled to the laser station's needs. For Nickel-Cadmium batteries, the cost range goes from $500 to $1450 per kWh [63]. For the solar arrays, the price range starts at $100/W and goes up to $500/W [64]. The overview of the expenses discussed is displayed in table 4.5.

Table 4.5: Cost estimates for a laser station

Main category	Sub-part / Provider	Cost [k$]	Reference
Development cost		to be derived	
Assembly cost	Structure & Payload & Operating cost	20000/ 5 years	[62]
	Laser	130000	[61]
	Power systems	to be derived	
	Propellant: Xenon	0.82 - 3.05 / kg	[65]
Launch cost	Falcon 9	69750	[66]

4.5.2. Competitveness to conventional CubeSat missions

To assess the competitiveness of orbit maintenance with LAP, the cost analysis is also made for existing means of orbit maintenance. One is that no orbit maintenance is made, and the other includes a thruster onboard the satellite. For comparability, it is assumed that the mission duration of the ”conventional” CubeSats is identical to that of an LAP operated mission. Since orbit maintenance prolongs a satellite's lifetime, it is assumed that the conventional CubeSats are replaced whenever necessary, to continue the mission.

Non-propelled CubeSats

Table 4.4 lists the estimated costs that occur for a non-propelled CubeSat. Its costs do not differ from a CubeSat being propelled using LAP, except for the ablative plate. Since an overview table for this kind of satellite does not provide any added value, it is omitted. The lifetime depends on the altitude at which it is deployed at the beginning of its mission. Simulations applying the environmental model described in section 4.1 were run at constant average solar activity to obtain those lifetimes for various altitudes, deploying a satellite at the respective altitude without propelling it until it crashed into Earth. The lifetimes are shown in table 4.6. Those results were used to define a trendline function so that the lifetime of a CubeSat at any altitude could be determined; the result being the function presented in equation 4.26 with R^2 = 0.9999 as the coefficient of determination, indicating a very accurate fit. L_d stands for the lifetime in days, and h represents the altitude at deployment in kilometers.

$$L_d = 3.969 \cdot 10^{-18} \cdot h^{7.956} \tag{4.26}$$

Table 4.6: Lifetime for CubeSat without propulsion

Deployment altitudes [km]	Lifetime [days]
200	8
300	209
400	1919
500	12020

Propelled CubeSats

The main advantage of propelled satellites over non-propelled satellites is their extended lifetime, reducing the frequency with which a replacement satellite must be launched. The satellite of NASA's Pathfinder Technology Demonstrator (PTD)-1 was chosen for the comparison. It was equipped with the HYDROS thruster, a cold gas thruster, the size of 1U, using water as the propellant, delivering 600 mN of thrust at an I_{sp} of 258 s [67]. Since the amount of water stored in the tank is not stated, it has been estimated based on technical drawings to be a third of the thruster's volume, resulting in a propellant mass of 33 g [68]. Applying the rocket equation results in an available ΔV of 6.97 m/s. The extension of the CubeSat's lifetime is calculated by dividing the available ΔV from the thruster by the ΔV lost over time due to air drag on the deployment altitude. The remainder of the CubeSat's lifetime, losing altitude, is taken equal to the non-propelled lifetimes.

The costs are taken equal to the non-propelled counterpart, but with the addition of the off-the-shelf thruster cost. The respective costs are listed in table 4.7. The cost of a thruster varies drastically between approximately $40000 and $120000 [69, 70], which, considering the other expenses, is a significant variation and therefore does not allow for simply averaging the price.

Table 4.7: Cost estimates for a propelling CubeSat

Main category	Sub-part / Provider	Cost [k$]	Reference
Subsystems	CubeSat payload	125	[56]
Assembly cost	Platform	140 – 260	[57]
	Thruster	40 – 120	[69, 70]
Launch cost	SpaceX rideshare	300	[58]
Operating cost		8 – 23%	[59]

4.6. Simulation Plotting

Some plots, such as those illustrating altitude profiles, were challenging to read and interpret, as in some cases, multiple lines that varied drastically over a short period obscured other lines in that plot. Therefore, curve smoothing, indicating the local average of the plot, was included in plots when necessary. The choice fell for the LOcally WEighted Scatterplot Smoothing (LOWESS) method.

LOWESS is a regression method that combines linear and non-linear methods. It works by fitting the curve locally with a low-order polynomial using the weighted least-squares method. The advantage of this method is that it does not require a specified function that is then fitted to the data; the only input necessary is the so-called smoothing parameter that indicates how smooth the fit shall be. On the other hand, however, LOWESS is computationally expensive and requires large data sets to reduce its proneness to outliers [71].

5
Sensitivity Study

Physical models, and therefore simulations, attempt to describe reality as precisely as possible. Doing so, however, can make them unnecessarily complex and computationally expensive. The sensitivity study aims to simplify a model while minimizing the deviation from reality. Thus, this section explains the impacts of changing parameters on the resulting simulation and justifies the disregard of parameters with little influence. Each model described in chapter 4 is analyzed in the subsequent sections.

5.1. Environmental Model

The environmental model's sensitivity study examines two sources of orbit perturbations: solar radiation pressure and the gravitational accelerations due to other celestial bodies in the Solar System.

5.1.1. Atmospheric drag

For a simulated CubeSat, the acceleration has been roughly estimated so that the effect of the atmosphere can be compared to other influences. The primary purpose is to assess which must be considered and which is negligible. Furthermore, it provides a minimal, but certainly not sufficient, verification of the results. The values shown in table 5.1 have been used for that estimation. For the drag coefficient C_D, measurements show that for a cuboid with a width-to-length ratio of the simulated CubeSats lies between 0.85 and 0.95 [72]; the average value of 0.9 is chosen. The atmospheric density is taken from Tudat's model at an altitude of 400 km. For v, the circular velocity at 400 km altitude is taken, the reasoning for the choice being presented in sections 5.4 and 5.5. Finally, for A, the frontal area of 10 cm by 20 cm is used. Applying equation 4.1 results in a drag force of 1.485 µN, thus in an acceleration of 0.124 µm/s^2. A similar estimation for a laser station has not been made, as its dimensions and mass were to be defined as part of this thesis.

Table 5.1: Values for estimation of atmospheric drag on a CubeSat

C_D	0.9	
ρ	2.803	ng/m^3
v	7673	m/s
A	0.02	m^2
$M_{CubeSat}$	12	kg

5.1.2. Solar radiation parameters

This section evaluates the significance of solar radiation pressure on both the CubeSats and laser stations. While the solar radiation pressure is nearly equal, their mass and exposure area differences make predictions difficult.

Impact on CubeSats

Similar to the atmospheric drag model, a rough estimate has been made for the SRP to allow for a comparison and ultimately assess the relative influence of the two. For the estimation, R_{Sun} was set to 1 AU for simplicity and because the deviation of that value of a spacecraft orbiting Earth is negligible. The predefined CubeSat mass of 12 kg was used. There is considerable variation in the reflectivity coefficient and the satellite area. On the one hand, it is dependent on the material of the satellite surface, making a precise estimation difficult. On the other hand, the CubeSat is rotating so that the area SRP acts on varies as well. Therefore, estimations have been made for the entire respective ranges, with the results shown in table 5.2.

Table 5.2: Acceleration due to SRP for different C_r and impact areas

in 10^{-8} m/s^2		Reflectivity coefficient C_r					
		1.0	1.2	1.4	1.6	1.8	2.0
Exposed Area [m^2]	0.02	0.76	0.91	1.06	1.21	1.36	1.51
	0.03	1.13	1.36	1.59	1.81	2.04	2.27
	0.04	1.51	1.81	2.11	2.42	2.72	3.02
	0.05	1.89	2.27	2.64	3.02	3.40	3.78
	0.06	2.27	2.72	3.17	3.62	4.08	4.53

Table 5.2 shows that SRP affects a CubeSat one order of magnitude less than atmospheric drag, for which an acceleration of 0.124 µm/s^2 has been estimated. Furthermore, it shows that the amount of exposed area and the reflectivity coefficient have a notable influence on the resulting acceleration. For these two reasons, the reasonability of implementing solar radiation pressure and, if implemented, the importance of the variation had to be evaluated, which is done in section 5.1.3.

Regardless of the comparison of SRP, its actual effect had also to be simulated, as the comparison in section 5.1.3 is not sufficient to set a limit for determining what influences must be included in the simulation. As the first step, the reflectivity coefficient's effect was analyzed using the average CubeSat surface area of 0.037 m^2. The choice fell for that value, as during an orbit, different sides of the CubeSat are exposed to the Sun at various angles, so that the area that the SRP acts upon changes. The average exposure area thus allows for a sensitivity study that does not require simulating the CubeSat's attitude. The impact of solar radiation pressure was investigated by comparing the orbit of a CubeSat at 400 km altitude over a year with the values of C_r of 0, 1, 1.5, and 2. While C_r = 1 and 2 represent the most extreme realistic outcomes with solar radiation pressure, C_r = 0 illustrates the case without it. In figure 5.1, no SRP was taken as the baseline, and the absolute altitude deviation from it due to solar radiation is shown. The shaded areas are the actual values, while the single lines are the respective averaged values using the LOWESS method.

The altitude differences are due to thrust events at different times, due to how they are triggered, as explained in section 4.4.1. Since the constellation of CubeSat and laser station was identical for every single case, there could not have been any third influence, such as different distances between spacecraft, resulting in different LAP performance or even infeasibility to have LAP. The thrust magnitudes are displayed in figure 5.2. It shows the thrust history for each case over that period, with the base case shown in black. The base case experiences only one thrust event over the entire course of a year. While all disturbed cases also experience a thrust around the same time as the base case, they already require additional thrust events at a much earlier stage. With more frequent thrust events necessary for a single CubeSat, the number of satellites maintained by the laser station is reduced. As a result, the solar radiation pressure must be considered for CubeSats. As elaborated in section 4.1.2, C_r was determined to be 1.403.

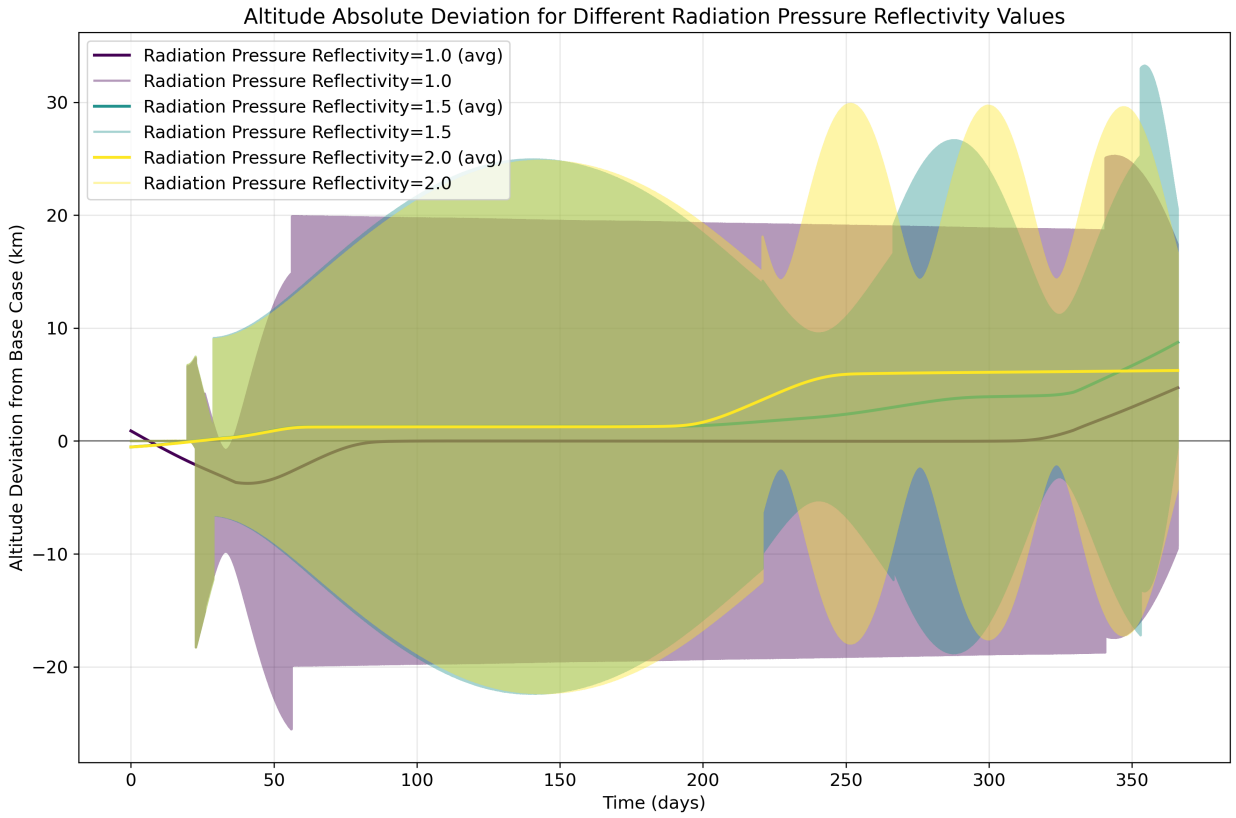

Figure 5.1: Altitude deviations for a CubeSat for different C_r with an area of 0.037 m^2 at 400 km altitude

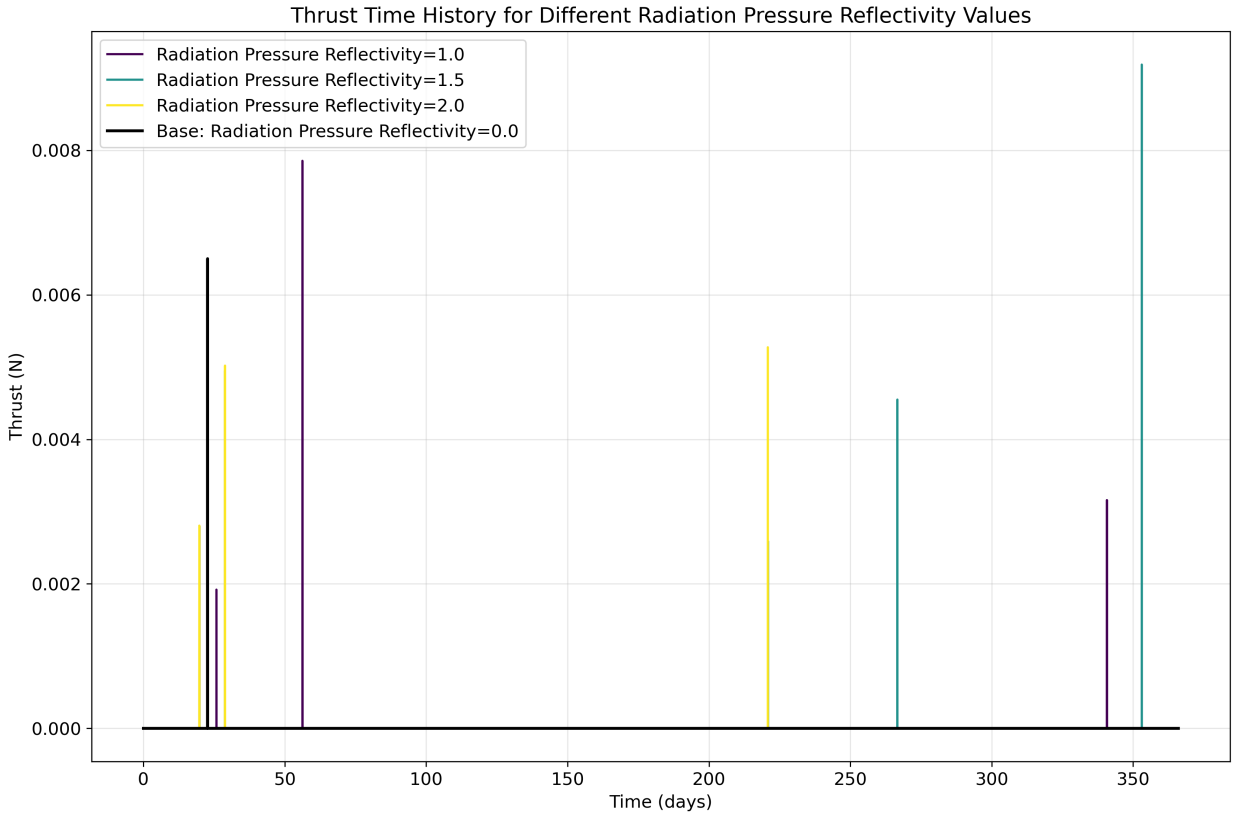

Figure 5.2: Thrust history for a CubeSat for different C_r

Impact on laser stations

For the laser stations, the same analysis was made as for the CubeSats. Again, the same reflectivity coefficients of 0, 1.0, 1.5, and 2.0 were plotted. Figure 5.3 shows the altitude profiles over a year, one for each of the reflectivities, the black line being the average of the case without any SRP. In the plot, the four transparent lines overlap with no clear distinction to be seen, as a change of color would otherwise be noticeable. Therefore, figure 5.4 was plotted to show the deviation due to SRP from the reference case of C_r =0. The transparent curves show that with increasing C_r, the deviation grows as well. For a value of 1.0, the deviation reaches approximately 55 m; for a value of 2.0, deviations of 100 m are achieved. The midpoint between the minimum and maximum deviations is shown for the reflectivity coefficient of 1.5.

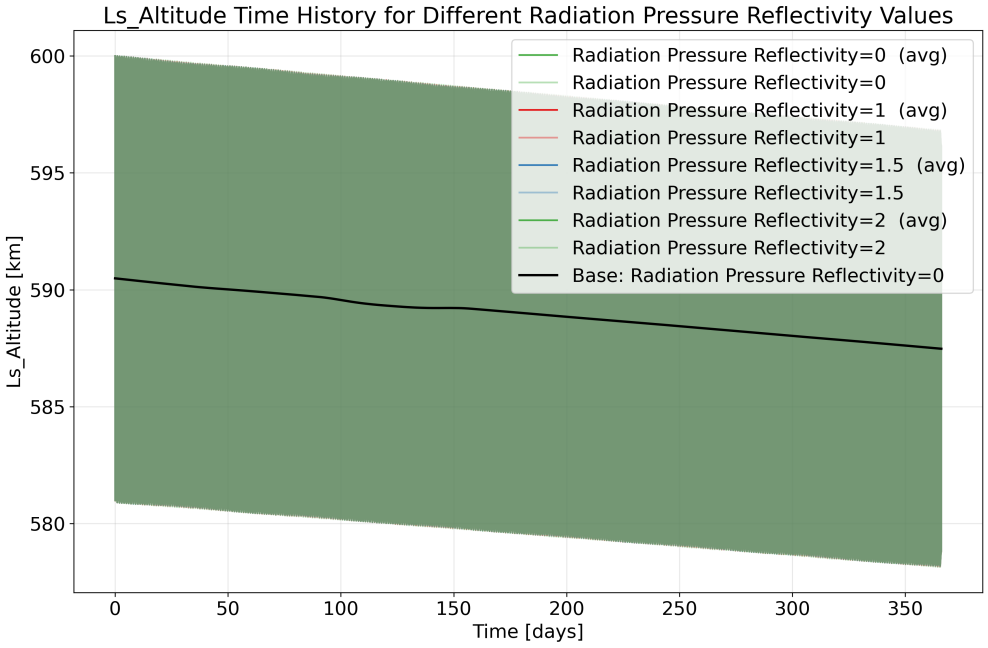

Figure 5.3: Altitude profiles of a laser station in 600 km altitude with different C_r

All average lines show that there is no trend of further deviating from the no-SRP case. Since the reflectivity has only a minimal effect on the altitude and also has no long-term influence in that regard, the choice of C_r does not require any further investigation in the case of the laser stations. As the analysis in section 5.4 concluded, the solar array area is larger than the spacecraft surface. Therefore, the spacecraft cannot be coated in them and needs solar arrays. Thus, based on the relative surface areas and the materials' reflectivity coefficients, an overall C_r of 1.127 was determined.

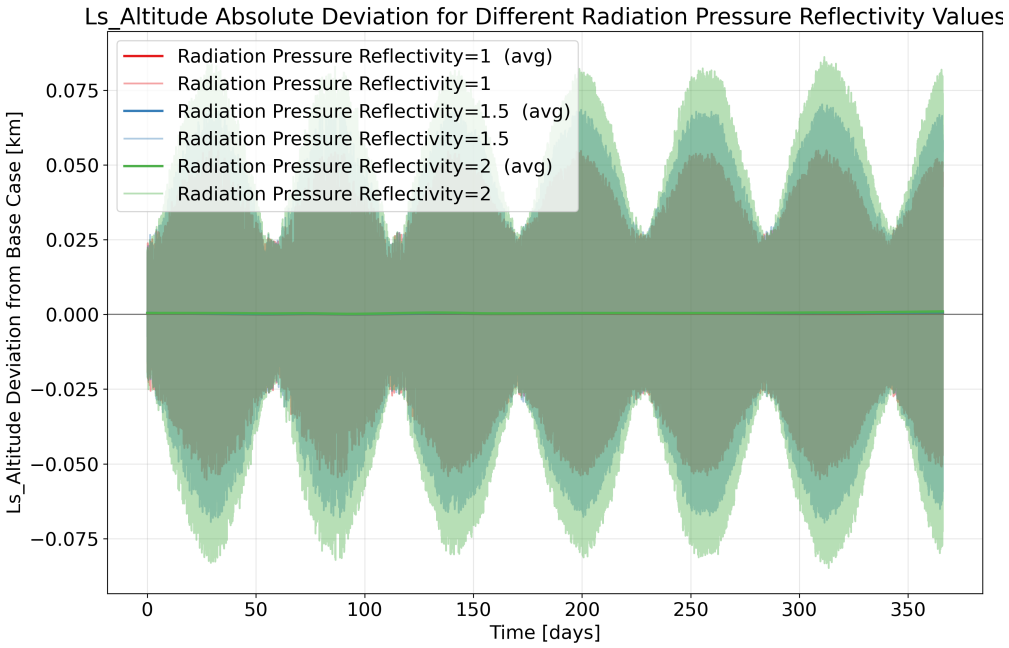

Figure 5.4: Altitude profile deviations of a laser station in 600 km altitude with different C_r

5.1.3. Third-body gravity

The orbits of the CubeSat and laser stations are determined by the perturbations they undergo during their mission. While Earth's gravity holds them in orbit, third-body influences accelerate and decelerate them, causing their orbits to change. Figure 5.5 shows the accelerations due to the celestial bodies' gravity, solar radiation pressure, and atmospheric drag that a CubeSat experiences over one year with an initial altitude of 400 km, a reflectivity coefficient C_r of 1.403, and a drag coefficient C_D of 1.2. It shows that the gravity of the Sun and the Moon are the most considerable perturbations in LEO, significantly surpassing the deceleration due to air drag. Therefore, their effects must be taken into account in the simulation.

Figure 5.5 indicates that the gravitational influences of the planets besides Earth are three to eight orders of magnitude smaller than air drag. Whether they can be deemed negligible in the simulation has been evaluated by plotting the deviation of only the Sun, the Moon, Venus, and Jupiter being simulated from the case where the Sun, the Moon, and all planets are simulated, which is illustrated in figure 5.6. The red, non-transparent line represents the average altitude deviation of the transparent

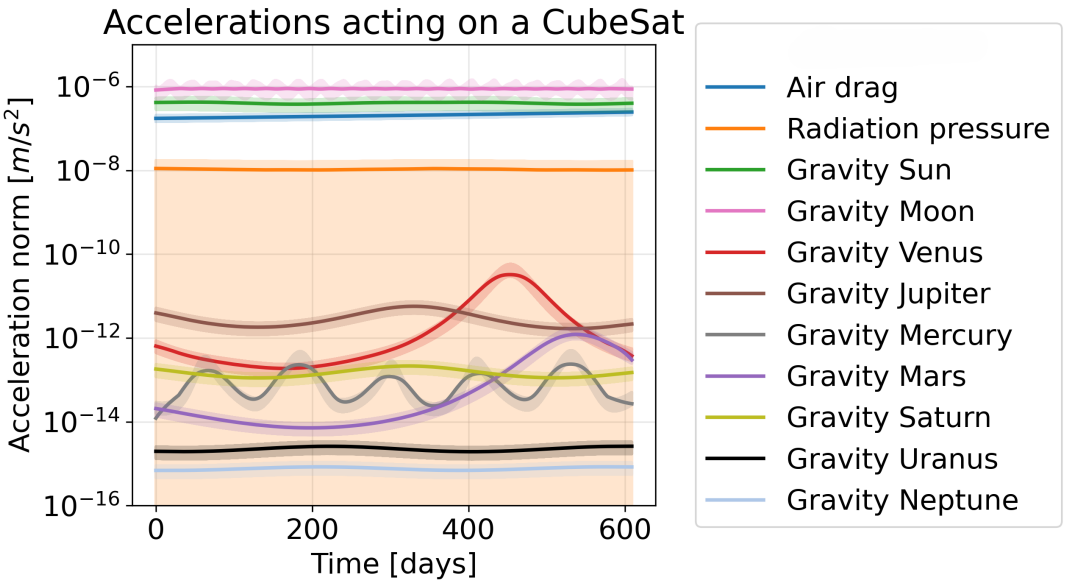

Figure 5.5: Relevant accelerations on a CubeSat at 400 km altitude, 10 x 20 cm frontal area, and C_r = 1.403

curve, which corresponds to the actual data. It shows that the maximum deviation lies in the order of 25 m, with an average deviation that is practically 0 m. Therefore, neglecting the gravitational influence of Mercury, Mars, Saturn, Uranus, and Neptune is reasonable.

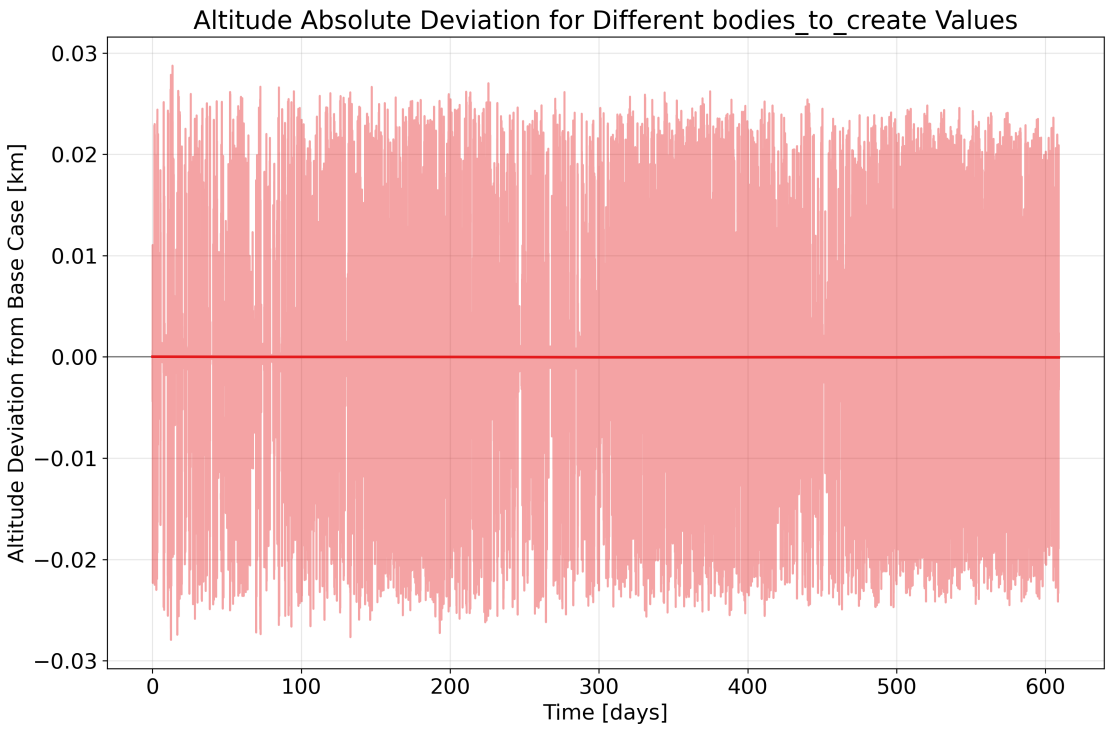

Figure 5.6: Third-body gravity effect of Mercury, Mars, Saturn, Uranus, and Neptune on CubeSat altitude combined

5.2. Laser Model

This section investigates what factors limit the laser range. This is done from different perspectives. First, section 5.2.1 considers the effect of the aiming accuracy together with the choice of the laser beam size. Then, section 5.2.2 takes the effect of the two FoV orientations into account. Finally, section 5.2.3 discusses how relevant Earth is in limiting the maximum laser range as it could obstruct the path from the laser station to the CubeSat.

5.2.1. Maximum emission distance

Since the calculations of the maximum distance over which a laser can be shot include a division by $\tan \varphi$ (see equation 4.8), a slight variation of the accuracy of a laser aiming system can have an enormous impact. Therefore, it is paramount that the most accurate aiming mechanisms available are implemented for LAP. The beam waist radius is the remaining variable that defines the distance over which the laser can be emitted. Figure 5.7 illustrates the required aiming accuracies for guaranteed targeting of the ablative surface for various beam waist radii w_0 between 0 and 4 cm. Furthermore,

it depicts the technological limit of 2 µrad established in chapter 2 with the red dashed line. Thus, the zone of possible designs lies above this line. The line for w_0 = 5 cm would not be visible, as it would require perfect aiming to achieve this case, which is equivalent to an aiming accuracy of 0 rad. The usage of a beam with this waist size would have the consequence that only a part of the beam would hit a CubeSat's ablative plate while the other part either misses the satellite completely so that energy is lost to space, or it hits the satellite somewhere next to the ablative plate which would lead to damages due to ablation. Furthermore, depending on the material, unintended LAP could occur in another direction, thus maneuvering the CubeSat out of its intended orbital plane or nearly circular orbit. The blue line for w_0 = 0 cm represents the limit with the smallest possible laser beam and, consequently, the maximum distance over which a laser beam can be emitted while still reaching the ablative surface. The maximum is reached at a 25 km distance between a laser station and a CubeSat. Considering equation 4.6, however, shows that a beam waist of 0 cm is impossible to reach. According to the equation, this is only achievable if both the distance from the laser to the ablative plate and the beam radius at the mirror are 0 m. A distance of 0 m defies the purpose of LAP and a beam with such a radius translates to that there is no beam. Therefore, this is an asymptotic upper limit of the situation at hand, and therefore, longer distances are physically unattainable.

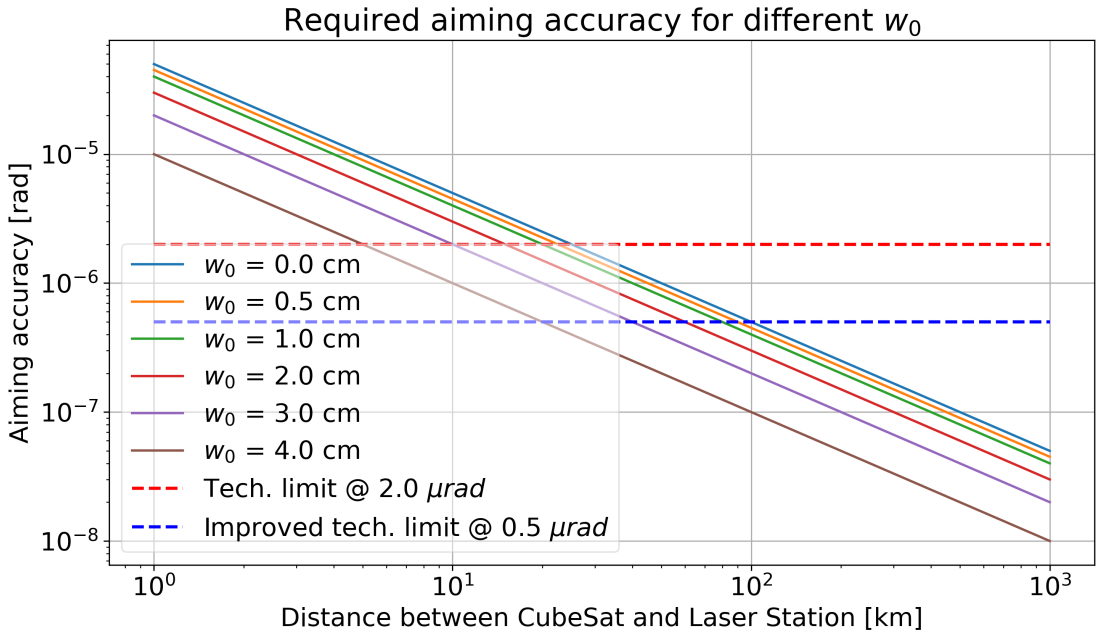

Figure 5.7: Aiming accuracies and waist radii required to achieve a certain laser emission range

Figure 5.7 illustrates the potential distance a laser can be emitted across by improving aiming mechanisms. From equation 4.8 and the approximation of $\tan x = x$ for small angles, a linear relation between aiming accuracy and maximum emission distance can be detected. Thus, by improving aiming accuracy by a factor of four, indicated by the blue dashed line, the w_0 = 0 cm case would reach a maximum distance of 100 km.

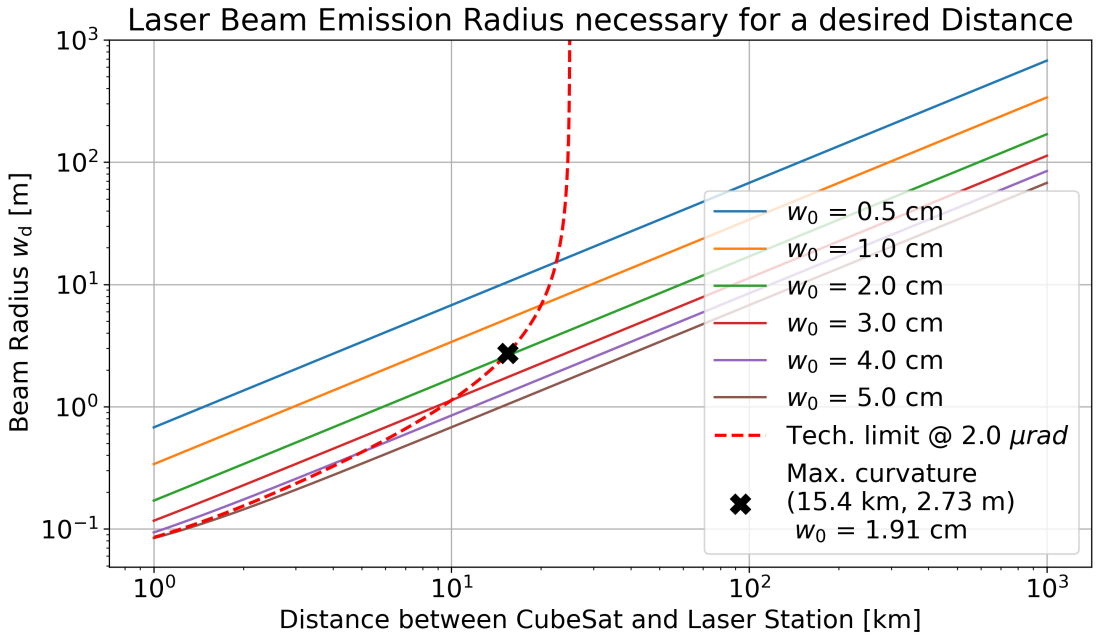

Figure 5.8: Mirror size required to achieve specific beam waist radii. The red dashed line indicates the technological aiming accuracy limit of 2 µrad. The maximum distance is valid for θ_{CS}=0°.

Since a laser beam is subject to diffraction, achieving small beam waist radii is not practical because it requires large mirrors or lenses to concentrate the light. The plot shown in figure 5.8 was used to determine the required mirror radius. Analogously to figure 5.7, this one depicts the technological limit of 2 µrad of aiming accuracy, so that the zone of possible designs lies above and to the left of the dashed red line. It shows the mirror size required over laser beam distance to obtain different beam waist radii w_0. The curves show that to attain smaller w_0, larger mirror radii are required; reducing the beam waist radius by one order of magnitude, the mirror radius must increase inversely proportionally for all distances, as is illustrated by the blue and brown curves. Furthermore, the technological limit indicates the maximum distance that can be achieved and the corresponding minimum mirror size. The dashed line grows continuously until it leaves the plot, hinting toward the already discussed

asymptotic limit of 25 km. For an optimized design, a point along the dashed line must be chosen so that the full beam range is used while also keeping the mirror radius as small as possible. In the end, a trade-off between range and mirror size must be made.

5.2.2. FoV angles

Since the laser beam range is also dependent on its incident angle on the ablative plate, the change of the maximum distance was investigated. For that figure 5.9 was plotted which shows the laser range in blue for each possible θ_{CS}. The red dashed lines indicate the limit angle for which it is still possible for the entire laser beam to hit the target with 100% certainty. It shows that the maximum viable semi-vertex angle for the CubeSat is 67.5°.

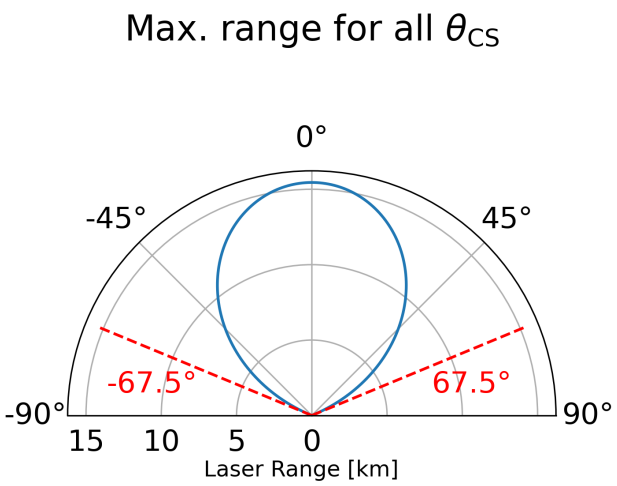

Figure 5.9: Maximum laser range over all θ_{CS}. The red dashed line indicates the maximum viable incident angle so that hitting the ablative plate is still ensured.

Regarding θ_{LS}, the semi-vertex angle of the laser station's FoV, there is no such influence on the range. Its limits are purely defined by structural and dimensional constraints. This would require a detailed structure plan on how the laser station would be constructed, and a load analysis would be necessary to determine the limits of θ_{LS}, which is beyond the scope of this thesis. Thus, θ_{LS} was set to 60°, to on one side allow for a lot of maneuverability while still taking into account that the mirror needs space to move and that it must be attached to the the laser station itself.

5.2.3. Earth obstruction

Despite the diffraction and aiming accuracy as limiting factors, the laser beam's proximity to Earth was investigated, as it also limits its emission distance, as illustrated in figure 4.4. The geometric maximum distances for various altitude combinations of a laser station and CubeSat are displayed in figure 5.10 using the minimum laser beam altitudes h_{L} of 200, 250, and 300 km, respectively. While the plots consider combinations of up to 500 km in altitude difference between laser station and CubeSat, LAP is only possible in the area between the white dashed lines, where the altitude difference is within the laser beam range based on the range limit caused by the aiming accuracy. In altitude combinations in the faded areas, the CubeSat cannot be propelled by the laser station. With an increased laser emission range, the area of possible altitude combinations widens.

For the case of h_{L} = 200 km, the maximum distances are larger than for the other two, as can be seen through the darker colors in the center and even more so in the right plot. Furthermore, the differences in maximum distance among the three cases decrease as altitude increases. In the situation where both spacecraft are at an altitude of 400 km, for instance, the maximum distances are 3267, 2834, and 2318 km, respectively, resulting in a difference of 949 km. Most drastically, this difference is evident when both spacecraft are at an altitude of 300 km (bottom left corners in the plots); the left case still allows the laser to be emitted over 2301 km, whereas the one on the right reduces to 0 km. On the other hand, when both spacecraft orbit at an altitude of 800 km (top right corner in the plots), the distance decreases to approximately 480 km. The main conclusion of those plots, however, is that unless the spacecraft are both at the same altitude of h_{L}, the maximum distance is practically limited by the aiming accuracy. For example, with h_{L} = 300 km, the scenario of one spacecraft being at the same altitude and the other being at an altitude of 301 km already allows for a distance of 115.5 km over which the laser can be emitted. So, to equate the two limits, the aiming accuracy would need to improve by a factor of 4.6.

Since geometric limitations are practically non-existent, as long as both laser stations and CubeSats orbit Earth at altitudes above 300 km are considered; thus, the aiming accuracy is regarded for the dimensioning of the mirror. To find the optimum, the limit curve in figure 5.8 was considered. Based on its shape, the optimum is found where its curvature is maximum, as for shorter mirror sizes the laser range decreases rapidly. In contrast, for even a slightly longer laser range the mirror radius grows quickly. At the point of the largest curvature, the two domains meet, and both a reasonable distance and a mirror that is not too large can be achieved. The black cross indicates the location of the point with the highest curvature and therefore the optimum, which lies at a laser beam range of 15.4 km and a mirror radius of 2.73 m, resulting in a beam waist radius w_0 of 1.91 cm.

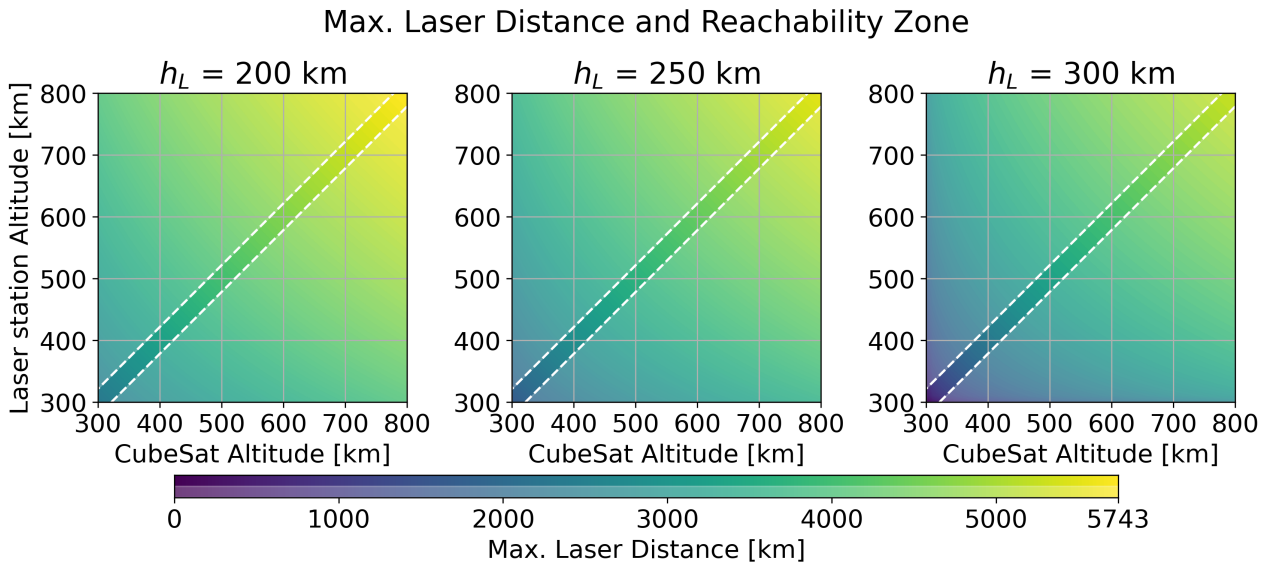

Figure 5.10: Maximum laser emission distance due to Earth and atmosphere obstruction. The white lines indicate the borders of eligible altitude combinations due to aiming accuracy. The whitened regions are not reachable.

5.3. Propulsion Model

This section examines the effect of laser power and altitude on the duration of the thrust event. The thrust duration varies with altitude because the ΔV required to increase a CubeSat's altitude by a fixed amount decreases at higher altitudes, as is derivable from equations 4.21 and 4.22. Figure 5.11 shows the thrust event durations for single complete thrust events where all CubeSats had an initial altitude 10 km lower than the laser station and then were propelled to an altitude 20 km above the laser station; it is assumed that the thrust event takes place at the maximum laser range of 15.4 km and the according losses. Those distances were chosen based on the laser's emission range and a possible goal altitude that the CubeSats can go to while still maintaining a nearly circular orbit. The heatmap reveals, on one hand, that the thrust duration is shorter as the laser power increases; more precisely, the two are inversely proportional. This is since mass loss and thrust magnitude are proportional to the laser power; thus, the thrust event must last longer to provide the same amount of ΔV. On the other hand, the thrust duration reduces slightly with higher altitudes, which confirms the statement made at the beginning of this paragraph. The values show that maneuvers at 300 km last approximately 9.1% longer than those at 700 km for all laser powers. Furthermore, with higher laser power levels, the thrust event is shorter; 10 kW lasers only need to be powered ten times longer than a 100 kW laser.

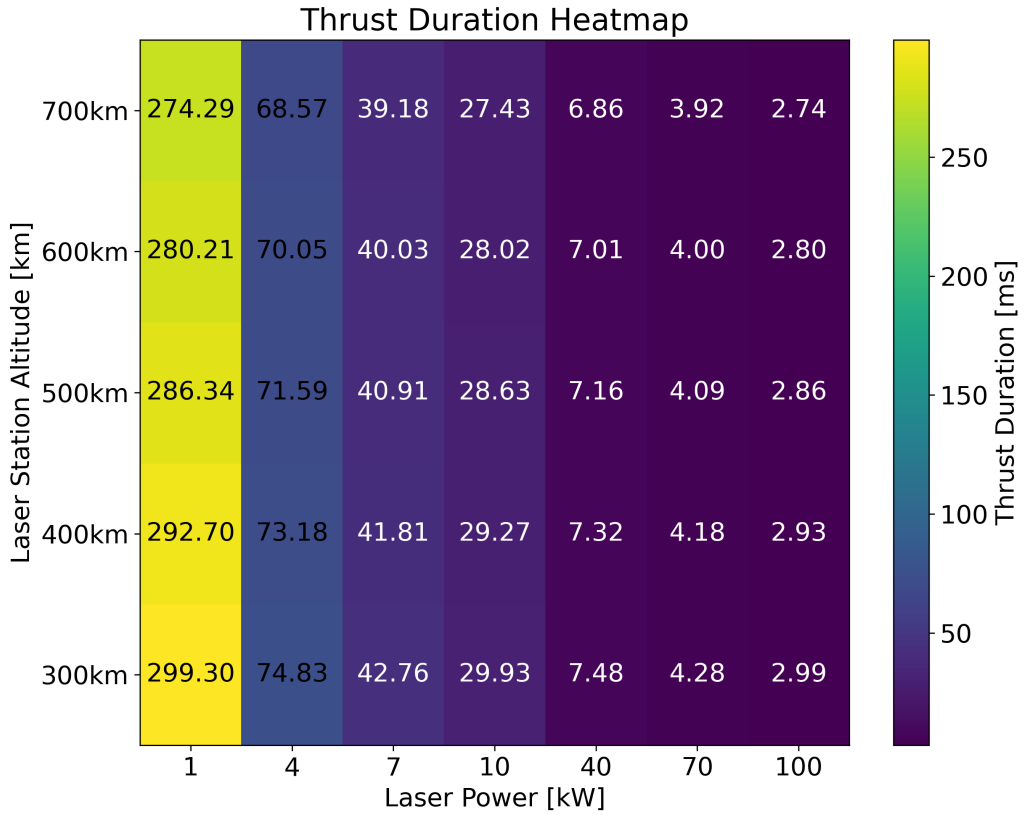

Figure 5.11: Thrust event durations for varying altitudes and laser power levels. In each case, the CubeSat was propelled from 10 km below the laser station to 20 km above the laser station. The maximum laser emission range of 20 km has been used for this heatmap.

While it could be argued that due to the shortest thrust duration, it would be most reasonable to perform LAP at the altitude of 700 km, as the energy consumption would be smaller and that more satellites could be maintained, the application at 700 km is not practical, as most CubeSats find their application around 400 km. Therefore, the laser station would also have to orbit Earth at that altitude so that it can reach the CubeSats with its laser. Moreover, with a pan speed of 25°/s, there is always a break of up to a few seconds for the laser's reorientation, so that the additional thrust event duration has only a minimal effect on the cycle time, the worst case being 25.01 ms when the laser is only powered with 1 kW.

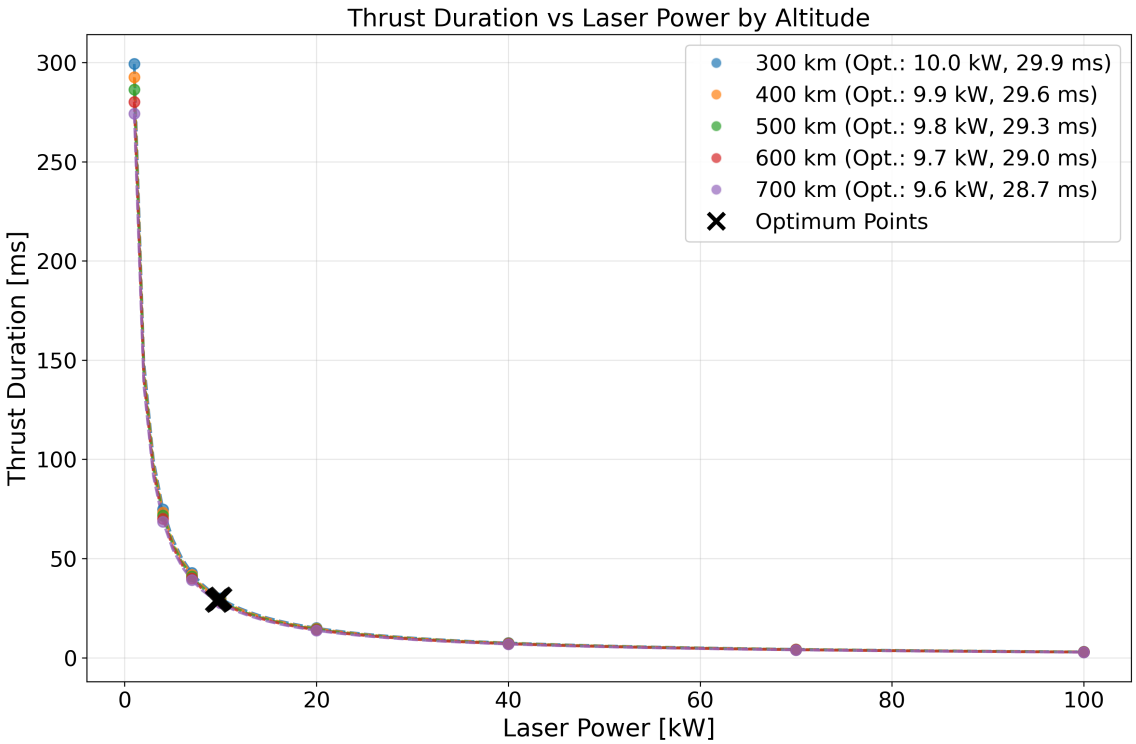

Figure 5.12: Optimization of thrust duration over laser power for different altitudes.

To find the optimal compromise between thrust duration and laser power, the values found in figure 5.11 have been plotted for each altitude in figure 5.12, and a trendline was drawn between the data points, each with a coefficient of determination of R^2 = 1.0000. The optimum is found where both the thrust duration and laser power are minimized. Therefore, the points closest to the plot's origin were chosen; in other cases, either the amount of power required to reduce the thrust duration increases rapidly, or reducing the laser power results in significantly higher thrust durations. The optima are found close on top of each other, so that the values are shown in figure 5.12's legend, the power level ranging from 9.6 to 10.0 kW and the thrust duration ranging from 28.7 to 29.9 ms. The effect of choosing different altitudes on the thrust duration is minimal, considering the time it can take to reorient the laser beam.

5.4. Energy Model

This section aims to determine how much battery capacity must be equipped to the laser station, which is discussed in section 5.4.1. section 5.4.2 then elaborates on the respective consequences regarding laser station dimensions and power generation.

5.4.1. Battery capacity

To evaluate the battery capacity, equations 4.16–4.19 have been used, the result being presented in figure 5.13. Long-term tests with nickel-cadmium batteries in orbit showed that the batteries fail after 10 years of operation due to the separator between the positive and negative side of the battery drying up, and not because of degradation [73]. Therefore, the change in battery capacity is only observed in that time frame. Figure 5.13 shows the laser station mass and volume over time, together with the mass and volume limits of the Falcon 9 launcher. With the defined laser power of 9.9 kW, the battery must hold at least 5.67 MJ of energy. At the defined combination of laser power and battery capacity, according to equation 4.15, the latter dictates the battery mass. Therefore, extra battery capacity must be equipped to the laser stations to allow for a 10-year lifetime, ultimately a total battery mass of 31.5 kg, thus a volume of 0.016 m^3, is required. In figure 5.13, the increase of the mass and volume of the battery, and therefore the laser station, is not visible, as their increase equates to 2.7 kg or 0.00135 m^3 to ensure surricient battery capacity over the mission lifetime. With the battery capacity and power usage being determined it can be estimated how much the power system costs. Assuming average prices in the ranges given in section 4.5.1, the entire power system costs $2.97 million.

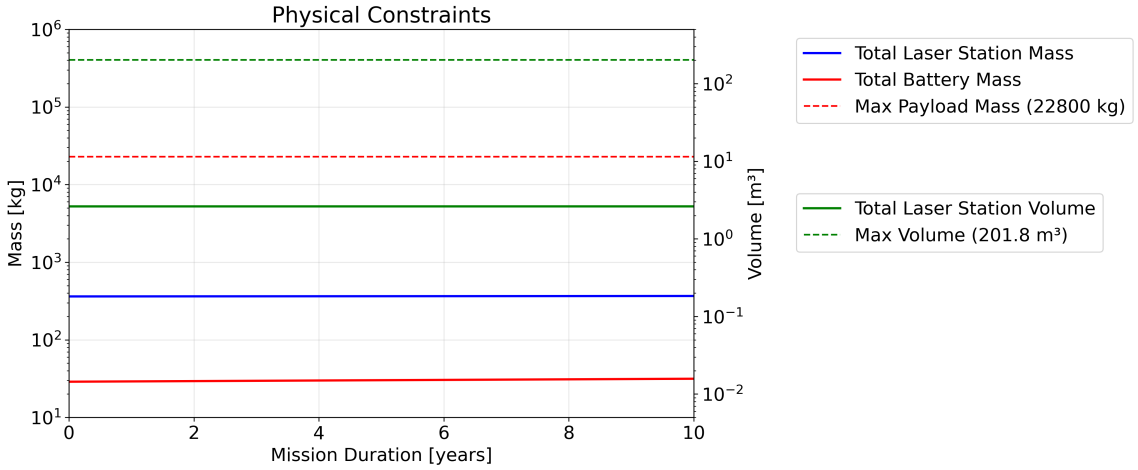

Figure 5.13: Nickel-cadmium battery mass and volume required for different operation durations. The increase in mass and volume over time is minute so that it is not visible.

5.4.2. Power generation and laser station dimensions

Based on the required energy capacity and power consumption, the solar array area was calculated using equation 4.19, resulting in 8.68 m^2, which adds 17.87 kg to the electrical power system of the laser station. For the laser station dimension estimate, a communication satellite was deemed

to be most suitable, as it is equipped with an antenna reflector which would act as the mirror for the laser, and because it otherwise is not equipped with other instruments like telescopes for space exploration that take up additional space on the satellite. For the estimation, a FLTSATCOM satellite, designed for military communication, was chosen, as data on the mass allocation of its components was available, helping to scale it to the laser station. FLTSATCOM's bus mass was 619 kg, of which 336 kg was designated for the electrical power system; additionally, the satellite contained a payload of 222 kg, totalling a dry weight of 841 kg. The antenna reflector diameter was 4.9 m [54].

The mass scaling of the bus was made linearly based on the electrical power mass, and the payload mass was scaled linearly from the antenna reflector to the laser mirror size. Regarding the bus mass of the laser station, the mass was scaled to 123.61 kg, and the payload mass was estimated to be 275.64 kg; the total mass of the laser station, therefore, resulted in 399.25 kg. Regarding the dimensions, FLATSATCOM had a hexagonal bus measuring 2.4 m flat-to-flat and 1 m deep, thus a volume of 4.99 m^3. Assuming the same bus density for the laser station, the laser station therefore has a volume of 1.00 m^3. For a bus of identical proportions as FLTSATCOM, its dimensions would thus be 1.40 m flat-to-flat and 0.58 m in depth.

At that size, however, the laser station's lifetime is only 35 days if released at 400 km altitude, which is not practical. Therefore, the laser station must also be equipped with a thruster. One option would be to have multiple laser stations propelling each other using LAP. However, the planning of a working laser station network that maintains its orbits is out of the scope of this thesis; therefore, the use of common means for orbit maintenance has been chosen. The simulation indicated a daily ΔV loss of 0.835 m/s, or a total ΔV loss of 3047.75 m/s over 10 years. Tests in the simulation showed that Hall Effect thrusters can maintain a laser station's orbit. Due to its maturity and, consequently, extensive information availability, the BHT-200 thruster was chosen. It can provide a thrust up to 13 mN and an I_{sp} of 1390 s and adds only 1.1 kg of mass to the laser station [74]. Based on the rocket equation, the laser station must be fuelled with 100.06 kg of xenon gas. Xenon is stored in a tank at a pressure of approximately 186 bar at a temperature of 60°C, so that the gas is stored in its supercritical state at a density of 1719.5 kg/m^3 [75]. Therefore, the volume that must be added for the propellant is 0.058 m^3, so that the laser station has a total volume of 1.058 m^3.

Regarding the dimensions of the laser station, they are constrained by the dimensions of the fairing of the rocket launcher. The Falcon 9 can house a cylindrical spacecraft the size of up to 12.14 m in length and 4.6 m in diameter with its extended fairing [76]. Since with a radius of 2.73 m the mirror exceeds the maximum diameter of the Falcon 9's fairing, it must be folded to fit. From the James Webb Space Telescope, it is known that for a mirror with a diameter of 6.4 m, the folding structure

behind the mirror and the mirror itself had a depth of 3.51 m [77]. Since the mirror of the laser station's mirror is smaller, the load the folding mechanism must bear is smaller as well, thus allowing for scaling down that thickness. Scaling it down based on the mirrors' diameters, therefore, results in a thickness of 2.55 m. Thus, in a folded state, a laser station would require the entire diameter of the fairing; the height of the laser station bus and twice the mirror thickness, for when it is folded, adds up to 5.68 m. Therefore, it is possible to fit two laser stations into one launcher, consequently halving the cost per laser station.

With the dimensions of the mirror and laser station known, it could also be estimated how large the drag coefficient would be. Literature says that disks and thin cylinders have a C_D in the range of 1.1 to 1.25 [78, 79]. A drag coefficient of 1.2 was deemed to be the most robust choice for the simulation. On one hand, it might slightly overestimate the actual C_D and therefore result in worse results for the simulation. However, if this was the case, feasibility would still be guaranteed if it could be demonstrated with the chosen value, as the actual ΔV loss would be lower than in the simulation. On the other hand, the deviation from 1.2 to 1.25 is only 4.2% so that the simulation would not deviate drastically from reality, if it was >1.2.

5.5. Financial Model

To assess the competitiveness of LAP compared to its propelled and non-propelled counterparts, their costs were plotted over time, allowing for the determination of break-eveneven point. Since the cost of the laser station is distributed across all CubeSats that are propelled by it, the number of the latter is essential. Equally, since the satellite lifetime of the competing maintenance depends on it, the altitude plays a role in the comparability as well.

To find the combinations of altitude and number of CubeSats that are financially competitive, a heatmap has been created that illustrates the time until break-even, as is shown in figure 5.14. It only demonstrates the altitudes up to 500 km, as higher-altitude cases did not result in break-evens with a reasonable number of CubeSats to be maintained; the 500 km case already requires 20000 satellites to become profitable. The cells with the value 'N/A' indicate the combinations that are not competitive to at least one of the propelled and non-propelled competitors.

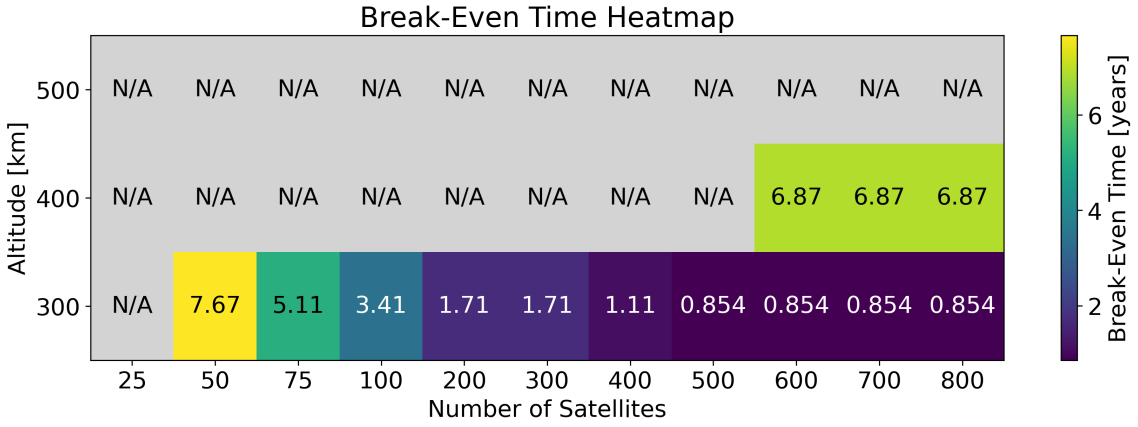

Figure 5.14: Break-even times for various altitudes and numbers of CubeSats to be propelled. Cells with 'N/A' represent combinations that are not competitive.

The cell values in figure 5.14 do not reduce with an increasing number of satellites, as can be seen for the viable cases for 400 km, and at 300 km for 200 and 300 satellites as well as from 500 CubeSats onwards. The reason for an unchanged break-even time can be discovered by analyzing the single cost developments over time, as illustrated in figure 5.15 for 400 km altitude and 600 CubeSats. The yellow and blue lines represent the total per satellite costs of the propelled and non-propelled CubeSats, respectively. In red, the actual cost of LAP is shown. The laser station costs are evenly distributed among the satellites. Due to requirement FIN-1.1, the green line showing the LAP cost with a 5% margin has been introduced. Finally, the dashed green line follows the cheapest competitor and indicates the maximum cost that LAP can be priced while still competing. The annotation in the graph indicates break-even point at which competitiveness is achieved. As the graph illustrates, the competing CubeSats must be replaced around day 2000 and 2509; thus, the competitiveness stems from the replacement of the conventional satellites while the LAP-maintained CubeSats remain in orbit. However, the competitiveness prevails only for 454 days, as the competitors become financially more attractive again due to their lower operational costs. With the distribution of the laser station cost on more CubeSat, the cost per CubeSat is reduced; in other words, the solid red and green lines are lower. However, since these curves are still not lower than the blue and yellow lines, break-even point is not moved in time; the only advantage in those cases is the reduced per-satellite cost. The earliest achievable break-even point is where the first replacement of the non-propelled competing CubeSat occurs, as the price of a LAP-maintained CubeSat itself is already higher.

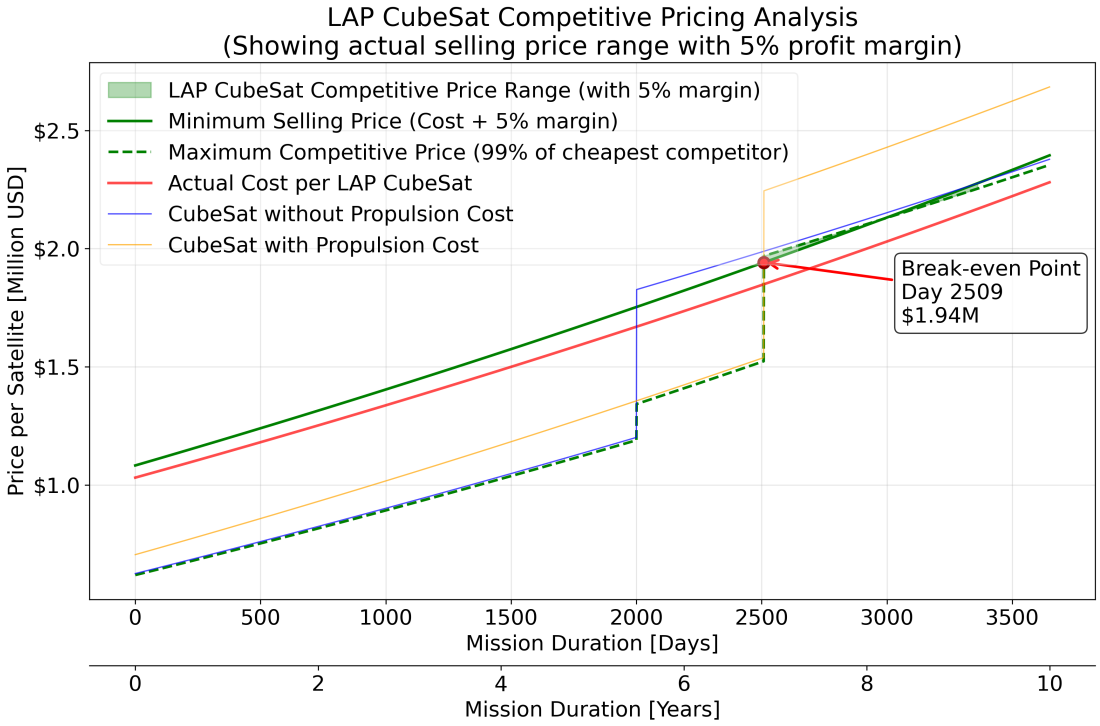

Figure 5.15: Cost evolution of LAP and the competitors over time.

For the determination of the altitude to answer the research questions, figure 5.14 makes it apparent that altitudes of 500 km and higher above are not reasonable to pursue. For the choice between 300 and 400 km, the cost heatmap in figure 5.16 was considered. Up to 500 satellites, the 300 km case is the only possible one, and in cases with more CubeSats, the 400 km instances are more expensive. However, the decision must also be made from another perspective. Satellites at 300 km altitude lose altitude at a significantly higher rate than those at 400 km; therefore, the risk of a CubeSat going out of range from the perspective of the laser station is significantly higher, which increases the attractiveness of self-propelling satellites due to practicality. Therefore, it was determined that the altitude of 400 km is to be preferred despite higher costs.

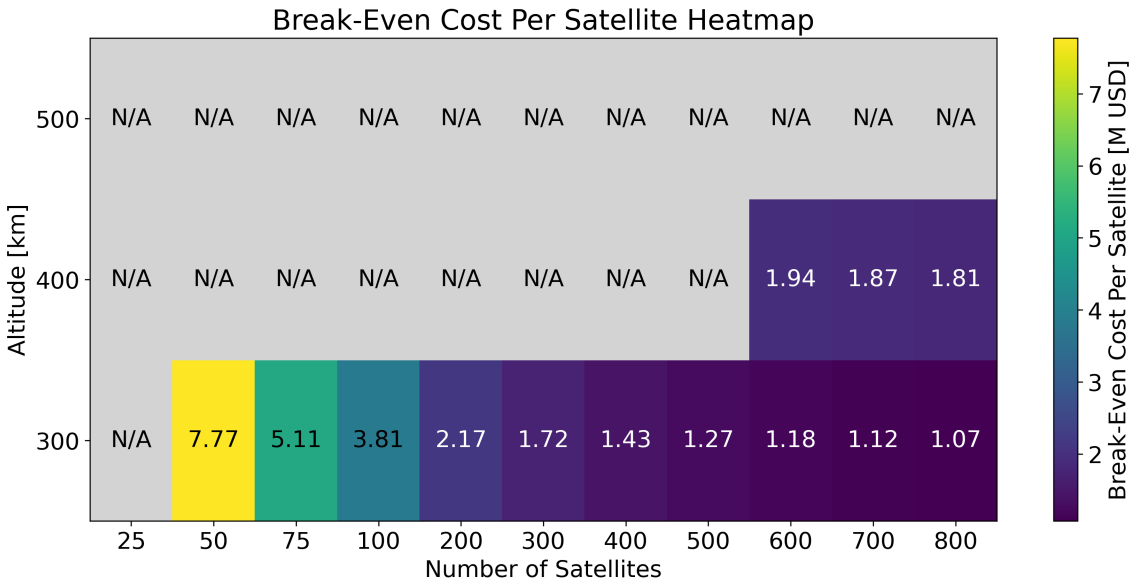

Figure 5.16: Break-even costs for various altitudes and numbers of CubeSats to be propelled. Cells with 'N/A' represent combinations that are not competitive.

6
Verification & Validation

This chapter aims to demonstrate that the simulation described in chapter 4 is both functional and in accordance with reality. First, the verification (section 6.1) shows the functionality of single models in the simulations and their interplay. Second, the validation (section 6.2) is used to confirm the accuracy of the simulation by comparing it with real-world data.

6.1. Verification

This section aims to demonstrate that single elements of the simulation work correctly and as expected. Since not all model functions are independently verifiable, it is shown that the interplay of the models is functioning.

6.1.1. Environmental Model

The no-thrust case for a CubeSat is investigated for the environmental model. Figure 6.1 depicts the altitude profile of the simulated CubeSat deployed at 400 km, the blue curve representing a time of high solar activity and the red curve standing for low solar activity. In this simulation, for comparison with literature, the ballistic coefficient ($\frac{M_{\text{sat}} C_{\text{D}}}{A}$) of the CubeSat was changed to 50 kg/m^2 by increasing its mass to 100 kg, and its front surface to 2.4 m^2, while the drag coefficient remained at 1.2. Depending on solar activity and its influence on a spacecraft with this ballistic coefficient, a lifetime of 77.4 to 552.2 days is expected [54]. Regarding figure 6.1, the satellite crashed on day 123 at high activity and on day 357 for low activity. The simulated results lie within the range given in the literature. Yet, despite releasing them at high and low peaks of activity, both curves do not indicate a lifetime similar to that in the literature. The consulted literature does not indicate whether the given lifetimes are valid for constant or changing solar activity. Since the simulation considers the varying solar activity over time, the change in atmospheric drag increases or decreases the lifetime of the

spacecraft, which becomes more noticeable over longer periods, as is the case for the red curve. Furthermore, deviations from literature might have arisen due to different assumptions made in this simulation in other areas.

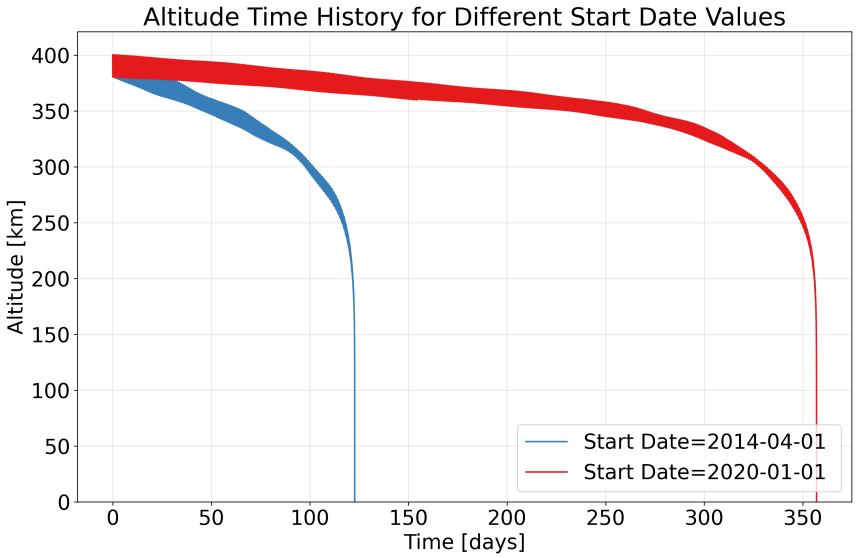

Figure 6.1: No-propulsion case for a satellite deployed at 400 km

To reduce the influence of the changing solar activity over time, the identical verification was repeated with identical parameters, but at an altitude of 300 km, so that the lifetime is shortened. According to literature, the lifetime at this altitude lies between 11.0 and 49.9 days for high and low solar activity, respectively [54]. Figure 6.2 displays the altitude profile for the lowered altitude, with the blue and red curves representing the lifetime for high and low solar activity, respectively. In the former case, the simulation tells that the spacecraft crashes with Earth after 10.83 days, and after 28.3 days for the latter. For the high activity, the simulation deviates only by approximately 4 hours, whereas for the low solar activity, the deviation is still 21.6 days. From the former result, it can be deduced that differences in simulation assumptions must be minimal, as otherwise the difference must be larger. Instead, the deviations for both the high and low solar activity cases must arise from the fact that the maximum and minimum activity are not equal in each cycle [80]. While a part of the deviation might still arise from the changing solar activity, this effect is not as prevalent here, since a shorter time period reduces the change in solar activity. Overall, the simulation lies within the bounds given by the literature and is practically spot on for the high-activity case at 300 km initial altitude. Thus, the simulation is accurate, and the environmental model is verified.

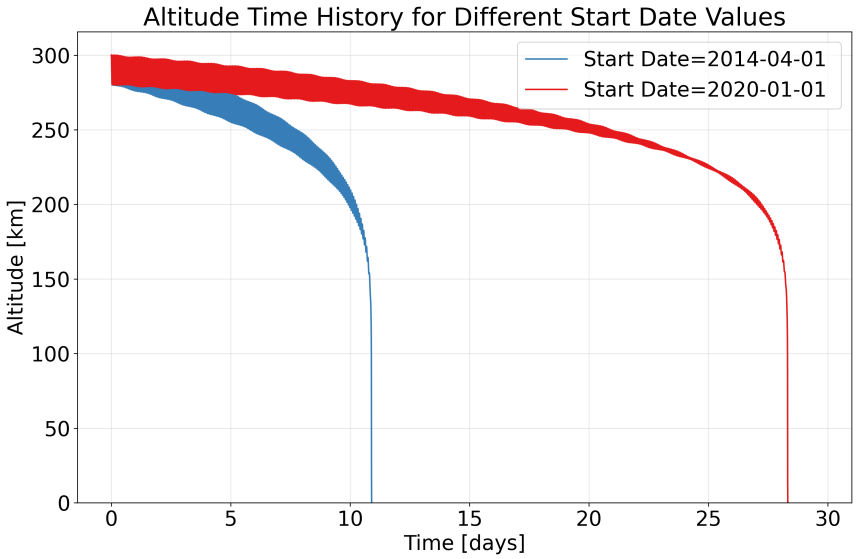

Figure 6.2: No-propulsion case for a satellite deployed at 300 km

6.1.2. Laser Station Energy and Thrust Interface

To check whether the laser station energy model accounts for the loss of energy when the laser is emitted to propel a CubeSat, their interplay has been considered. Thus, stored energy must decrease when a thrust event takes place. Figure 6.3 shows the energy stored on the top, the energy usage in the center, and the thrust magnitude at the bottom. This figure was created based on the values defined in chapter 5 with one CubeSat to be maintained. The top plot shows the energy level of the battery that is equipped on the laser station over time, the center plot illustrates the power usage for the laser, and the bottom plot presents the thrust a CubeSat experienced on each thrust event. The energy level plot shows that the battery starts the simulation empty and therefore charges on the first day. Two thrust events occur during the observed time, one on day 1 and the other on day 102, with a maximum thrust of 0.424 N and 0.429 N, respectively, as is presented in the bottom plot. The top and center plots indicate energy usage at the identical times as the thrust events occur, indicating that the energy is consumed for said thrust events. The center plot shows that for both thrust events, the full laser power of 9.9 kW is used. The top plot, however, demonstrates that for the two thrust events, a different amount of energy was consumed, the first event using 0.41 MJ, thus lasting for 41 s, and the second thrust event using 1.50 MJ over 152 s.

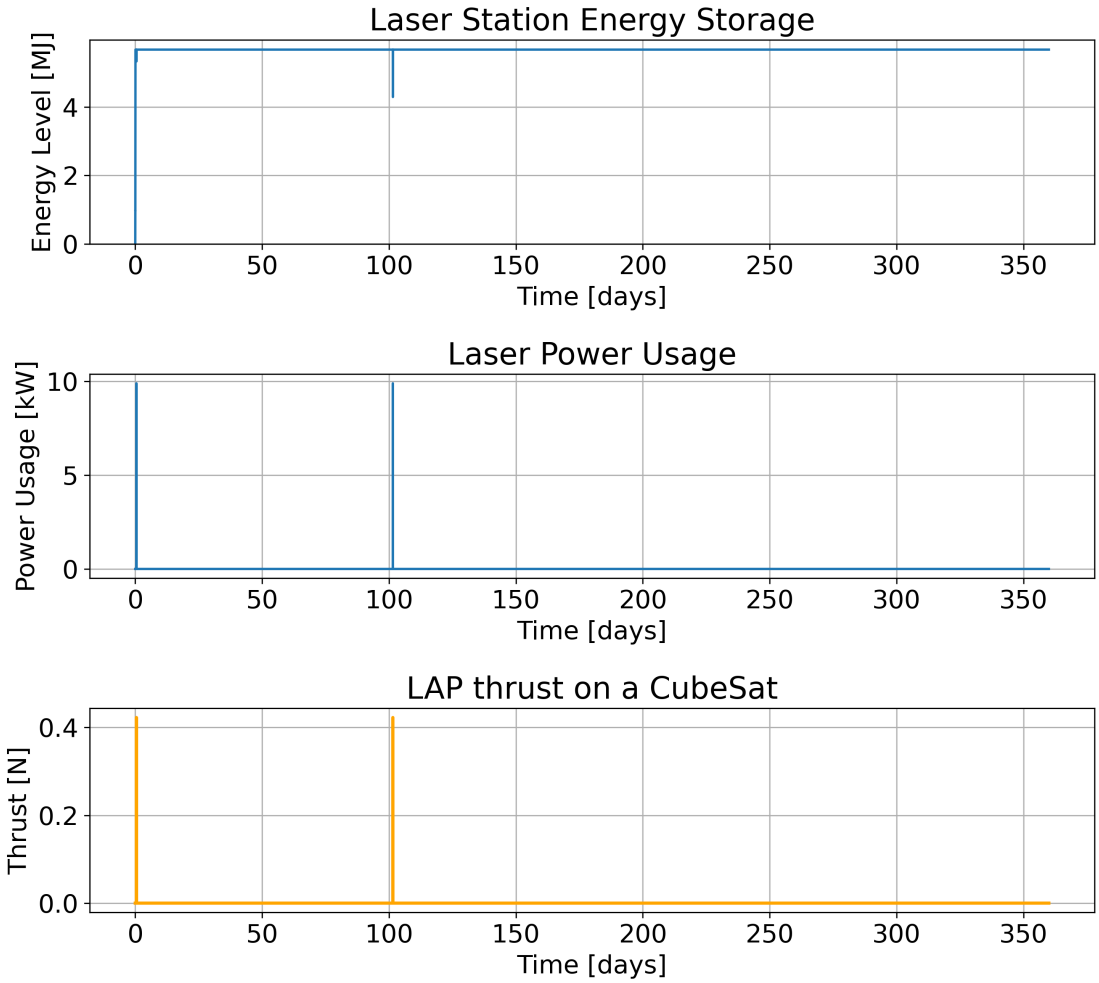

Figure 6.3: Energy storage and usage during thrust events

To prove the functioning of the interplay of the models, the second thrust event is investigated more thoroughly and recalculated separately. During the thrust event, the distance between the laser station and CubeSat reduced to approximately 6.1 km. Over that distance, the absorption and diffraction efficiencies are 92.66% and practically 100%, so that 9173 W of laser power arrived at the ablative plate, which translates into 4.2 N. This value is smaller than the shown thrust event; however, since the thrust event starts as soon as the CubeSat is in range, the thrust increases over time due to increased diffraction efficiency. Since the exact start and end times of the thrust event are unknown,

the distance where the thrust is maximum cannot be determined. Regardless, the separate calculation and the plots show that the timing is correct, that the thrust values are within a reasonable range, and that the modules' interplay is functional.

6.1.3. Laser Power and Thrust Frequency

From equations 4.21 and 4.23, it is to be expected that with higher laser power, more thrust is generated, and the ΔV required for the orbit maintenance is reached with shorter and fewer laser pulses. To check whether this is the case in the simulation, the thrust events have been plotted for when both laser station and CubeSat are deployed at 400 km for laser powers of 50, 100, and 200 kW, which are displayed in figure 6.4 in red, black, and blue, respectively. The expected trend is observable in this plot. Between the first two thrusts of the 100 kW case, a CubeSat that is only propelled with a 50 kW laser must be propelled four times. Similarly, the blue curve has its second peak more than twenty days after the second black peak, while the two have the first peak simultaneously. Those behaviors show that the simulation is operating reasonably.

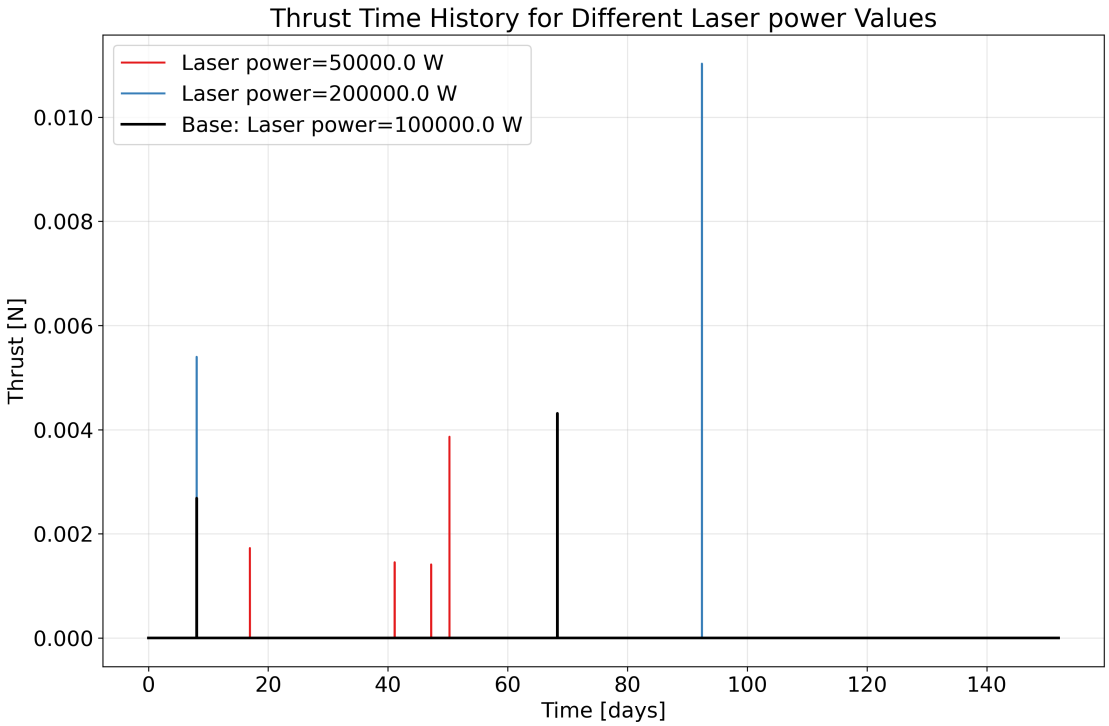

Figure 6.4: Thrust events for different laser powers

Thanks to the first black and blue peak in figure 6.4 that take place at the same time, it also allows to show that the linearity of the laser power to the thrust, as indicated in equation 4.23, is represented in the simulation: the black peak indicates a thrust of approximately 2.75 mN and the blue one a thrust of roughly 5.50 mN, therefore being double the thrust for twice the laser power. This comparison is possible due to the CubeSats and laser stations starting at the same location, and because this is the first thrust event, the losses are identical. Such a comparison is not feasible for later peaks, as the altitudes and the distances to the laser stations differ.

6.2. Validation

For the validation of the simulation, the flight of the ISS has been reconstructed. This method offered a simple method for the validation, as the ISS's flight data has been made publicly accessible by NASA's Trajectory Operations and Planning office [81]. Since the data provided consisted of only 15 days, only a short-term validation is possible. For the reconstruction, the simulation parameters were altered to match the ISS: the mass was set to 438914.5 kg, the drag area increased to 1314.60 m^2, and the drag coefficient C_D changed to 0.8. The starting date was set to March 22, 2021, at 12:00:00 UTC. The starting location and velocity were set to the first coordinates given in the data set, as shown in equation 6.1. On April 2, 2021, at 12:29:00 a thrust event took place, adding a ΔV of 0.2 m/s to the ISS.

$$\vec{r}_0 = \begin{pmatrix} 5026.086172275360 \\ 4313.723403421940 \\ -1548.539588725320 \end{pmatrix} \text{km} \qquad \vec{v}_0 = \begin{pmatrix} -2.15404992881804 \\ 4.56591472319758 \\ 5.75541822478933 \end{pmatrix} \text{km/s} \tag{6.1}$$

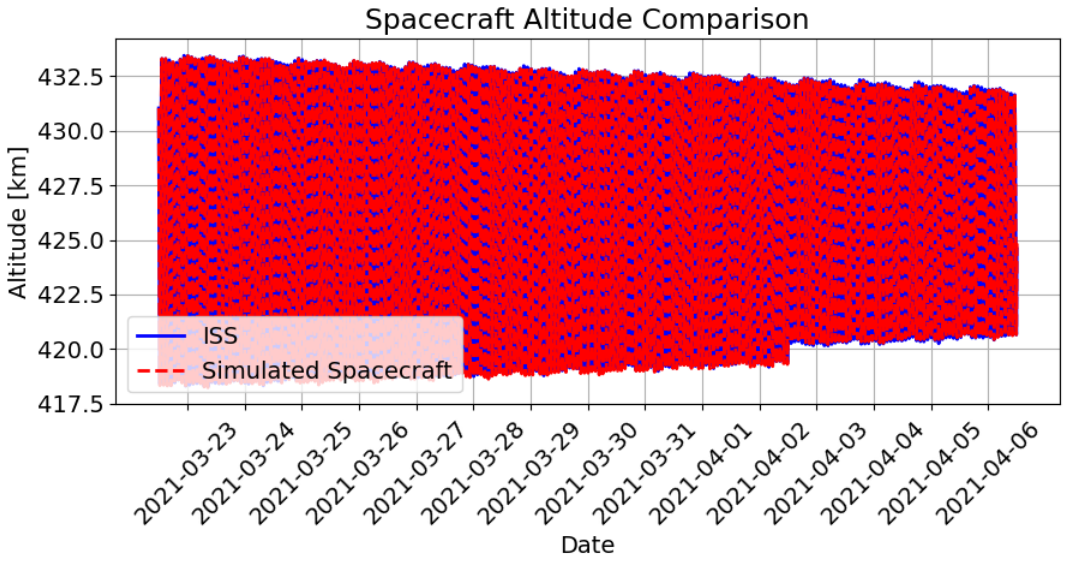

Figure 6.5: Actual and reconstructed ISS altitude

Figure 6.5 shows the altitude profiles of the actual flight in blue and the reconstructed one obtained through the simulation. This graph shows that the simulation follows the same trends as the ISS did in reality. However, for a more precise analysis, an altitude deviation plot has been made, which is depicted in figure 6.6. This plot's transparent curve shows that the simulation's deviation remains within 240 m throughout the entire period. Nevertheless, the trend plot indicates that the simulated ISS tends to lose altitude more slowly in reality by approximately 4.75 m/day. A possible reason for this discrepancy could be that the actual ISS is more decelerated due to changes of the frontal area or the changes in the station's orientation, changing the drag coefficient C_D, which both affect atmospheric drag. The simulation does not intend to modify those parameters over time and, therefore, remains fixed at the initial values provided by the data.

On April 2, 2021, the ISS underwent a thrust event as can be seen through the sudden increase of the perigee in figure 6.5. From NASA's provided data, it is known that the required ΔV for the maneuver was 0.2 m/s and that the ISS's initial mass of the validation period was 438914.50 kg. The simulation was conducted by applying a continuous thrust of 700 N for 125.4 s. In a first-order approximation, this results in an applied $\Delta V = \frac{F_\mathrm{T} \cdot \Delta t}{M_\mathrm{ISS}} = 0.20$ m/s. As can be seen in figure 6.6a, the trend of the increasing deviation from the actual trajectory continues after the thrust event as it did beforehand. This indicates that the thrust event increases the simulated ISS's altitude by a comparable amount as the actual ISS was.

As proof of the thrust model working in the validation, the altitude profile has been plotted where no thrust was exerted to the ISS. This plot is shown in figure 6.6b. The deviation is unchanged until the thrust event on April 2. After the thrust event, the deviation increases so that on April 6, it reaches 1 km in altitude difference toward the end of the observed time span.

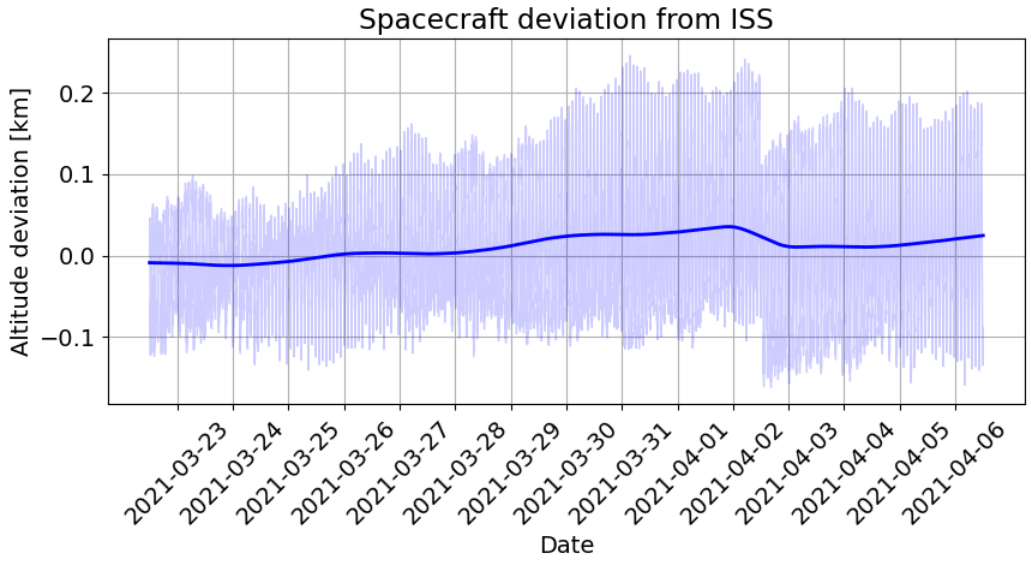

(a) Deviation of reconstructed to actual ISS altitude with ΔV = 0.20 m/s

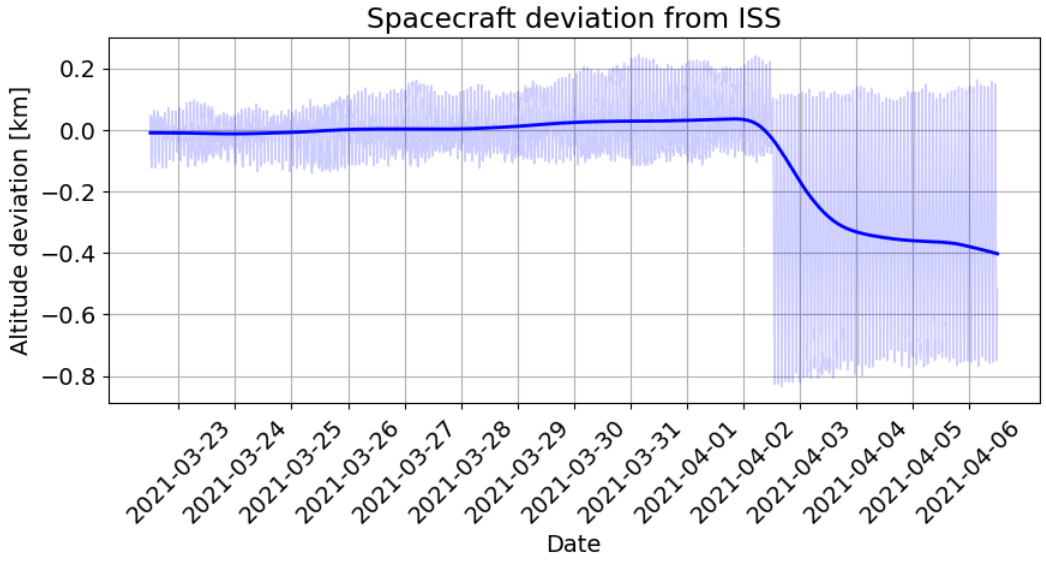

(b) Deviation of reconstructed to actual ISS altitude with ΔV = 0.00 m/s

Figure 6.6: Altitude profile reconstruction deviations with and without thrust event. The ISS underwent a thrust event on April 2.

7
Results

This chapter presents the results generated using the simulation described, characterized, verified, and validated in chapters 4 to 6. Due to the simulation being computationally expensive, results could only be generated with one laser station and one CubeSat, as the computation scales $\mathcal{O}(nmt)$ with n and m standing for the number of each of the two spacecraft types and t representing the simulated duration. Therefore, the simulation was only performed over one year instead of 10 years. This makes it difficult to make statements that are true for the entire duration that a laser station would be operating. Otherwise, the parameters determined in chapter 5 are used in the simulation. This chapter makes multiple references to figure 6.3, which has also been plotted together with the results presented here and therefore provides information for this chapter. Since it could be used as verification of the model, it is already depicted in section 6.1.2.

7.1. Orbital characteristics

First, the altitude profile of the laser station and CubeSat are investigated, and are presented in figure 7.1. The laser station is represented by the orange and the CubeSat by the blue curve. After deployment, the CubeSat oscillates roughly 20 km in altitude and slowly loses altitude as expected, due to atmospheric drag, SRP, and third-body gravitational accelerations. The oscillation poses an additional hurdle to the reachability of the CubeSat: The maximum range being 15.4 km, it is possible that the CubeSat passes the laser station out of reach so that an opportunity for orbit maintenance is lost. On the other hand however, the orange curve indicates that the laser station oscillates in altitude as well, and reaches altitudes lower than the CubeSat. Two examples of that situation being illustrated between days 6 and 35 as well as between 67 and 243 where the laser station reaches altitudes 10.69 km and 27.21 km below the CubeSat, respectively. On the other hand, however, throughout the entire simulated period, the laser station also reaches higher altitudes than the CubeSat. The most extreme case took place on day 98 where the laser station is up to 28.83 km above the maximum CubeSat altitude.

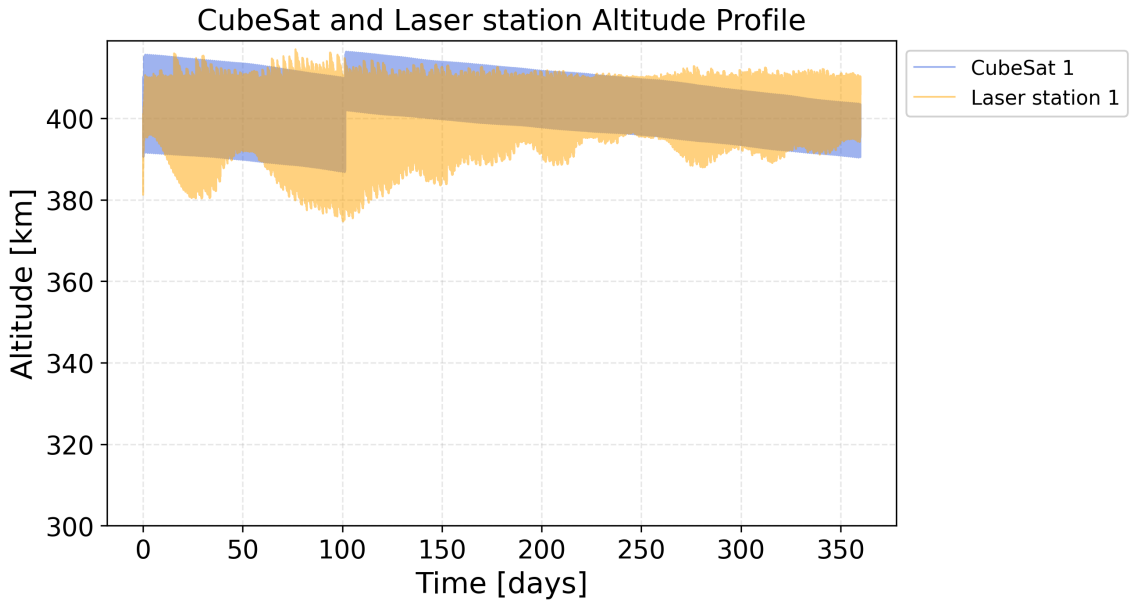

Figure 7.1: Altitude profile of a laser station and CubeSat deployed at 400 km altitude. The arrows indicate show the thrust events as presented in section 6.1.2 and the ΔV added at each thrust event.

From figure 6.3 the thrust magnitudes of 0.424 and 0.429 N are already known. On the first thrust event on day 1, a ΔV of 1.45 m/s was executed, by ablating 0.46 g of propellant. On day 102, 1.72 g of propellant were ablated to achieve a ΔV of 5.43 m/s.

Next to the altitude, the eccentricity and inclination of the two spacecraft provide relevant information. They are shown in figure 7.2, the eccentricity on the left and the inclination on the right, and again the laser station being represented by the orange curve and the CubeSat by the blue curve. The eccentricity plot on the left proves that both spacecraft remain on nearly circular orbits throughout the simulated period, as was intended in section 3.2, the highest eccentricity being 0.00392 for the laser station on day 102, and 0.00320 on day 46 for the CubeSat. The inclination difference shows that the two spacecraft differ in by 0.00252° at most on day 309. To put this in perspective, if the two spacecraft were both at 400 km altitude with this difference in inclination, the two could still be nearing each other to approximately 298 m in the worst case. Therefore, the inclination difference plays only a minor role in the laser station's potential inability to reach the CubeSat compared to the altitude.

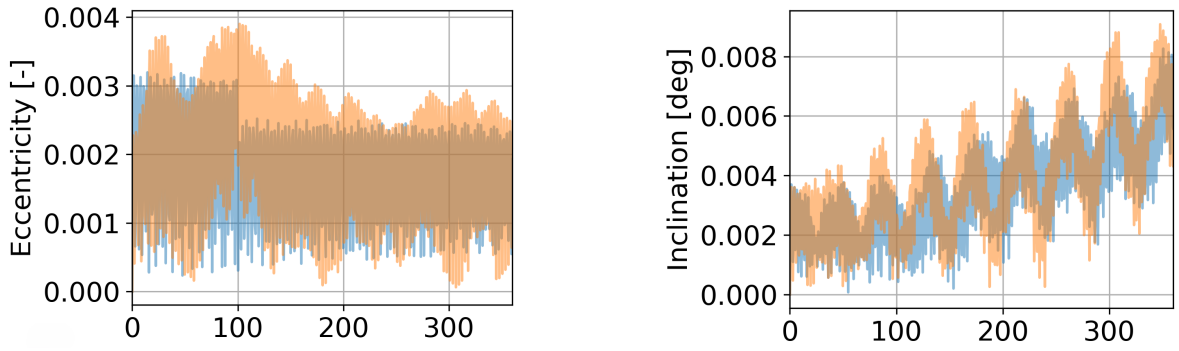

Figure 7.2: Eccentricity and inclination of the laser station and CubeSat. The orange curve represents the laser station, the blue curve the CubeSat.

7.2. Spacecraft proximity

To analyze the thrust events, as has been made in section 6.1.2, the distance between the laser station and the CubeSat is essential, as it illustrates the available time windows when LAP would have been possible, and indicates how large the losses due to absorption and diffusion are. For that reason, figure 7.3 has been plotted. It depicts the distance between the two spacecraft with the blue curve. The dashed red line is the maximum range of the laser. Therefore, the time windows where LAP is possible are when the blue curve is below the dashed one.

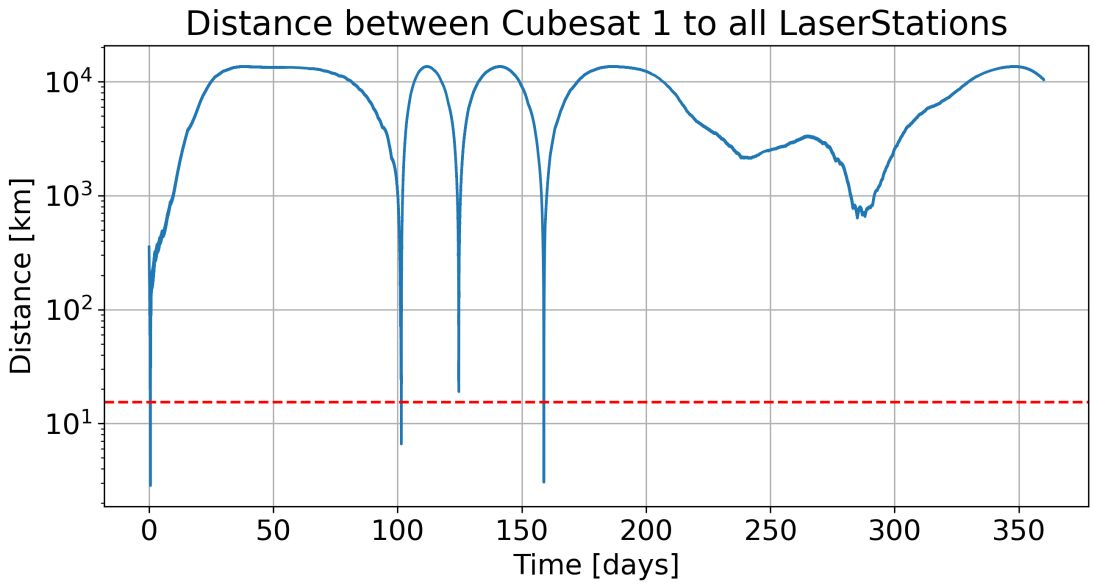

Figure 7.3: Distance between the laser station and the CubeSat

From figure 7.3, it can be derived that there are three time windows where thrust events could be performed; in detail, on days 1, 102, and 159. By comparing the thrust plot in figure 6.3, it becomes clear that only the first and second window were used, on day 159, the third encounter of the two spacecraft, no thrust event took place. The reason for that is that the second thrust event already increased the CubeSat altitude, so that by day 159, its periapsis was still too high for the simulation to start a thrust event.

Figure 7.3 shows a potential complication which is visible from day 200 onwards. Up until then, the laser station and the CubeSat encountered each other occasionally which allows for the opportunity to initiate a thrust event. However, after the third thrust event window, the two spacecraft do not come close again. Moreover, on day 298, they increase the distance between each other. This behavior can be explained by considering figure 7.1 which shows that the two spacecraft orbit Earth at roughly the same altitudes, resulting in neither of them ”catching up” with the other; thus a significant amount of time passes until the next thrust event can take place, which can be too late when the CubeSat has lost too much altitude. Between days 340 and 350, however, the two spacecraft are on opposite sides again, and the altitude difference increases towards the end of the simulated period, therefore, it can be estimated that the next encounter would have occurred a few days after day 365.

8

Conclusion

This chapter aims to answer the research questions based on the findings in chapter 7 and their interpretation in section 8.1. In section 8.6, the limitations are discussed, and what research can be done based on the results and answers of this thesis.

8.1. Answers on the Research Questions

The first research question asks what possible orbits for laser stations are so that energy consumption and the laser station orbit maintenance are minimal, and that the number of reachable CubeSats is maximal. This question is not entirely answerable, due to the rapid scaling of the simulation. The last part of the question would require simulating 600 or more satellites until one simulation shows that a satellite crashes into Earth, because it could not be maintained by the laser station anymore. The remainder of the question is answered in detail in the subquestion answers. Nevertheless, energy consumption and orbit maintenance frequency decrease with the altitude of the CubeSat and laser station, respectively, as can be derived from the propulsion model in section 4.4.

8.1.1. Possible CubeSat & laser station altitude

Research questions 1.1 and 1.2 are answered together, since due to the short maximum range of roughly 20 km, the altitude difference of both CubeSats and laser stations must mainly remain within this range, so that LAP is still possible. Question 1.1 asked at what altitudes the laser station can propel CubeSats in LEO; question 1.2 asked at what altitudes the laser station's orbit has to be maintained as little as possible while still being able to reach CubeSat.

Regarding the second question, the laser station must remain at a similar altitude as the CubeSats, due to the limited laser range of 15.4 km, regardless of altitude. To keep the laser station's orbit maintenance at a minimum, its altitude should be as high as physically possible. The first question can be answered from two perspectives. From a general and purely physical view, LAP is possible

at all altitudes, the difference being the frequency at which the CubeSats require orbit maintenance. However, considering the financial aspect, LAP is only feasible at altitudes of 400 km and below. For the investigated case of maintaining 600 CubeSats, figure 5.15 clearly shows that financial feasibility is possible for a time frame of 454 days before it becomes unattractive again. Therefore, a viable altitude for a laser station lies at 400 km; its orbit maintenance must occur quite often, as due to the large mirror that causes relatively high air drag, regular thrust events must maintain its altitude.

8.1.2. Longest laser range

Research question 1.3 wanted to know how far a laser station and a CubeSat can be apart from each other while still being able to conduct orbit maintenance due to technological limits of today. The aiming accuracy of 2 µrad presented itself as the limiting factor as to how far a laser beam can reach and still hit the ablative plate of a CubeSat. In section 5.2.1 it was found out that the asymptotic range limit to hit a 10 cm x 10 cm ablative plate is 25 km, yet due to diffraction, the laser beam waist radius w_0, and the radius of the mirror where the laser originates from, an optimum laser range of 15.4 km has been derived. For that distance, a mirror radius of 2.73 m is required; the incident beam radius is 1.91 cm.

8.1.3. Suitable laser types

Research question 1.4 focuses on what types of lasers are viable for LAP. The palette of possible laser types is limited to solid-state and CO_2 lasers. Since for the former, only a few models achieve the determined power level of 9.9 kW, a larger selection can be found with the latter to fit the power level needed for LAP, as they can provide up to 100 kW. Since lasers that would be necessary for LAP are still in the experimental or prototype phase, a definitive choice could not be made.

8.1.4. Orbit improvement with technological advancement

Question 1.5 asked in what way the laser station's orbit could be improved with more accurate aiming technology in the future. To answer that question, it has been assumed that the aiming accuracy was enhanced by one order of magnitude, thus to 0.2 µrad. A similar analysis to that with figure 5.7 enables an answer. Figure 8.1 shows the mirror radius required to aim a laser over a distance for different beam waist radii, illustrated by the solid lines. The dashed red line represents the aiming accuracy of 0.2 µrad. The solid lines are identical to those in figure 5.7, the only difference being the changed technological limit. The plot here indicates that with increasing the aiming accuracy by one order of magnitude, both the laser range and the mirror radius grow by one order of magnitude. The

optimum values of the trade-off between maximizing distance and minimizing mirror radius, indicated by the black cross, increased proportionally as well, now indicating a beam range of 154.5 km with a mirror radius of 27.42 m. The beam waist radius remains at 1.91 cm.

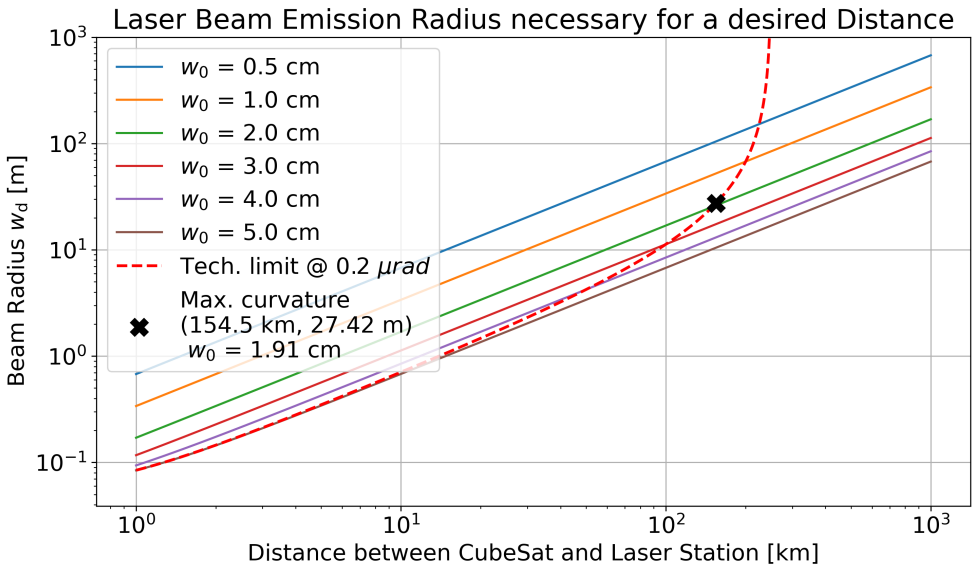

Figure 8.1: Mirror size required to achieve specific beam waist radii. The red dashed line indicates the technological aiming accuracy limit of 0.2 µrad.

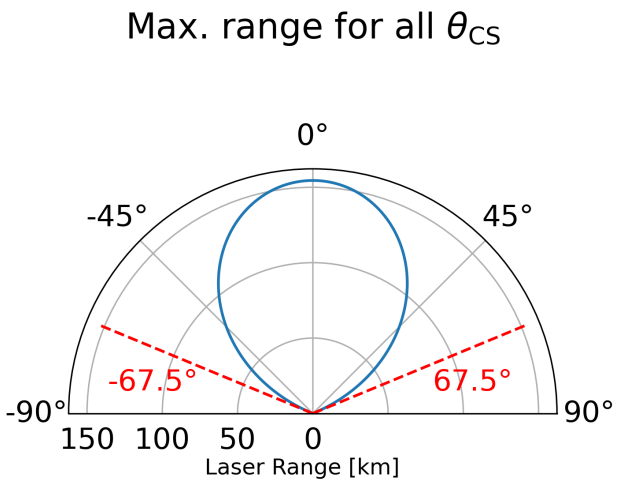

Figure 8.2: Maximum laser range over all θ_{CS} for the improved case. The red dashed line indicates the maximum viable incident angle so that hitting the ablative plate is still ensured.

With the increased range of the laser station, three advantages arise. First, there is the possibility of reaching more CubeSats, especially those on different orbital planes, as the time window to maintain their orbits is relatively short with the FoV model (see section 4.2). The FoV becomes wider the farther away one is located from the laser emitter, scaling linearly with the distance as is illustrated by figure 8.2 when compared to figure 5.9. As a result, one laser station can propel more CubeSats, provided the energy level allows for it. What does not change, however, is the maximum incident angle of the laser at the ablative plate; it remains at 67.5°. Second, increasing the laser range allows the laser station to be at a higher altitude, which increases the frequency of how often a CubeSat passes by to be hit with the laser, thus reducing the risk that it loses too much altitude to be out of reach for the laser station between two encounters, as was elaborated in connection with figure 7.3 in section 7.2. The third advantage is derived directly from the previous advantage. The extended range also allows the laser station to be put into orbit at a higher altitude, so that the orbit lifetime of the laser station is longer, or the CubeSats can be deployed at a lower altitude for improved competitiveness, if a mission requires that, or to reduce launch costs.

On the other hand, it is questionable whether the deployment and operation of a laser station with such a large mirror is practical and financially viable. On the practical side, a significantly larger launcher structure would be required to transport the entire mirror in one piece compared to the Falcon 9 used in this thesis, regardless of its foldability. Thus, it would have to be deployed with multiple launchers, which would significantly increase the cost. If Falcon 9 rocket launchers were used, each additional launch would cost $69.75 million. Thus, financial viability and competitiveness are not a given.

8.2. Minimum number of Laser stations

The second research question asked for the minimum number of laser stations necessary to ensure nearly circular orbits for CubeSats. The answer to that question can only be given for one CubeSat orbit that is maintained, for which it is 1. Due to the drag that the CubeSats experience, there is always a slight eccentricity of up to 0.0064, as was shown in figure 7.2. This eccentricity allows for orbit maintenance where the perigee can be increased until a less eccentric orbit can be achieved; the eccentricity, however, grows again over time due to said perturbations. This behavior could be observed for any number of satellites, as they are all subject to atmospheric drag. Yet, it is unknown whether one laser station can maintain 600 satellites on its own. Since this thesis only considered one orbital plane, it remains unknown how the minimum number of necessary laser stations changes, as the FoV model allows for thrust events for CubeSats on a different orbital plane to take place.

8.3. Maximum number of CubeSats

The third research question seeks to determine the maximum number of CubeSats that a laser station can maintain due to its energy limitations. The laser station was designed so that the solar arrays generate enough energy to power the laser, the board computer, and other control systems while exposed to the Sun. This energy also charges the battery, ensuring the power supply does not deplete during eclipses. Therefore, there is no limitation based on the energy.

8.3.1. Power supply options

Research question 3.1 asks what power supply options provide the most energy to the laser station for operation. In section section 4.3.1, it was established that the only viable and therefore most efficient power generation option for a laser station's energy supply is solar arrays due to cost and practical issues. Again, due to limited computation resources, it is not known whether the calculated array area of 8.68 m^2 suffices to provide power for the orbit maintenance of 600 CubeSats; figure 6.3 only confirms this for one satellite.

8.3.2. Degradation implications

Questions 3.3 and 3.4 can be answered together; the former asks what the degradation implications are on the power storage, while the latter inquires about the laser station dimensions to house energy storage and supply. As was discussed in section 5.4.1, the degradation of 0.02% per full discharge cycle results in the battery accumulating to a mass of 31.5 kg, of which 2.7 kg are added to ensure enough battery capacity for the 10-year lifetime of the laser station, which corresponds to roughly 9.38% of additional battery mass. While this is a significant addition in terms of battery mass, with the overall mass being 499.35 kg, it equates to an increase of 0.54% of the total mass, and therefore, does not have a significant impact in terms of mass. In terms of volume, it adds 0.00135 m^3 to a bus of the size of 1.00 m^3, so the volumetric impact is negligible. The laser station size is not dependent on the size of the solar arrays, as they must be mounted externally, because their area of 8.68 m^2 is larger than the laser station surface area, which is 6.09 m^3. Also, with that mass and volume, the laser station is not close to either the mass or volumetric limit of the launcher structure, so that a slight increase in both becomes problematic.

8.4. Financial viability of LAP

The fourth research question asked whether LAP is financially viable as opposed to replacing satellites. As was shown in figures 5.14 and 5.16, financial viability is given for 300 km and 400 km from 50 and 600 satellites that are maintained, respectively. The chosen case of maintaining 600 satellites at 400 km altitude shows competitiveness for 454 days after a mission duration of 6.87 years, as is presented by figure 5.15 where the green area displays the viable profit margins. Afterward, replacing the satellites becomes financially more attractive again due to the lower operation costs, as presented in section 4.5.

8.5. Requirement Conformity

This section investigates whether all requirements stated in section 3.3 are met throughout the thesis. The requirements are discussed in the same order as they were introduced.

8.5.1. Operational requirements

The CubeSat thrust model forces the thrust direction to be in the same direction as the CubeSat's direction of movement. Therefore, no thrust is lost to changing the inclination and right ascension of the ascending node, but also to rotating the orbit within its plane. Thus, no extra energy is required to maintain a CubeSat's orbit. Consequently, the maneuver is compliant with requirements OPS-1, that the laser station shall operate energy-efficiently, and OPS 1.1, that CubeSats shall perform Hohmann transfers in their orbit maintenance. Nevertheless, the requirement for Hohmann transfers, and therefore a pair of thrust events, turned out to be obsolete, as single thrust events were sufficient to maintain the satellites in orbit by exploiting the eccentricity caused by atmospheric drag. OPS-1.2, requiring electrical self-sufficiency, is met, as is demonstrated in figure 6.3. The battery charges at the beginning of the mission and recharges after a thrust event. The requirements for OPS-2, that only minimal time shall be spent per CubeSat, were mainly obeyed. By limiting the laser emission distance so that, with the maximum inaccuracy being present, the ablative plate is still hit, requirement OPS-2.1 is fulfilled at all times. While the power levels allow for single thrust events to maintain a CubeSat's orbit, the short emission distance and the FoV model can force a premature interruption of said thrust event. Thus, conformity with OPS-2.2, requiring single events for one maneuver, is not guaranteed at all times. Finally, OPS-2.3 is obeyed at all times, due to the CubeSat mass and ablative surface size of 10 cm x 10 cm, which are parameters that are fed into

the simulation. Therefore, this requirement can be regarded as fulfilled. Similar to OPS-2.3, OPS-3 is obeyed simply by entering the correct inputs into the simulation, thereby fixing the orbit to the equatorial plane.

8.5.2. State of Technology

The TRL has been considered and obeyed throughout the thesis whenever possible. It has not been considered very strictly regarding the choice of the laser, since no high-power laser has reached level 8. The laser TRL might currently reach six at maximum [61]. However, the remaining design choices have been made based on technology that has been available for multiple years, such as the nickel-cadmium battery, or relatively recent developments, such as SpaceX's Falcon 9 rocket.

8.5.3. Financial requirements

The compliance with requirement FIN-1, requiring profitability and competitiveness, and FIN-1.1, which requires a 5% profit, can be demonstrated simply. The financial simulations considered the 5% margin, as could be seen in the competitive pricing analysis with the green line in figure 5.15 for instance. The comparison with the cost of the competitors, profitability, and competitiveness is identified quickly.

8.6. Limitations & Recommendations for Future Work

The simulation was conducted in a somewhat restricted environment, as it only considered orbit maintenance for one type of CubeSat, which are all orbiting Earth on the equatorial plane. The influence of having a laser station and CubeSats orbiting on different planes was not investigated. However, the laser model, for instance, has been designed so that it also works in those scenarios with the help of the Field of View approach.

The second limitation is evident in the financial model. While there was detailed information on the costs of launchers, estimates of the costs for the laser station are subject to significant uncertainty. Unfortunately, since laser stations do not exist as proposed in this thesis, a verification or validation of those costs is impossible.

Regarding the maximum number of satellites possible to be maintained by one laser station, the simulation scales poorly with increasing numbers of CubeSats and laser stations. Therefore, already small numbers of satellites could not be simulated and verified due to limited computational resources.

Overall, there are four possible directions for continuing this work. First, optimizing the orbit and laser station characteristics concerning spacecraft lifetime, and in turn, the costs and competitiveness of LAP, might offer valuable insights. It might allow the discovery of configurations that are profitable, which, in this thesis, have not been identified as viable options or have not been considered.

Requirement OPS-3 limited this thesis to the analysis of LAP in the equatorial plane. Removing said requirement opens up LAP to a variety of missions. For instance, the dimensions of the laser stations may differ if they were in a sun-synchronous orbit. Furthermore, the application of the FoV model could be used to its full extent and improved if necessary.

Third, it has not been investigated if it is feasible to operate a network of laser stations that maintain each other's orbits. The main question would be how many of those stations would be necessary to realize such a network. Based on the laser station size, larger ablative plates can be attached, allowing lasers to be directed over longer distances. Consequently, the number of necessary laser stations may decrease. This is worth investigating for both cases: one where all spacecraft orbit in the same plane, and the other where they operate on multiple planes.

Finally, with the suboptimal technological limitation in aiming accuracy, an option to consider is the application of LAP on larger satellites. Already by applying it on 12U CubeSats in a 2x2x3 configuration, an ablative plate with twice the sidelength can be used compared to the one used in this thesis, with the consequence that the laser range increases. A laser station can then provide orbit maintenance to more CubeSats, provided the energy levels allow for it.

References

[1] Stephen D. Heister et al. *Rocket Propulsion*. Cambridge Aerospace Series. Cambridge University Press, 2019. ISBN: 978-1-108-42227-7. DOI: 10.1017/9781108381376. URL: www.cambridge.org/9781108422277.

[2] CU Aerospace. *Propulsion Unit for CubeSats*. 2024. URL: https://cuaerospace.com/products-services/space-propulsion-systems/propulsion-unit-for-cubesats-puc (visited on Apr. 16, 2025).

[3] Claude Phipps and James R. Luke. "Laser Space Propulsion". In: *Laser Ablation and its Applications*. Ed. by Claude Phipps et al. 1st ed. Springer New York, NY, 2007, pp. 407–434. ISBN: 978-0-387-30453-3. DOI: https://doi.org/10.1007/978-0-387-30453-3. URL: www.springer.com/series/624.

[4] ACSYS Lasertechnik GmbH. *Laser ablation: material removal with laser technology*. 2024. URL: https://acsyslaser.com/en/insights-en/laser-ablation-material-removal-with-laser-technology/ (visited on Dec. 11, 2024).

[5] Claude Phipps et al. *Review: Laser-ablation propulsion*. 2010. DOI: 10.2514/1.43733.

[6] Ayesha Abbas et al. "Characteristic investigation of ablative laser propulsion parameters using barium ferrites BaFe12O19 irradiated by Nd:YAG laser at 1064 nm". In: *CEAS Space Journal 2025* (Jan. 2025), pp. 1–8. ISSN: 1868-2510. DOI: 10.1007/S12567-024-00590-8. URL: https://link.springer.com/article/10.1007/s12567-024-00590-8.

[7] Leonard David. *Russian Fireball Explosion Shows Meteor Risk Greater Than Thought*. Nov. 2013. URL: https://www.space.com/23423-russian-fireball-meteor-airburst-risk.html (visited on Dec. 18, 2024).

[8] Massimiliano Vasile et al. "Improved laser ablation model for asteroid deflection". In: *Acta Astronautica* 103 (Oct. 2014), pp. 382–394. ISSN: 0094-5765. DOI: 10.1016/J.ACTAASTRO.2014.01.033.

[9] Nola Taylor Tillman. *Incoming! New Warning System Tracks Potentially Dangerous Asteroids*. Sept. 2016. URL: https://www.space.com/34149-asteroid-impact-warning-system-scout.html (visited on July 10, 2025).

[10] NASA. *Space Debris*. Nov. 2023. URL: https://www.nasa.gov/headquarters/library/find/bibliographies/space-debris/ (visited on Dec. 20, 2024).

[11] Claude R. Phipps. "Basic theory of laser propulsion". In: *Laser Propulsion in Space*. Ed. by Claude Phipps. Aerospace Engineering. Elsevier, 2024, pp. 1–38. ISBN: 978-0-443-15903-9. DOI: https://doi.org/10.1016/B978-0-44-315903-9.00007-0. URL: https://www.sciencedirect.com/science/article/pii/B9780443159039000070.

[12] John E. Sinko. "Laser Propulsion Science and Technology". In: *Aerospace* 11 (10 Oct. 2024). ISSN: 22264310. DOI: 10.3390/aerospace11100806. URL: https://www.mdpi.com/2226-4310/11/10/806.

[13] Michael Tsay et al. "Integrated Testing of Iodine BIT-3 RF Ion Propulsion System for 6U CubeSat Applications". In: Oct. 2017.

[14] Humaima Saeed et al. "Quantitative Measurements of Ablative Laser Propulsion Parameters of Metal Foils Using Pulsed Nd:YAG Laser". In: *Arabian Journal for Science and Engineering* 47 (1 Jan. 2022), pp. 895–901. ISSN: 21914281. DOI: 10.1007/S13369-021-05739-9/FIGURES/8. URL: https://link.springer.com/article/10.1007/s13369-021-05739-9.

[15] ESA. *CubeSats*. Sept. 2023. URL: https://www.esa.int/Enabling_Support/Preparing_for_the_Future/Discovery_and_Preparation/CubeSats (visited on Jan. 10, 2025).

[16] ESA. *Galileo - Facts and figures*. June 2014. URL: https://www.esa.int/Applications/Satellite_navigation/Galileo/Facts_and_figures (visited on Jan. 11, 2025).

[17] NASA. *The Future of CubeSats*. 2024. URL: https://www.nasa.gov/missions/the-future-of-cubesats/ (visited on Jan. 30, 2025).

[18] Ludwig Bergmann, Clemens Schäfer, and Heinz Niedrig. *Optik: Wellen- und Teilchenoptik*. 10th ed. Vol. 3. Walter de Gruyter, Sept. 2004, p. 370. ISBN: 3-11-017081-7.

[19] Alessandro Golkar. "Overview of the New Space CubeSat market". In: *Next Generation CubeSats and SmallSats*. Ed. by Francesco Branz et al. Elsevier, 2023, pp. 605–620. ISBN: 978-0-12-824541-5. DOI: https://doi.org/10.1016/B978-0-12-824541-5.00013-3. URL: https://www.sciencedirect.com/science/article/pii/B9780128245415000133.

[20] Lukas Urech et al. “Designed polymers for laser-based microthrusters: correlation of thrust with material, plasma, and shockwave properties (Plenary Paper)”. In: *High-Power Laser Ablation V*. Ed. by Claude R. Phipps. Vol. 5448. International Society for Optics and Photonics. SPIE, 2004, pp. 52–64. DOI: 10.1117/12.544771. URL: https://doi.org/10.1117/12.544771.

[21] David P. Resendes et al. “Laser Propulsion for Ground Launch”. In: *Journal of Propulsion and Power* 23.1 (2007), pp. 73–80. DOI: 10.2514/1.24527. eprint: https://doi.org/10.2514/1.24527. URL: https://doi.org/10.2514/1.24527.

[22] Bahman Zohuri. “Atmospheric Propagation of High-Energy Laser Beams”. In: Springer International Publishing, Aug. 2016, pp. 379–414. ISBN: 978-3-319-31288-0. DOI: 10.1007/978-3-319-31289-7_8.

[23] Hao Zhu et al. “Enhancing payload capacity to low earth orbit via a relay solution trajectory with laser-powered vehicles”. In: *Geo-Spatial Information Science* (2024). ISSN: 10095020. DOI: 10.1080/10095020.2024.2372499.

[24] Claude R. Phipps. “L′ADROIT – A spaceborne ultraviolet laser system for space debris clearing”. In: *Acta Astronautica* 104 (1 Nov. 2014), pp. 243–255. ISSN: 0094-5765. DOI: 10.1016/J.ACTAASTRO.2014.08.007.

[25] Jifei Ye et al. “Development of a Laser Micro-Thruster and On-Orbit Testing”. In: *Aerospace* 11.1 (1 Jan. 2024). ISSN: 2226-4310. DOI: 10.3390/aerospace11010023. URL: https://www.mdpi.com/2226-4310/11/1/23.

[26] Gunter D Krebs. *Chuangxing Leishen*. 2023. URL: https://space.skyrocket.de/doc_sdat/chuangxing_leishen.htm (visited on Jan. 6, 2025).

[27] Xizheng Ke. “Acquisition, Pointing, and Tracking”. In: *Handbook of Optical Wireless Communication*. Singapore: Springer Nature Singapore, 2024, pp. 357–391. ISBN: 978-981-97-1522-0. DOI: 10.1007/978-981-97-1522-0_12. URL: https://doi.org/10.1007/978-981-97-1522-0_12.

[28] Xizheng Ke. “Research Progress on Satellite Laser Communication Networks”. In: *Handbook of Optical Wireless Communication*. Singapore: Springer Nature Singapore, 2024, pp. 357–391. ISBN: 978-981-97-1522-0. DOI: 10.1007/978-981-97-1522-0_2. URL: https://doi.org/10.1007/978-981-97-1522-0_2.

[29] Riccardo Antonello et al. “High-Precision Dual-Stage Pointing Mechanism for Miniature Satellite Laser Communication Terminals”. In: *IEEE Transactions on Industrial Electronics* 68.1 (2021), pp. 776–785. DOI: 10.1109/TIE.2020.2972452.

[30] Anthony E Bentley. *Pointing Control Design for a High Precision Flight Telescope Using Quantitative Feedback Theory*. Tech. rep. Control Subsystems Department, Sandia National Laboratories, URL: https://www.osti.gov/servlets/purl/769051 (visited on July 6, 2025).

[31] Jeff Foust. *NASA to add fourth pair of roll-out arrays to ISS*. June 2023. URL: https://spacenews.com/nasa-to-add-fourth-pair-of-roll-out-arrays-to-iss/ (visited on June 29, 2025).

[32] NASA. *Second of the New Solar Arrays Successfully Deployed*. June 2021. URL: https://www.nasa.gov/blogs/spacestation/2021/06/25/second-of-the-new-solar-arrays-successfully-deployed/ (visited on June 29, 2025).

[33] ESA. *Power Systems*. URL: https://www.esa.int/Enabling_Support/Space_Engineering_Technology/Power_Systems (visited on Jan. 12, 2025).

[34] NASA Science. *Power: Radioisotope Thermoelectric Generators*. 2024. URL: https://science.nasa.gov/planetary-science/programs/radioisotope-power-systems/power-radioisotope-thermoelectric-generators/ (visited on Jan. 12, 2025).

[35] *Safety Framework for Nuclear Power Source Applications in Outer Space*. Non-serial Publications. Vienna: INTERNATIONAL ATOMIC ENERGY AGENCY. URL: https://www.iaea.org/publications/8251/safety-framework-for-nuclear-power-source-applications-in-outer-space.

[36] Claudia Toro and Noam Lior. “Analysis and comparison of solar-heat driven Stirling, Brayton and Rankine cycles for space power generation”. In: *Energy* 120 (Feb. 2017), pp. 549–564. ISSN: 0360-5442. DOI: 10.1016/J.ENERGY.2016.11.104.

[37] Anil D. Pathak et al. “A review on battery technology for space application”. In: *Journal of Energy Storage* 61 (May 2023), p. 106792. ISSN: 2352-152X. DOI: 10.1016/J.EST.2023.106792.

[38] Susanne Dörfler et al. “Recent Progress and Emerging Application Areas for Lithium–Sulfur Battery Technology”. In: *Energy Technology* 9 (1 Jan. 2021), p. 2000694. ISSN: 2194-4296. DOI: 10.1002/ENTE.202000694.

[39] Jesus Gonzalez-Llorente et al. “In-orbit feasibility demonstration of supercapacitors for space applications”. In: *Acta Astronautica* 174 (Sept. 2020), pp. 294–305. ISSN: 0094-5765. DOI: 10.1016/J.ACTAASTRO.2020.05.007.

[40] Tholkappiyan Ramachandran et al. “Asymmetric supercapacitors: Unlocking the energy storage revolution”. In: *Journal of Energy Storage* 73 (Dec. 2023), p. 109096. ISSN: 2352-152X. DOI: 10.1016/J.EST.2023.109096.

[41] Mina Mitry. “Routers in space: Kepler communications’ CubeSats will create an Internet for other satellites”. In: *IEEE Spectrum* 57.2 (2020), pp. 38–43. DOI: 10.1109/MSPEC.2020.8976900.

[42] Arianda Farres and Jeremy Petersen. “Solar radiation pressure effects on the orbital motion at SEL2 for the James Webb Space Telescope”. In: (Aug. 2019), pp. 19–657. URL: https://ntrs.nasa.gov/citations/20190029609 (visited on Feb. 10, 2025).

[43] Leandro Zardaín et al. “HIGH-FIDELITY MODELING AND VISUALIZING OF SOLAR RADIATION PRESSURE: A FRAMEWORK FOR HIGH-FIDELITY ANALYSIS”. In: (Aug. 2020). URL: https://ntrs.nasa.gov/api/citations/20205005240/downloads/AAS_srpframeworkpaper_Final02.pdf.

[44] Meike List et al. “Modelling of Solar Radiation Pressure Effects: Parameter Analysis for the MICROSCOPE Mission”. In: *International Journal of Aerospace Engineering* 2015 (1 Jan. 2015). ISSN: 1687-5974. DOI: 10.1155/2015/928206. URL: https://onlinelibrary.wiley.com/doi/full/10.1155/2015/928206%20https://onlinelibrary.wiley.com/doi/abs/10.1155/2015/928206%20https://onlinelibrary.wiley.com/doi/10.1155/2015/928206.

[45] Schaeffler Technologies AG Co. KG. *Technisches Taschenbuch*. 3rd ed. Herzogenaurach, Germany: Schaeffler Technologies AG Co. KG, 2017, pp. 127, 216.

[46] Zuu-Chang Hong, Jia Ming Liu, and Jeng-Shing Chern. “Overall payload ratio of a combined laser and chemical propulsion system for geo launch”. In: *Acta Astronautica* 50.7 (2002), pp. 417–426. ISSN: 0094-5765. DOI: https://doi.org/10.1016/S0094-5765(01)00169-2. URL: https://www.sciencedirect.com/science/article/pii/S0094576501001692.

[47] Anthony E. Siegman. “Physical Properties of Gaussian Beams”. In: *Lasers*. Univ. Sci. Bks., U.S., 1986, pp. 56, 663–669. ISBN: 0-935702-11-3.

[48] Hans Joachim Eichler, Jürgen Eichler, and Oliver Lux. “Laser Types”. In: *Lasers: Basics, Advances and Applications*. Cham: Springer International Publishing, 2018, pp. 51–62. ISBN: 978-3-319-99895-4. DOI: 10.1007/978-3-319-99895-4_3. URL: https://doi.org/10.1007/978-3-319-99895-4_3.

[49] Department of Energy. *Energy and Power by Battery Type*. Jan. 2010. URL: https://www.energy.gov/eere/vehicles/fact-607-january-25-2010-energy-and-power-battery-type.

[50] J. D. Dunlop and J. F. Stockel. “Nickel-Hydrogen Battery Technology-Development and Status”. In: *Journal of Energy* 6.1 (1982), pp. 28–33. DOI: 10.2514/3.62569. URL: https://doi.org/10.2514/3.62569.

[51] T R Ayodele and A S O Ogunjuyigbe. “Mitigation of wind power intermittency: Storage technology approach”. In: (2015). DOI: 10.1016/j.rser.2014.12.034. URL: http://dx.doi.org/10.1016/j.rser.2014.12.034.

[52] NASA Science. *Electrical Power*. URL: https://science.nasa.gov/mission/hubble/observatory/design/electrical-power/ (visited on July 28, 2025).

[53] Peter Kurzweil and Wolfgang Scheuerpflug. “State-of-Charge Monitoring and Battery Diagnosis of NiCd Cells Using Impedance Spectroscopy”. In: *Batteries* 6.1 (2020). ISSN: 2313-0105. DOI: 10.3390/batteries6010004. URL: https://www.mdpi.com/2313-0105/6/1/4.

[54] James Richard. Wertz and Wiley J. Larson. *Space mission analysis and design*. 3rd ed. Microcosm Press, Kluwer Academic Publishers, 1999, pp. 147–148, 312, 342–345, 611, 914, 985. ISBN: 1-881883-10. DOI: Wertz1999.

[55] Yuri Rezunkov. *High Power Laser Propulsion*. Ed. by Gordon W. F. Drake. 1st ed. Springer Cham, 2021, pp. 18, 19. ISBN: 978-3-030-79693-8. DOI: https://doi.org/10.1007/978-3-030-79693-8. URL: http://www.springer.com/series/411.

[56] Bright Ascension. *What is a 6U CubeSat and when would you use one?* Feb. 2020. URL: https://brightascension.com/what-is-a-6u-cubesat-and-when-would-you-use-one/ (visited on June 25, 2025).

[57] SatCatalog. *6U CubeSat Platform*. URL: https://www.satcatalog.com/component/6u-cubesat-platform/ (visited on Mar. 24, 2025).

[58] SpaceX. *Rideshare*. URL: https://www.spacex.com/rideshare/ (visited on Mar. 24, 2025).

[59] Olivier de Weck et al. *Communications Satellite Constellations ”Technical Success and Economic Failure”*. Tech. rep. Massachusetts Institute of Technology, Oct. 2003, pp. 10, 11.

[60] Jared Keller. *Here’s the Status of Every Known US Military Laser Weapon*. Feb. 2025. URL: https://laserwars.substack.com/p/us-military-laser-weapons-programs-list (visited on Apr. 22, 2025).

[61] Jen Judson. *Dynetics-Lockheed team beats out Raytheon to build 100-kilowatt laser weapon*. May 2019. URL: https://www.defensenews.com/land/2019/05/16/dynetics-lockheed-team-beats-out-raytheon-to-build-100-kilowatt-laser-weapon/ (visited on July 4, 2025).

[62] Sergey Reznik, D Reut, and M Shustilova. “Comparison of geostationary and low-orbit “round dance” satellite communication systems”. In: *IOP Conference Series: Materials Science and Engineering* 971 (Dec. 2020), p. 052045. DOI: 10.1088/1757-899X/971/5/052045.

[63] D. Steward et al. “Lifecycle Cost Analysis of Hydrogen Versus Other Technologies for Electrical Energy Storage”. In: (Nov. 2009). DOI: 10.2172/968186. URL: https://www.researchgate.net/publication/237393792_Lifecycle_Cost_Analysis_of_Hydrogen_Versus_Other_Technologies_for_Electrical_Energy_Storage.

[64] Shanghai YIM Machinery and Equipment Co.ltd. *Multi-Junction Solar Cells Price: Understanding the Market and Applications*. URL: https://www.shanghaiyim.com/news/industry/153.html.

[65] IMARC Group. *Xenon Prices, Trend, Chart, Demand, Market Analysis, News, Historical and Forecast Data Report 2025 Edition*. 2025. URL: https://www.imarcgroup.com/xenon-price-trend (visited on July 25, 2025).

[66] SpaceX. *Falcon 9*. 2025. URL: https://www.spacex.com/vehicles/falcon-9/ (visited on Apr. 22, 2025).

[67] Karsten James et al. *Performance Characterization of the HYDROS Water electrolysis Thruster*. Tech. rep. Tethers Unlimited, Inc., 2015.

[68] John Hanson. *Pathfinder Technology Demonstrator ”Enabling the Next Generation of CubeSat missions”*. Apr. 2019.

[69] CubeSatShop. *Nanosatellite Micropropulsion System*. URL: https://www.cubesatshop.com/product/nanosatellite-micropropulsion-system/ (visited on Mar. 24, 2025).

[70] CubeSatShop. *IFM Nano Thruster for CubeSats*. URL: https://www.cubesatshop.com/product/ifm-nano-thruster/ (visited on Apr. 18, 2025).

[71] National Institute of Standards and Technology. *LOESS (aka LOWESS)*. URL: https://www.itl.nist.gov/div898/handbook/pmd/section1/pmd144.htm (visited on Apr. 20, 2025).

[72] Yanan Wang, David Thompson, and Zhiwei Hu. “Effect of aspect ratios on flow and noise from cuboids”. In: *25th AIAA/CEAS Aeroacoustics Conference*. DOI: 10.2514/6.2019-2671. eprint: https://arc.aiaa.org/doi/pdf/10.2514/6.2019-2671. URL: https://arc.aiaa.org/doi/abs/10.2514/6.2019-2671.

[73] Jacques Goualard. “Cycle life status of SAFT VOS nickel-cadmium cells”. In: *NASA. Marshall Space Flight Center, The 1992 NASA Aerospace Battery Workshop* (1993). URL: https://ntrs.nasa.gov/citations/19930011322.

[74] Busek Co. Inc. *BHT-200 Hall Effect Thruster*. Tech. rep. Busek Co. Inc, 2021. URL: https://www.busek.com/bht200.

[75] National Institute of Standards and Technology. *Isothermal Properties for Xenon*. 2025. URL: https://webbook.nist.gov/cgi/fluid.cgi?T=60&PLow=180&PHigh=190&PInc=1&Digits=5&ID=C7440633&Action=Load&Type=IsoTherm&TUnit=C&PUnit=bar&DUnit=kg%2Fm3&HUnit=kJ%2Fkg&WUnit=m%2Fs&VisUnit=Pa*s&STUnit=N%2Fm&RefState=DEF.

[76] SpaceX. *Falcon User's Guide*. Tech. rep. Sept. 2021, p. 84.

[77] NASA. *NASA's Webb Telescope's Last Backbone Component Completed*. June 2013. URL: https://www.nasa.gov/news-release/nasas-webb-telescopes-last-backbone-component-completed/.

[78] B. R. Munson et al. *Fundamentals of fluid mechanics*. 6th ed. John Wiley & Sons, 2009, p. 511. ISBN: 978-0470-26284-9.

[79] Jovan Nedić, Bharathram Ganapathisubramani, and J. Vassilicos. "Drag and near wake characteristics of flat plates normal to the flow with fractal edge geometries". In: *Fluid Dynamics Research* 45 (Aug. 2013), p. 061406. DOI: 10.1088/0169-5983/45/6/061406.

[80] SpaceWeatherLive.com. *Historical solar cycles*. URL: https://www.spaceweatherlive.com/en/solar-activity/solar-cycle/historical-solar-cycles.html (visited on July 18, 2025).

[81] NASA. *NASA Open Data Portal*. URL: https://data.nasa.gov/dataset/iss-coords-2021-03-23 (visited on Apr. 20, 2025).

A
Research Plan

A.1. Original plan

Table A.1 depicts the original research plan for this thesis. It breaks down the thesis into six main steps: literature study, simulations, sensitivity analysis, verification and validation, results, and defense preparation. Each of those steps consists of work packages that are planned in the Gantt chart.

The simulations are divided into four work packages, each focusing on a specific part of the model that describes a laser station's task and environment. The work packages are planned serially because the individual topics depend on the previous ones. For the optimization algorithm, intended as the final simulation work package, a minor exception is made by addressing its requirements at the beginning to clarify which outputs the remaining three simulations are expected to return. Step three, the sensitivity analysis, occurs toward the end of the simulation period, allowing for the detection of possible trends across topics. Next, the verification and validation are conducted after the simulations are finished.

The answers to the research questions in section 3.1, the results, are derived after the mid-term review. Those answers are obtained by running the optimization algorithm, finding the system's limits, and generating diagrams. Those outputs are interpreted and ultimately elaborated in the report. After the report has been submitted, preparation for the thesis defence begins.

A.2. Actual outcome

A.2.1. Simulations

The main deviations that occurred in the simulation part originate, on the one hand, from underestimating the time needed to complete the models. On the other hand, time was lost at the beginning to familiarize with Tudat. Those two factors resulted in abandoning the optimization part, allowing the other three parts to be completed. Ultimately, the mid-term review was postponed to calendar week 17 to account for the additional time needed. A minor change was made by switching the laser propulsion and orbital mechanics parts, as it became clear that the outputs of the propulsion model needed in the main simulation, which contains the orbital mechanics, had to be known first.

A.2.2. Sensitivity analysis

The sensitivity analysis was postponed by roughly a month for two reasons. First, there was the misunderstanding that the sensitivity analysis had to be completed by the mid-term review. Second, coding the models did not leave time to do the sensitivity analysis simultaneously. In the end, however, the sensitivity analysis has been continually expanded as necessary to answer the research questions.

A.2.3. Verification & Validation

Due to the additional time required for the simulations, verification and validation commenced only in calendar week 16, shortly before the mid-term review, and therefore lasted longer than initially planned, extending roughly until calendar week 20. Gathering external data had already begun during the literature study, as the sources collected in that phase could be referenced.

A.2.4. Results

The time to generate results and interpret them was shortened due to the postponements made during the earlier stages; yet, as planned, the visualization, interpretation, and inclusion in this report took place simultaneously. Nevertheless, the green light has been postponed by a week as well.

Table A.1: Gantt chart research plan

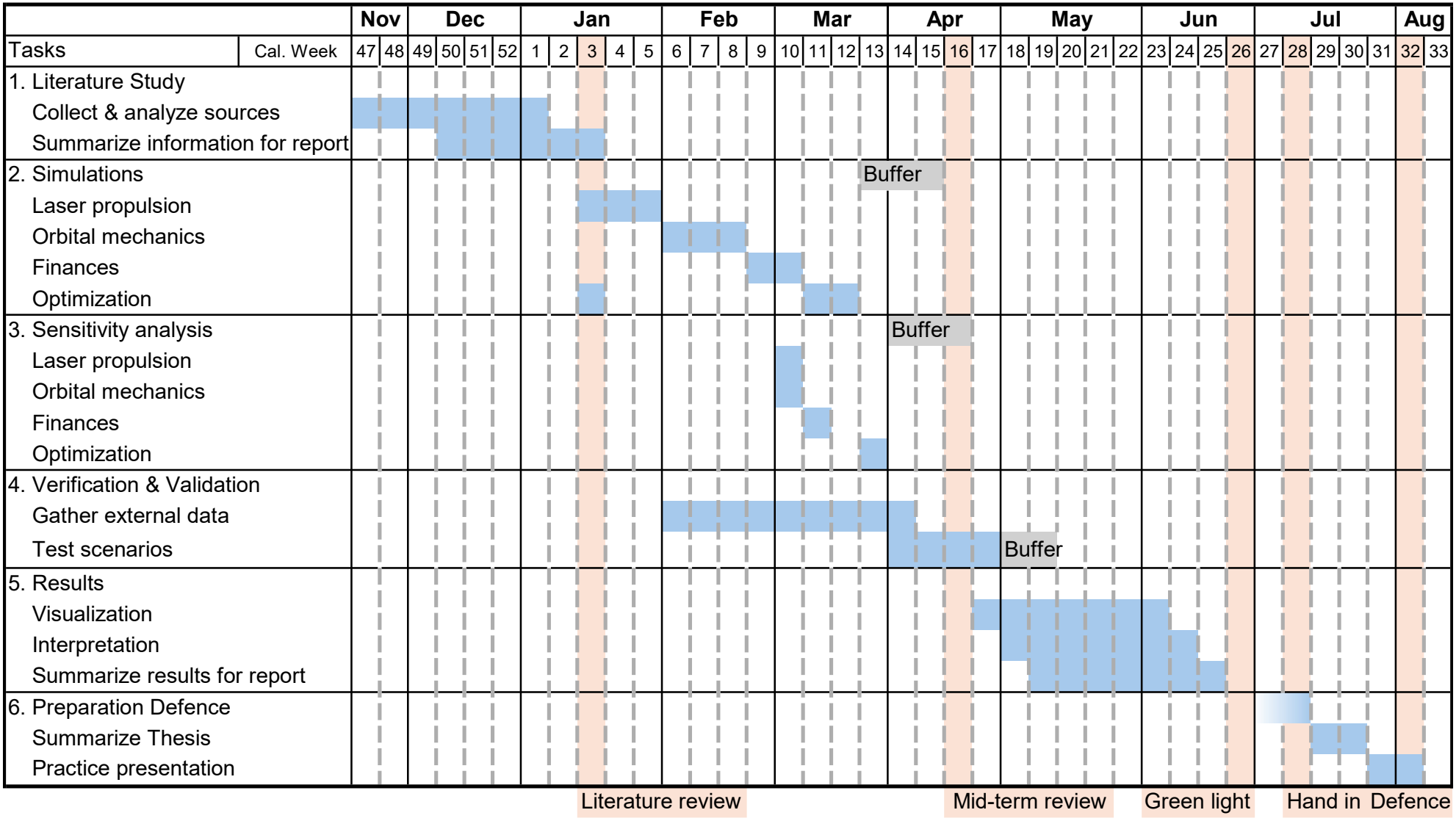

B
Adjustments

B.1. Changes made in the Research Proposal

In section 3.1, research question RQ-3.2 ”What energy storage options can store electricity most efficiently in space?” has been removed. This is because this question is analyzed in the methodology in section 2.4.2 and is not answered via the results of the simulation made for this thesis. The method of determining the laser station’s battery mass and size is indeed tied to the battery properties; however, the question of the laser station’s dimensions has already been posed with RQ-3.4, which makes RQ-3.2 obsolete.